High-transition-temperature superconducting quantum interference devices

D. Koelle

II. Physikalisches Institut, Lehrstuhl für Angewandte Physik, Universität zu Köln, D-50937 Köln, Germany

R. Kleiner

Physikalisches Institut III, Universität Erlangen-Nürnberg, D-91058 Erlangen, Germany

F. Ludwig

Physikalisch-Technische Bundesanstalt, Section Cryosensors, D-10587 Berlin, Germany

E. Dantsker* and John Clarke

Physics Department, University of California, Berkeley, and Materials Sciences Division, Lawrence Berkeley National Laboratory, Berkeley, California 94720

The advent of high-T_c superconductors gave great impetus to the development of thin-film superconducting quantum interference devices (SQUIDs) for operation at temperatures up to the boiling point of liquid nitrogen, 77 K. The spectral density of the white flux noise can be calculated analytically for rf SQUIDs and by computer simulation for dc SQUIDs; however, observed noise spectral densities are typically an order of magnitude higher. Low-frequency $1/f$ noise from thermally activated vortex motion is a much bigger issue in high-T_c SQUIDs at 77 K than in low-T_c SQUIDs because of the low flux-pinning energies in high-T_c superconductors. The magnitude of the noise depends strongly on the quality of the thin films, and much effort has been expended to improve techniques for depositing $YBa_2Cu_3O_{7-x}$ (YBCO) on lattice-matched single-crystal substrates. Substantial effort has also been invested in the development of new types of Josephson junctions, of which grain-boundary junctions are the most widely used in SQUIDs. Appropriate electronic read-out schemes largely eliminate $1/f$ noise from fluctuations in the junction critical current in both rf and dc SQUIDs. Typical levels of white flux noise are a few $\mu\Phi_0\,\mathrm{Hz}^{-1/2}$ (Φ_0 is the flux quantum). Magnetometers—consisting of a superconducting flux transformer coupled to a SQUID—achieve a white magnetic-field noise as low as $10\ \mathrm{fT\,Hz}^{-1/2}$, increasing to typically $30\ \mathrm{fT\,Hz}^{-1/2}$ at 1 Hz. When these devices are operated in an unshielded environment, it is important to minimize the motion of trapped vortices and induced supercurrents, which can greatly increase the $1/f$ noise. The ambient noise is far greater than the intrinsic noise of the devices, but can be substantially reduced by various gradiometer configurations. There is now considerable effort to apply high-T_c SQUIDs in magnetocardiology, nondestructive evaluation, microscopy, and geophysics. [S0034-6861(99)00403-1]

CONTENTS

*Current address: TRW, Electronics & Technology Division, Redondo Beach, California 90278.

I. INTRODUCTION

The discovery of superconductivity in ceramic oxides (Bednorz and Müller, 1986) such as $YBa_2Cu_3O_{7-x}$ (YBCO) (Wu *et al.*, 1987) with transition temperatures (T_c) above the boiling point of liquid nitrogen (77 K) generated a worldwide furor to develop new superconducting technologies for both large- and small-scale applications. This frenzy of activity was of course driven by the perception that superconductors cooled in liquid nitrogen at 77 K would quickly become much more widely applicable than superconductors cooled in liquid ^{4}He at 4.2 K. There were two broad reasons behind this perception: liquid nitrogen is much cheaper than liquid helium, and, for a given heat load, liquid nitrogen boils away much more slowly than liquid helium. It was immediately apparent that small-scale devices would require the development of thin-film techniques, and to provide a framework for this research many groups focused on the superconducting quantum interference device (SQUID). Thus at a very early stage of the field Koch *et al.* (1987) and subsequently Nakane *et al.* (1987) fabricated the first thin-film dc SQUIDs; the first rf SQUIDs appeared a little later (Colclough *et al.*, 1987; Zimmerman *et al.*, 1987), although they were actually formed from bulk YBCO. There were several good reasons for choosing the SQUID as a vehicle for the development of this new technology. Low-T_c SQUIDs are by far the most widely used superconducting thin-film devices at liquid ^{4}He temperatures, and it was a natural assumption that this trend would continue at liquid N_2 temperatures. Furthermore, the SQUID incorporates most of the components needed for a broader range of electronic devices. The first is a photolithographically patterned thin film with high crystalline quality and a transition temperature essentially equal to that of the bulk material. A second, essential component is the Josephson junction (Josephson, 1962), for which one would like a process that yields highly reproducible parameters. A third ingredient is an interconnect technology, that is, a multiple-level process that enables one to fabricate crossovers—two intersecting superconducting films separated by an insulating layer—and *vias*—superconducting contacts through the insulating layer. Progress in high-T_c dc and rf SQUIDs over the last decade has been dramatic, and the purpose of this review is to give a perspective on the current state of the art.

The dc SQUID (Jaklevic *et al.*, 1964) consists of two Josephson junctions connected in parallel on a superconducting loop. When the magnetic flux Φ threading the loop is changed monotonically, the maximum supercurrent the SQUID can sustain (the critical current) is modulated with a period of one flux quantum, $\Phi_0 \equiv h/2e$. Provided the current-voltage (I-V) characteristic is nonhysteretic (Sec. II.A), this modulation results in a concomitant modulation of the voltage across the SQUID when it is biased with a constant current greater than the maximum critical current. In essence, the SQUID is a flux-to-voltage transducer, characterized by the transfer coefficient $|\partial V/\partial\Phi|_I$. The flux resolution of the SQUID is determined by its intrinsic noise, which has a spectral density that is white at frequencies above a certain threshold and that scales approximately as $1/f$ at frequencies f below the threshold. In low-T_c SQUIDs the threshold frequency can be 0.1 Hz or lower, while, as we shall see, in high-T_c SQUIDs it can be substantially higher. In Secs. II.B and C, we outline the theory of operation of the dc SQUID and solve its equations of motion numerically for both the transfer function and white noise. From the results of our simulations we discuss the optimum choice of parameters for operation at 77 K.

The rf SQUID (Zimmerman *et al.*, 1970; Mercereau, 1970; Nisenoff, 1970) involves a single Josephson junction that interrupts a superconducting loop. This loop is inductively coupled to the inductor of an LC-resonant circuit that is driven by an rf current at or near its resonant frequency, which ranges from 20 MHz to 10 GHz. The amplitude of the rf voltage across the tank circuit is periodic in the magnetic flux in the SQUID with period Φ_0, so that, after demodulating this voltage, one obtains a quasistatic voltage that is periodic in Φ just as for the dc SQUID. For operation at 4.2 K the rf SQUID has been largely abandoned in favor of the dc SQUID, but the advantage in sensitivity of the latter device at 77 K is much narrower. In Secs. II.D–F, we outline the theory of operation and noise limitations of the rf SQUID.

Low-T_c SQUIDs have been used as sensors in a broad range of applications, including biomagnetism, nondestructive evaluation, geophysics, susceptometers, voltmeters, scanning SQUID microscopes, and nuclear magnetic and nuclear quadrupole resonance (Weinstock, 1996). Of these, the largest number of SQUIDs are deployed in multichannel systems for magnetoencephalography and, to a lesser extent, magnetocardiology. A major requirement for biomagnetic measurements is high magnetic-field sensitivity at frequencies down to 1 Hz. Although this requirement is readily met with niobium based SQUID magnetometers, which achieve a sensitivity of a few fT $Hz^{-1/2}$, the issue of $1/f$ noise in high-T_c SQUIDs has been a major challenge, and will emerge repeatedly throughout this review. There are two separate sources of $1/f$ noise (Koch *et al.*, 1983): fluctuations in the critical current of the junction(s) and the ther-

mally activated hopping of flux vortices among pinning sites in the thin-film loop. Fortunately, as will be described, $1/f$ noise due to critical-current fluctuations in both dc and rf SQUIDs can be largely eliminated electronically by means of appropriate schemes (Secs. V.B and VII.C). In the case of low-T_c SQUIDs, $1/f$ noise from vortex motion is rarely a problem, but for high-T_c SQUIDs it is a major issue. The reason is simple: flux-pinning energies are lower and thermal energies are higher. At an early stage, Ferrari *et al.* (1988, 1989) used a low-T_c dc SQUID to show that vortex motion in unpatterned high-T_c films indeed produced copious levels of $1/f$ flux noise and that the level diminished dramatically as the microstructural quality of the film was improved. This theme is first raised in Sec. III, in which we briefly review issues concerning the fabrication of thin films. We confine our discussion to YBCO, the only material that has been used for practical devices. Of the possible substrate materials only a handful are admissible. Pulsed laser deposition, sputtering, and recently, coevaporation have emerged as the deposition techniques of choice. Issues of patterning and multilayer processing as well as $1/f$ noise are also discussed in this section.

The other major challenge in the development of SQUIDs, and indeed for high-T_c electronics circuits in general, has been the need to develop an appropriate technology for Josephson junctions (Sec. IV). Many approaches have been tried, ranging from a single layer of YBCO in which grain-boundary junctions are formed along the misorientation boundary of a bicrystal substrate or at a step edge milled in a substrate, to multilayers in which insulating or metallic barriers are formed between two YBCO films. It seems fair to say that the ideal technology has not yet been invented. For virtually all applications, the figure of merit is the I_0R product, where I_0 is the critical current and R is the resistance for currents much greater than I_0. Although one might hope to achieve values of several millivolts at 77 K, in practice the highest values achieved to date are more like 300 μV. For SQUIDs, the technique most widely used today is the grain-boundary junction formed on either a bicrystal or a step edge.

Section V reviews practical high-T_c dc SQUIDs. The two widely used readout schemes, flux modulation and direct readout, are briefly described, and the use of bias reversal to eliminate the $1/f$ noise due to critical-current fluctuations is outlined. Achieved levels of white noise and $1/f$ noise are summarized in a series of figures. For reasons that are not well understood, the levels of white noise are generally higher than the predictions of the computer model described in Sec. II.

Although dc SQUIDs are exquisitely sensitive to changes in magnetic flux—typical devices have a white noise of a few $\mu\Phi_0\,\mathrm{Hz}^{-1/2}$—their small area implies that they are relatively insensitive to changes in magnetic field. To increase this sensitivity, as described in Sec. VI, one almost invariably couples the SQUID to a flux transformer that increases its effective area. Broadly speaking, there are two classes of such magnetometers. In the first, the so-called directly coupled magnetometer, a large pickup loop—perhaps 10 mm across—is patterned in the same layer as the SQUID so that the supercurrent produced by an applied magnetic field is injected directly into the body of the SQUID. This scheme has the advantage that it involves only a single superconducting layer but suffers from the disadvantage that the inductances of the pickup loop and SQUID are mismatched, thereby reducing the flux-coupling efficiency of the transformer. The mismatch is overcome in the second approach, mimicking that used for low-T_c magnetometers, in which a pickup loop is connected to a multiturn input coil that in turn is inductively coupled to the SQUID. The flux transformer can be either deposited directly onto the SQUID or deposited on a separate substrate and coupled to the SQUID in a flip-chip arrangement. This flux transformer matches the inductance of the pickup loop to the SQUID, but the multilayer structure required for the input coil complicates the fabrication. The best of these magnetometers have achieved a white noise below 10 $\mathrm{fT\,Hz}^{-1/2}$. An alternative, multilayer magnetometer is the fractional-turn SQUID described in Sec. VI.D.

Section VII is concerned with practical rf SQUIDs, usually fabricated from single layers of YBCO. As discussed in Sec. II, the inductance of the rf SQUID can be somewhat larger than its dc counterpart, enabling one to obtain a higher effective area. Early devices consisted of square washers with step-edge, grain-boundary junctions, and were operated at typically 150 MHz. The sensitivity has been improved by increasing the frequency substantially; as shown in Sec. II, the spectral density of the flux noise is expected to scale inversely with the rf frequency. In the best device reported to date, the white noise was 16 $\mathrm{fT\,Hz}^{-1/2}$. Section VII.C describes how the $1/f$ noise due to critical-current fluctuations is eliminated by the combination of rf biasing and flux modulation.

Sections VIII and IX are concerned with using SQUID magnetometers in real-world environments. Most notably in biomagnetism, one needs to measure a tiny magnetic signal against a magnetically noisy background. The standard approach to this problem is to use a spatial gradiometer, usually in conjunction with a magnetically shielded room. The gradiometer discriminates against distant noise sources in favor of a nearby signal source. Given the lack of a suitable high-T_c superconducting wire, two approaches have been adopted (Sec. VIII): electronic subtraction of the signals from two or more spatially separated magnetometers, usually to form axial gradiometers, and the use of planar, thin-film gradiometers that measure off-diagonal gradients. Section IX is largely concerned with the operation of magnetometers or gradiometers in the ambient magnetic field of the earth, which has two deleterious effects. The additional vortices created by the penetration of the earth's field into the thin films can greatly increase the level of $1/f$ noise. Fortunately, this problem can be largely alleviated by making the thin-film structures sufficiently narrow, if necessary, by patterning slots or holes

in them. A related problem is hysteresis produced by the entry of vortices when the device is rotated in the earth's field. Flux entry can be greatly reduced, fortunately, by patterning straight, near-vertical edges which provide high edge-pinning forces. Other issues discussed in Sec. IX include rf interference and temperature fluctuations.

In Sec. X we briefly review several applications of high-T_c SQUIDs, which are still in their infancy. Nonetheless, impressive progress has been made in biomagnetism, particularly magnetocardiology, and useful demonstrations have been made in both nondestructive evaluation and scanning SQUID microscopy. Prototype geophysical systems have been successfully deployed. Section XI contains our conclusions.

Writing this review brought home to us the enormous amount of effort that has been expended in developing the technology of high-T_c SQUIDs, and the vastness of the literature. Regrettably, it was out of the question to list more than a fraction of the publications in the space of this review. We have attempted to give a broad perspective on the field, but we are acutely aware that our choice of topics is subjective and far from exhaustive.

II. THEORY

A. Resistively shunted junction model

The Josephson junction (Josephson 1962, 1965; Barone and Paterno, 1982) consists of two weakly coupled superconducting electrodes separated—in the case of the low-T_c tunnel junction—by a thin insulating barrier. Cooper pairs tunneling through the barrier constitute a supercurrent $I=I_0\sin\delta$, where I_0 is the critical current and δ is the difference between the phases of the order parameters in the two superconductors. For zero applied current, the two electrodes are coupled by an energy $I_0\Phi_0/2\pi$. In the absence of thermal fluctuations, the voltage V across the barrier is zero for $I<I_0$; for $I>I_0$ a voltage is developed and δ evolves with time as $\dot{\delta}=2\,\mathrm{eV}/\hbar=2\pi\,\mathrm{V}/\Phi_0$. At least for low-$T_c$ junctions, the current-voltage characteristics are well explained by the resistively and capacitively shunted junction (RCSJ) model (McCumber, 1968; Stewart, 1968). In this model, the Josephson element is in parallel with a resistance R (which may be an external shunt) and a capacitance C. For SQUIDs, one generally needs nonhysteretic I-V characteristics, a requirement that is met if $\beta_c\equiv 2\pi I_0R^2C/\Phi_0\lesssim 1$. In the limit $\beta_c\ll 1$, which as we shall see is often the case for high-T_c junctions, the RCSJ model reduces to the RSJ model and the I-V characteristic in the absence of thermal noise is given by $V=R(I^2-I_0^2)^{1/2}$ for $I\geqslant I_0$.

Particularly in the case of devices operating at 77 K, however, noise has an appreciable effect, and is added to the model by associating a Nyquist noise current I_N with spectral density $S_I(f)=4k_BT/R$ with the shunt resistor. This noise term rounds the I-V characteristic at low voltages and reduces the apparent critical current (Ambegaokar and Halperin, 1969). To maintain a reasonable degree of Josephson coupling one requires the noise parameter $\Gamma\equiv 2\pi k_BT/I_0\Phi_0=I_{th}/I_0\lesssim 1$; at 77 K, $I_{th}\approx 3.3\,\mu$A.

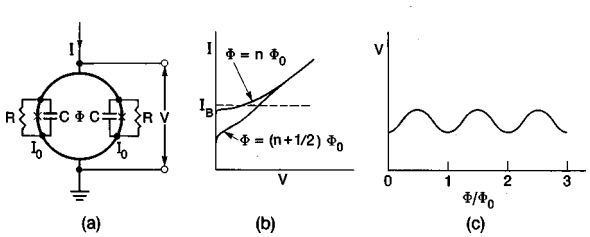

FIG. 1. The dc SQUID: (a) schematic, (b) I-V characteristic, (c) V vs Φ/Φ_0 at constant bias current I_B.

B. dc SQUID: Overview

The dc SQUID (Jaklevic *et al.*, 1964) consists of two Josephson junctions connected in parallel on a superconducting loop of inductance L [Fig. 1(a)]. If one biases the SQUID with a constant current $I_B(>2I_0)$ the voltage V across the SQUID oscillates with a period Φ_0 as one changes the external magnetic flux Φ [Figs. 1(b) and (c)]. To measure small changes in Φ ($\ll\Phi_0$) one generally chooses the bias current to maximize the amplitude of the voltage modulation and sets the external flux at $(2n+1)\Phi_0/4$ ($n=0,1,2,\ldots$), so that the flux-to-voltage transfer coefficient $|\partial V/\partial\Phi|_I$ is a maximum, which we denote as V_Φ. Thus the SQUID produces a maximum output voltage signal $\delta V=V_\Phi\delta\Phi$ in response to a small flux signal $\delta\Phi$. For frequencies f well below the Josephson frequency $f_J=V/\Phi_0$, the two independent Nyquist noise currents in the shunt resistors produce a white voltage noise across the SQUID with a spectral density $S_V(f)$ (Tesche and Clarke, 1977) and a white current noise around the SQUID loop with a spectral density $S_J(f)$; in fact, these two noise terms are partially correlated (Tesche and Clarke, 1979). The intrinsic white flux noise of the SQUID is given by $S_\Phi(f)=S_V(f)/V_\Phi^2$; it is often convenient to introduce a noise energy per unit bandwidth $\varepsilon(f)=S_\Phi(f)/2L$. We note that noise imposes a second constraint on the parameters, namely that the magnetic energy per flux quantum $\Phi_0^2/2L$ must be substantially greater than k_BT. We can express this requirement as $\Gamma\beta_L=L/L_{th}\ll 1$, where we define $\beta_L=2LI_0/\Phi_0$, and $L_{th}\equiv\Phi_0^2/4\pi k_BT=321$ pH at 77 K. As we shall see, this restriction, which can also be written as $\Phi_0^2/2L\gg 2\pi k_BT$, will play a key role in our choice of parameters.

There have been extensive computer simulations of dc SQUIDs operated at 4.2 K (Tesche and Clarke, 1977, 1979; Bruines *et al.*, 1982; Voss, 1981; de Waal *et al.*, 1984; Ryhänen *et al.*, 1989). These simulations show that the minimum noise energy is obtained for $\beta_L\approx 1$ and that, for a representative value of the noise parameter $\Gamma=0.05$, $V_\Phi\approx R/L$, $S_V(f)\approx 16k_BTR$ and $\varepsilon\approx 9k_BTL/R\approx 9k_BT\Phi_0/2I_0R$. Thus ε inevitably increases with temperature and, for optimized parameters, scales as $1/I_0R$. In addition to the white noise, there is usually low-

frequency $1/f$ noise generated by both $1/f$ noise in the critical current and by the motion of flux vortices trapped in the body of the SQUID. We defer the issue of $1/f$ noise to Sec. V.D, and turn our attention to optimizing the parameters of the SQUID at 77 K with regard to white noise.

C. dc SQUID: Transfer function and thermal noise

It is straightforward to show that the phase differences $\delta_1(t)$ and $\delta_2(t)$ across the two junctions obey the following equations (Tesche and Clarke, 1977):

$$\frac{\hbar C}{2e}\ddot{\delta}_1+\frac{\hbar}{2eR}\dot{\delta}_1+I_0\sin\delta_1+I_{N1}=\frac{I}{2}-J, \tag{2.1}$$

$$\frac{\hbar C}{2e}\ddot{\delta}_2+\frac{\hbar}{2eR}\dot{\delta}_2+I_0\sin\delta_2+I_{N2}=\frac{I}{2}+J, \tag{2.2}$$

$$\delta_1-\delta_2=\frac{2\pi}{\Phi_0}(\Phi+LJ), \tag{2.3}$$

and

$$\dot{\delta}_1+\dot{\delta}_2=\frac{4\mathrm{eV}}{\hbar}. \tag{2.4}$$

The Langevin Eqs. (2.1) and (2.2) are coupled via the circulating current J, which is related to the external flux Φ in Eq. (2.3). Equation (2.4) expresses the voltage across the SQUID as the rate of the change of the phase differences. In all our simulations we set $\beta_c=0.5$; the results change only slightly for the smaller values of β_c that we expect for many high-T_c junctions operated at 77 K. To find the transfer function we set $\Phi=\Phi_0/4$, integrate Eqs. (2.1)–(2.3) numerically over 10^4 to 10^6 time units ($\Phi_0/2\pi I_0R$), and use Eq. (2.4) to obtain the average voltage across the SQUID (Kleiner, 1996). We compute $\partial V/\partial\Phi$ as a function of I to find the maximum value V_Φ. To explore the dependence on the inductance L, it is convenient to plot V_Φ vs $\Gamma\beta_L=L/L_{th}=(4\pi k_BT/\Phi_0^2)L$. The range of interest for $\Gamma\beta_L$ extends from well below 0.05 to unity. For convenience, we start from $\Gamma\beta_L=(0.05)2^{-2}=\frac{1}{80}$ and increase $\Gamma\beta_L$ in powers of $2^{1/2}$ up to $(0.05)2^{9/2}\approx1.13$. For $T=77$ K this corresponds to inductances between 4 and 362 pH, while for $T=4.2$ K the corresponding range is 74 pH to 6.7 nH. For most high-T_c devices $\Gamma\beta_L\geq0.1$, whereas for typical low-T_c devices $\Gamma\beta_L\lesssim0.05$.

On calculating the dimensionless transfer function $v_\phi=V_\Phi\Phi_0/I_0R$ vs $\Gamma\beta_L$ for values of β_L ranging from 0.6 to 4 one finds that, although v_ϕ for a given value of $\Gamma\beta_L$ decreases with β_L, its functional dependence on $\Gamma\beta_L$ is essentially the same for all values of β_L. Thus, on normalizing curves of v_ϕ vs $\Gamma\beta_L$ to their value at, say, $\Gamma\beta_L=\frac{1}{80}$, one obtains a universal curve $g(\Gamma\beta_L)=v_\phi(\beta_L;\Gamma\beta_L)/v_\phi(\beta_L;\Gamma\beta_L=\frac{1}{80})$, which is independent of β_L. Note that the value of $\Gamma\beta_L=\frac{1}{80}$ is an arbitrary but convenient choice suggested by the smallest value of $\Gamma\beta_L$ used in the simulations. We denote the normalization factor $v_\phi(\beta_L;\Gamma\beta_L=\frac{1}{80})$ as $f(\beta_L)$. Figure 2 shows

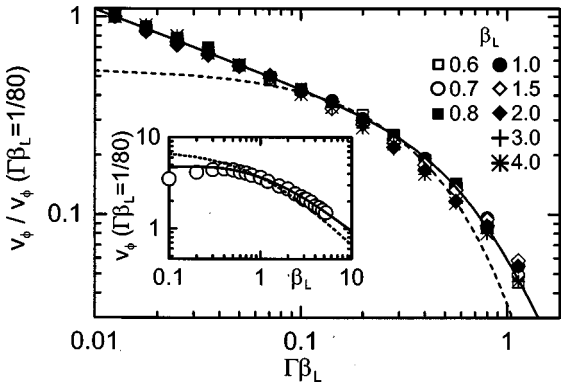

FIG. 2. Computed normalized transfer function $v_\phi/v_\phi(\beta_L;\Gamma\beta_L=\frac{1}{80})$ vs $\Gamma\beta_L$ for $\beta_c=0.5$. Solid line corresponds to Eq. (2.5), dashed line to $(4/7.3)\exp(-2.75\Gamma\beta_L)$. Inset shows $v_\phi(\beta_L;\Gamma\beta_L=\frac{1}{80})$ vs β_L; solid line corresponds to Eq. (2.6), dashed line to $7.3/(1+\beta_L)$.

the normalized curve $g(\Gamma\beta_L)$ vs $\Gamma\beta_L$ for eight values of β_L ranging from 0.6 to 4.0. As discussed, the results collapse onto a single curve. The solid line in Fig. 2 is an empirical fit to the computed values

$$g(\Gamma\beta_L)=v_\phi(\beta_L;\Gamma\beta_L)/v_\phi(\beta_L;\Gamma\beta_L=1/80)$$
$$=[(80\Gamma\beta_L)^{0.4}+0.35(4\Gamma\beta_L)^{2.5}]^{-1}. \tag{2.5}$$

For $\Gamma\beta_L<0.2$, Eq. (2.5) can be approximated as $g(\Gamma\beta_L)\approx(80\Gamma\beta_L)^{-0.4}$. The inset of Fig. 2 shows $f(\beta_L)$ vs β_L for the fixed value $\Gamma\beta_L=1/80$ for $0.1\leq\beta_L\leq5.2$. For $\beta_L\gtrsim0.5$, the range of experimental interest, one can fit the transfer function with the expression

$$f(\beta_L)=v_\phi(\beta_L;\Gamma\beta_L=1/80)=7.3\beta_L^{0.15}/(1+\beta_L), \tag{2.6}$$

shown as a solid line in the inset. With the aid of the factorization $v_\phi=f(\beta_L)g(\Gamma\beta_L)$, these two curves, or Eqs. (2.5) and (2.6), enable one to calculate v_ϕ immediately for any value of β_L and $\Gamma\beta_L$ within the specified ranges. Note that v_ϕ, calculated numerically, decreases for $\beta_L\lesssim0.4$. This decrease is not reproduced by Eq. (2.6). Furthermore, since the SQUID will no longer function when Γ becomes much greater than unity, the range of validity of Eqs. (2.5) and (2.6) is restricted to $\Gamma\lesssim1$, that is $\Gamma\beta_L\lesssim\beta_L$. Note that in the range $\Gamma\beta_L<0.2$, where $g(\Gamma\beta_L)\approx(80\Gamma\beta_L)^{-0.4}$, we can also factorize v_ϕ as $\hat{f}(\beta_L)\hat{g}(\Gamma)$, where $\hat{f}(\beta_L)=f(\beta_L)/\beta_L^{0.4}$ and $\hat{g}(\beta_L)=(80\Gamma)^{-0.4}$. Thus for $\Gamma\beta_L<0.2$ the variables β_L and $\Gamma\beta_L$ are not the only possible choices for factorization. In order to confirm the validity of Eq. (2.6) for larger values of β_L, we also calculated v_ϕ for $\beta_L=20$ and $\Gamma\beta_L=1/80$. The numerical result is $v_\phi\approx0.6$ whereas Eq. (2.6) yields 0.55.

It is of interest to compare our results with the expression of Enpuku, Doi *et al.* (1995) and Enpuku, Tokita *et al.* (1995),

$$v_\phi=\frac{4}{1+\beta_L}\exp\left(-\frac{3.5\pi^2(\delta\Phi_n)^2}{\Phi_0^2}\right)$$
$$=\frac{4}{1+\beta_L}\exp(-2.75\Gamma\beta_L), \tag{2.7}$$

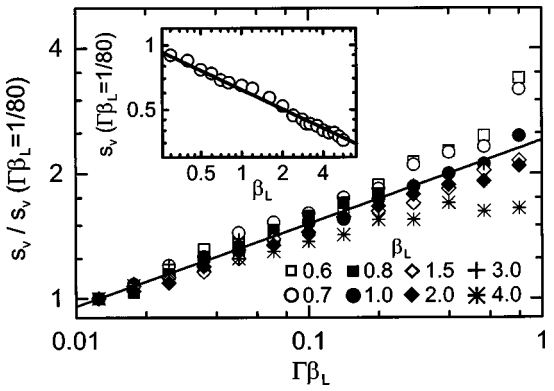

FIG. 3. Computed normalized voltage noise power $s_v/s_v(\beta_L;\Gamma\beta_L=\frac{1}{80})$, vs $\Gamma\beta_L$ for $\beta_c=0.5$. Solid line shows $s_v(\beta_L;\Gamma\beta_L)/s_v(\beta_L;\Gamma\beta_L=\frac{1}{80})=(80\Gamma\beta_L)^{0.2}$. Inset shows $s_v(\beta_L;\Gamma\beta_L=\frac{1}{80})$ vs β_L, solid line is $s_v(\beta_L;\Gamma\beta_L=\frac{1}{80})=0.62\beta_L^{-0.3}$.

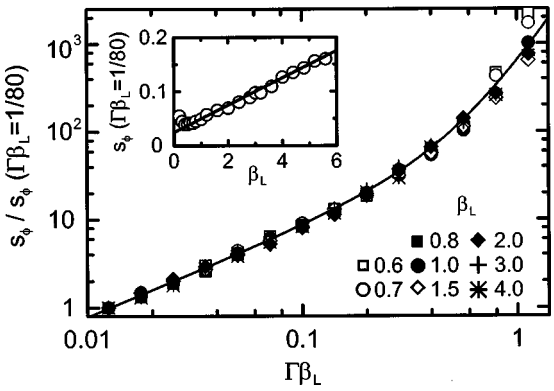

FIG. 4. Computed normalized flux noise power $s_\phi/s_\phi(\beta_L;\Gamma\beta_L=\frac{1}{80})$ vs $\Gamma\beta_L$ for $\beta_c=0.5$. Solid line corresponds to Eq. (2.8). Inset shows $s_\phi(\beta_L;\Gamma\beta_L=\frac{1}{80})$ vs β_L. Solid line corresponds to Eq. (2.9).

where $(\delta\Phi_n)^2=k_BTL$ is the mean square flux noise. This expression also factorizes into two terms, which depend on β_L and $\Gamma\beta_L$, respectively. Equation (2.7) agrees well with our results for intermediate values of β_L and $\Gamma\beta_L$, but underestimates v_ϕ outside this region. For example, for $\beta_L=1$ the agreement is better than 5% for $0.09<\Gamma\beta_L<0.35$. The dashed line in Fig. 2 is given by $(4/7.3)\exp(-2.75\Gamma\beta_L)$, and the dashed line in the inset of Fig. 2 corresponds to $7.3/(1+\beta_L)$. The prefactor $(\frac{7.3}{4})$ was chosen to obtain the best agreement with our simulations for $\beta_L=1$. Similar results have been found by Koch (1994), Keene *et al.* (1995), and Foglietti *et al.* (1995).

We turn now to the voltage noise at frequencies well below the Josephson frequency, where its spectral density is white. Using Eqs. (2.1)–(2.4) we compute the Fourier transform of the time-varying voltage across the SQUID and hence the dimensionless power spectrum $s_V(f)=2\pi S_V(f)/I_0R\Phi_0$. We set $\Phi=\Phi_0/4$, vary the bias current so that V_Φ takes its maximum value and calculate $S_V(f)$. In Fig. 3 we plot $s_v(\beta_L;\Gamma\beta_L)/s_v(\beta_L;\Gamma\beta_L=\frac{1}{80})$ vs $\Gamma\beta_L$ for eight values of β_L. For a given value of β_L, the noise power increases with $\Gamma\beta_L$. However, the overall variation in $s_v(\beta_L;\Gamma\beta_L)$ is weak: within a factor of 2, $s_v\approx1$ or $S_V\approx I_0R\Phi_0/2\pi$. In contrast to the transfer function (Fig. 2), there is no universal behavior for the noise power, although roughly speaking, s_v scales as $(80\Gamma\beta_L)^{0.2}$ (line in Fig. 3). The inset to Fig. 3 shows $s_v(\beta_L;\Gamma\beta=\frac{1}{80})$ vs β_L. For fixed $\Gamma\beta_L$, β_L is proportional to I_0/T; the decrease in noise with increasing β_L thus reflects either the decrease in temperature if I_0 is fixed or the increase in I_0 if T is fixed. The line is a fit to $s_v(\beta_L;\Gamma\beta_L=\frac{1}{80})=0.62\beta_L^{-0.3}$; within the range $0.2<\beta_L<5.2$, we can approximate $s_v\approx1.5\beta_L^{-0.3}(\Gamma\beta_L)^{0.2}$. For $\Gamma=0.05$ and $\beta_L=1$ we find $s_v=0.82$, in excellent agreement with the result of Tesche and Clarke (1977), $S_V\approx16k_BTR$. (To make the comparison, note that $s_v=(2\pi/I_0R\Phi_0)16k_BTR=16\Gamma=0.8$.)

We find the flux noise of the dc SQUID from the relation $S_\Phi(f)=S_V(f)/V_\Phi^2$ or $s_\phi(f)=s_v/v_\phi^2=(2\pi I_0R/\Phi_0^3)S_\Phi(f)$. Figure 4 shows $s_\phi(\beta_L;\Gamma\beta_L)/s_\phi(\beta_L;\Gamma\beta_L=\frac{1}{80})$ vs $\Gamma\beta_L$, obtained from the results in Figs. 2 and 3. The computed data very nearly follow a universal curve, because of the universal, strong dependence of v_ϕ on $\Gamma\beta_L$ and the weak dependence of s_v. For $0.01<\Gamma\beta_L<1$ we can fit the curve reasonably well by the expression

$$s_\phi(\beta_L;\Gamma\beta_L)/s_\phi(\beta_L;\Gamma\beta_L=\tfrac{1}{80}) = 0.8[80\Gamma\beta_L+(1+4\Gamma\beta_L)^{4.1}-1]. \quad (2.8)$$

For $\Gamma\beta_L<0.1$, $s_\phi(\beta_L;\Gamma\beta_L)/s_\phi(\beta_L;\Gamma\beta_L=\frac{1}{80})$ reduces to approximately $80\Gamma\beta_L$, while for larger values of $\Gamma\beta_L$ it increases rapidly because of the rapid drop in v_ϕ. In the inset to Fig. 4 we plot $s_\phi(\beta_L;\Gamma\beta_L=\frac{1}{80})$ vs β_L, together with the fitted curve

$$s_\phi(\beta_L;\Gamma\beta_L=\tfrac{1}{80})=(1+\beta_L)/40. \quad (2.9)$$

Note that the increase of $s_\phi(\beta_L;\Gamma\beta_L=\frac{1}{80})$ for $\beta_L\lesssim0.5$, which arises from the decrease of $v_\phi(\beta_L;\Gamma\beta_L=\frac{1}{80})$, is not reproduced by Eq. (2.9). Thus, for the range $\Gamma\beta_L<0.1$ and $\beta_L\gtrsim0.5$, we find $s_\phi\approx2(1+\beta_L)\Gamma\beta_L$ or $S_\Phi\approx4(1+\beta_L)\Phi_0k_BTL/I_0R$. For $\beta_L=1$, this result becomes $16k_BTL^2/R$, in excellent agreement with the value of Tesche and Clarke (1977). As an example, from Fig. 4 for $\beta_L\Gamma=0.1$ and $\beta_L=1$ we find $s_\phi\approx0.4$; with $I_0R=200$ μV, this value corresponds to $S_\Phi\approx0.6\times10^{-12}\Phi_0^2$ Hz^{-1}.

Finally, we derive the noise energy $\varepsilon(f)=S_\Phi(f)/2L$; in dimensionless units, $e=\varepsilon I_0R/2\Phi_0k_BT=s_\phi/2\Gamma\beta_L$. Figure 5 shows $e(\beta_L;\Gamma\beta)/e(\beta_L;\Gamma\beta_L=\frac{1}{80})$ vs $\Gamma\beta_L$, obtained from the results in Figs. 2 and 3. For $\Gamma\beta_L<0.2$, the reduced noise energy is almost constant, while for higher values of $\Gamma\beta_L$ it increases rapidly. The rapid increase in noise energy arises from the rapid degradation of the transfer function over the same values of $\Gamma\beta_L$ (Fig. 2). In the inset of Fig. 5 we plot $e(\Gamma\beta_L=1/80)$ as a function of β_L: the dependence is linear for $\beta_L\gtrsim0.5$, and to a good approximation $e(\beta_L;\Gamma\beta_L=1/80)\approx(1+\beta_L)$ for $\beta_L\gtrsim0.5$. For a SQUID with $\Gamma=0.05$ and $\beta_L=1$, Tesche and Clarke (1977) find $\varepsilon\approx9k_BTL/R$, corresponding to $e=\varepsilon I_0R/2\Phi_0k_BT\approx9LI_0/2\Phi_0=9\beta_L/4=2.25$. From Fig. 5, we predict $e\approx2$, in good agreement,

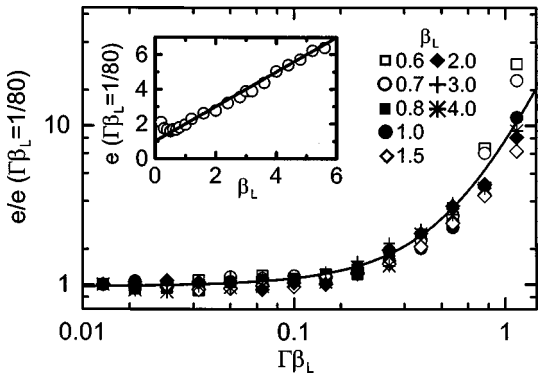

FIG. 5. Computed normalized energy resolution $e/e(\beta_L;\Gamma\beta_L=\frac{1}{80})$ vs $\Gamma\beta_L$ for $\beta_c=0.5$. Solid line corresponds to Eq. (2.8) divided by $(80\Gamma\beta_L)$. Inset shows $e(\beta_L;\Gamma\beta_L=\frac{1}{80})$ vs β_L, solid line is the function $(1+\beta_L)$.

and observe that this value remains valid for $\Gamma\beta_L<0.2$. More generally, for $\Gamma\beta_L<0.2$ and for an arbitrary value of β_L we find $e\approx(1+\beta_L)$ or $\varepsilon\approx 2(1+\beta_L)\Phi_0 k_B T/I_0 R$.

This concludes our description of the signal and noise theory for the dc SQUID. The results dictate the range of parameters required to achieve near optimal performance. Low-T_c SQUIDs are usually optimized under the constraint $I_0R^2=$constant (Tesche and Clarke, 1977), in order to keep β_c fixed. For a given value of L we then have $I_0\propto\beta_L$ and $R\propto I_0^{-1/2}$, so that $I_0R\propto\beta_L^{1/2}$. Since $e\propto(1+\beta_L)$ we find $\varepsilon\propto(1+\beta_L)\beta_L^{1/2}$, which has a minimum at $\beta_L=1$. The situation for high-T_c SQUIDs is more complicated. One way to optimize the SQUID is to vary the junction width on a given substrate. We then have $I_0R=$constant, and the dependence of ε on β_L can be scaled from the plots in Fig. 5; in this case, the minimum is at $\beta_L\approx 0.5$. However, we again emphasize that this value is at the lower end of the validity of our equations. A discussion of smaller values would be purely academic, since one generally couples the SQUID to a pickup loop with an inductance that is much higher than the SQUID inductance L (Sec. VI). Thus, to reduce the inductance mismatch, there is a strong incentive to make L as high as possible. As a result, values of $\beta_L\ll 1$ would require values of Γ that are outside the validity of our equations. An alternative philosophy is to fix the junction area and to vary the critical current, for example, by changing the barrier thickness. Since for many high-T_c junctions $I_0R\propto j_c^{1/2}$ (Sec. IV), this approach leads to $I_0R^2=$constant as for low-T_c SQUIDs, so that $\beta_L=1$ is the optimum value.

Figure 5 shows clearly that the reduced noise energy increases rapidly once $\Gamma\beta_L=L/L_{th}$ is raised above about 0.15; for $T=77$ K, this constraint implies $L\lesssim 50$ pH. However, one can use higher inductances either by adding a damping resistor across the SQUID loop (Enpuku, Sueoka *et al.*, 1985; Enpuku, Muta *et al.*, 1985; Enpuku, *et al.*, 1993; Enpuku, 1993) and/or a third Josephson junction (Enpuku, 1993; Enpuku *et al.*, 1994; Enpuku, Doi *et al.*, 1995). It is shown that with these additional circuit elements one may increase the SQUID inductance up to 500 pH. Recently, high-T_c SQUIDs with integrated damping resistors have been studied by Kang *et al.* (1997), and three-junction SQUIDs have been investigated by Schultze, Ijsselsteijn *et al.* (1997). In both cases, an enhanced voltage modulation was observed. However, for the three-junction SQUID, large modulation was obtained only over a few periods and the authors concluded that this SQUID has no advantage over the conventional SQUID.

Finally, the fact that ε scales as $1/I_0R$ emphasizes the need to develop junction technologies with the largest possible value of I_0R. In particular, one would like a type of junction in which I_0 and R can be varied independently. For example, for $L=40$ pH, the requirement $\beta_L=1$ leads to $I_0=25\,\mu$A; increasing I_0R solely by increasing I_0 will not lead to significantly enhanced performance.

D. rf SQUID: Overview

The rf SQUID (Mercereau, 1970; Nisenoff, 1970; Zimmerman *et al.*, 1970) consists of a single Josephson junction integrated into a superconducting loop that is inductively coupled to the inductance L_T of an LC-resonant (tank) circuit [inset Fig. 6(b)]. The tank circuit is driven by an rf current, and the resultant rf voltage is periodic in the flux applied to the SQUID with period Φ_0. Detailed reviews have been written by many authors (for example, Jackel and Buhrman, 1975; Ehnholm, 1977; Likharev and Ulrich, 1978; Likharev, 1986; Ryhänen *et al.*, 1989; Clarke, 1996).

The total flux Φ_T in the SQUID is related to the applied flux Φ by

$$\Phi_T=\Phi-LI_0\sin(2\pi\Phi_T/\Phi_0). \tag{2.10}$$

We see immediately that Eq. (2.10) can exhibit two distinct kinds of behavior [Fig. 6(a)]. For $\beta_L'=2\pi LI_0/\Phi_0<1$, the slope $d\Phi_T/d\Phi=[1+\beta_L'\cos(2\pi\Phi_T/\Phi_0)]^{-1}$ is everywhere positive and the Φ_T vs Φ curve is nonhysteretic. On the other hand, for $\beta_L'>1$, there are regions in which $d\Phi_T/d\Phi$ is positive, negative, or divergent so that the Φ_T vs Φ curve becomes hysteretic. Radio frequency superconducting quantum interference devices have been operated in both modes. In the hysteretic mode the SQUID makes transitions between quantum states and dissipates energy at a rate that is periodic in Φ. This periodic dissipation in turn modulates the quality factor Q of the tank circuit, so that when it is driven on resonance with a current of constant amplitude the rf voltage is periodic in Φ. In the case $\beta_L'<1$, the nondissipative mode, the SQUID behaves as a parametric inductance, modulating the effective inductance and hence the resonant frequency of the tank circuit as the flux is varied. Thus when the tank circuit is driven at constant frequency, the variations in its resonant frequency cause the rf voltage to be periodic in Φ.

Historically, it appears that most low-T_c rf SQUIDs were operated in the hysteretic mode, although as we shall see, there are advantages to the nonhysteretic mode. However, the theory of noise in the nondissipa-

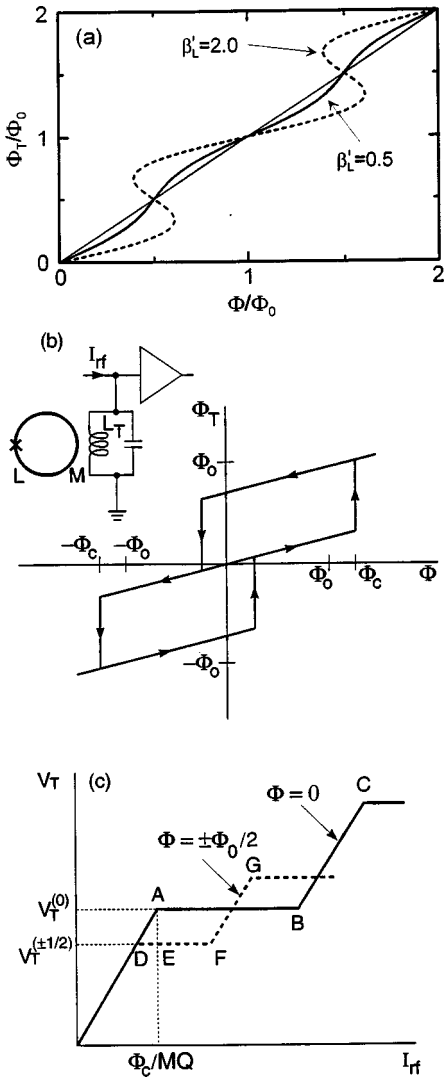

FIG. 6. The rf SQUID: (a) Normalized total flux Φ_T/Φ_0 vs normalized applied flux Φ/Φ_0 for $\beta_L'=0.5,2$. (b) Total flux Φ_T vs applied flux Φ for rf SQUID with $LI_0/\Phi_0=\frac{5}{4}$, showing transitions between quantum states in absence of thermal noise as Φ is increased and subsequently decreased. Inset shows rf SQUID inductively coupled to the inductor of a resonant circuit. (c) Peak rf voltage V_T across tank circuit vs peak rf current I_{rf} in absence of thermal noise for $\Phi=0$ (solid line) and $\Phi=\pm\Phi_0/2$ (dashed line).

tive regime was worked out in the late 1970s, just as dc SQUIDs began largely to replace rf SQUIDs. As a result, the importance of the nonhysteretic rf SQUID was not widely exploited experimentally. The advent of 77 K operation has changed this situation dramatically, largely due to the systematic experimental effort of the group at Jülich and the very recent theoretical work of Chesca (1998). In the following two sections we briefly outline the theory of the dissipative and nondissipative rf SQUIDs.

E. rf SQUID: Hysteretic mode

For the case $\beta_L'>1$, the unstable nature of the Φ_T vs Φ curve in Fig. 6(a) causes the SQUID to make transitions between stable quantum states as Φ is changed [Fig. 6(b)]. For example, when Φ is increased from 0, there is a transition from the $k=0$ flux state to the $k=1$ state at a critical flux (neglecting fluctuations) $\Phi_c=LI_0$. In rf operation, a current $I_{rf}\sin\omega_{rf}t$ is applied to the resonant circuit. The peak voltage V_T across the resonant circuit increases linearly with I_{rf} until, for $\Phi=0$, $I_{rf}=\Phi_c/MQ$, at which value

$$V_T^{(0)}=\omega_{rf}L_T\Phi_c/M, \tag{2.11}$$

where $M=\kappa(LL_T)^{1/2}$. At this point [A in Fig. 6(c)] the SQUID makes a transition to the $k=+1$ or -1 state. As the SQUID traverses the hysteresis loop, energy ΔE is extracted from the tank circuit. Because of this loss, the peak flux on the next half cycle is less than Φ_c, and no transition occurs. The tank circuit takes many cycles to recover sufficient energy to induce a further transition, which may be into either the $k=+1$ or -1 states. If we now increase I_{rf}, transitions are induced at the same values of I_T and V_T but, because energy is supplied at a higher rate, the stored energy builds up more rapidly after each energy loss ΔE, and transitions occur more frequently. At B, a transition is induced on each positive and negative rf peak, and a further increase in I_{rf} produces the "riser" BC. At C, transitions from the $k=\pm1$ states to the $k=\pm2$ states occur, and a second step begins. A plot of the peak values $V_T^{(0)}$ vs I_{rf} produces the "steps and risers" shown in Fig. 6(c).

If we now apply an external flux $\Phi_0/2$, the hysteresis loops in Fig. 6(b) are shifted by this amount, and one finds

$$V_T^{(\pm 1/2)}=\omega_{rf}L_T(\Phi_c-\Phi_0/2)/M. \tag{2.12}$$

As I_{rf} is increased, this voltage remains constant until the point F, at which the SQUID traverses the hysteresis loop corresponding to the $k=0\leftrightarrow k=+1$ transitions once per rf cycle. A further increase in I_{rf} produces the riser FG; at G, corresponding to a peak rf flux $-(\Phi_c+\Phi_0/2)$, transitions $k=0\leftrightarrow k=-1$ begin. Thus an applied flux other than $n\Phi_0$ (n is an integer) causes the step AB to split as shown in Fig. 6(c).

The model outlined above enables us to calculate the transfer function at values of I_{rf} that maintain the SQUID biased on a step: the change in V_T as we increase Φ from 0 to $\Phi_0/2$ is $V_T^{(0)}-V_T^{(\pm 1/2)}=\omega_{rf}L_T\Phi_0/2M$, so that for small changes in flux in the range $0<\Phi<\Phi_0/2$ we find $V_\Phi=\omega_{rf}L_T/M$. At first sight, this result seems to imply that V_Φ can be increased indefinitely by reducing κ. This is not the case, since one must ensure that the point F in Fig. 6(c) lies to the right of E, that is, DF must exceed DE. To calculate DF we note that the power dissipated in the SQUID is zero at D and approximately $I_0\Phi_0\omega_{rf}/2\pi$ at F, since the energy dissipated per rf cycle is approximately $I_0\Phi_0$ for a device with $LI_0\approx\Phi_0$. Thus, taking account of the fact that the rf currents and voltages are peak values, we find $(I_{rf}^{(F)}-I_{rf}^{(D)})=V_T^{(\pm 1/2)}/2\approx I_0\Phi_0\omega_{rf}/2\pi$. Furthermore, we can easily see that $I_{rf}^{(E)}-I_{rf}^{(D)}=\Phi_0/2MQ$. Assuming LI_0

$\approx\Phi_0$ and using Eq. (2.12), we can write the requirement that DF exceeds DE in the form

$$\kappa^2 Q \gtrsim \pi/4. \tag{2.13}$$

Taking $\kappa\approx 1/Q^{1/2}$, we find that the expression for V_Φ becomes

$$V_\Phi \approx \omega_{\rm rf}(QL_T/L)^{1/2} \approx \omega_{\rm rf}(L_T/L)^{1/2}/\kappa. \tag{2.14}$$

We note that V_Φ scales with $\omega_{\rm rf}$ and as $L^{-1/2}$.

A detailed theory has been developed for noise in the hysteretic rf SQUID operating at liquid helium temperatures (Kurkijärvi, 1972, 1973; Jackel and Buhrman, 1975; Giffard *et al.*, 1976; Ehnholm, 1977; Hollenhorst and Giffard, 1980; Ryhänen *et al.*, 1989). Although in a noise-free model the steps are flat, thermal noise causes them to tilt to a slope η. In addition, thermal noise induces voltage noise on the step arising from fluctuations in the value of flux at which transitions between flux states occur. The corresponding intrinsic flux noise of the SQUID is (Kurkijärvi, 1973)

$$S_\Phi^i(f) \approx \frac{(LI_0)^2}{\omega_{\rm rf}}\left(\frac{2\pi k_B T}{I_0\Phi_0}\right)^{4/3}. \tag{2.15}$$

In the case of helium-cooled rf SQUIDs in which the tank circuit voltage is detected with a room-temperature amplifier, there is a second, extrinsic contribution to the flux noise. This arises in part because the noise temperature of the rf amplifier is above the bath temperature and in part because a fraction of the coaxial line connecting the tank circuit to the amplifier is at room temperature. We can represent these two contributions by an effective noise temperature $T_a^{\rm eff}$, enabling us to write the noise energy due to intrinsic and extrinsic noise sources as (Jackel and Buhrman, 1975; Giffard *et al.*, 1976)

$$\varepsilon \approx \frac{LI_0^2}{2\omega_{\rm rf}}\left(\frac{2\pi k_B T}{I_0\Phi_0}\right)^{4/3} + \frac{2\pi\eta k_B T_a^{\rm eff}}{\omega_{\rm rf}}. \tag{2.16}$$

Equation (2.16) makes two important points. First, ε scales as $1/\omega_{\rm rf}$, up to a limiting value R/L. Second, for low-T_c SQUIDs, the extrinsic noise energy generally dominates the intrinsic noise: if we take the representative values $T=4$ K, $\Gamma=0.1$, $\eta=0.2$, $\beta_L'=2\pi$ and $T_a^{\rm eff}=100$ K, we find that the extrinsic noise energy is about 20 times the intrinsic value. Thus, although we should be wary of extrapolating these results to 77 K where, to our knowledge, there are no simulations or calculations, the overall noise energy of the hysteretic rf SQUID should not increase very much as we raise the temperature from 4 K to 77 K. This result is in contrast to the dc SQUID, which for properly designed circuitry is limited largely by intrinsic noise at 4.2 K, so that the overall noise energy will increase significantly as the temperature is raised to 77 K.

F. rf SQUID: Nonhysteretic mode

To give an approximate account of the operation of the nonhysteretic rf SQUID we follow the description of Hansma (1973), which is valid in the limits $\beta_L' \ll 1$, where the total magnetic flux threading the SQUID is nearly equal to the applied flux, and $\omega_{\rm rf} \ll I_0 R/\Phi_0$. More general treatments are given, for example, by Jackel and Buhrman (1975), Erné *et al.* (1976), Danilov *et al.* (1980), Likharev (1986), and Ryhänen *et al.* (1989).

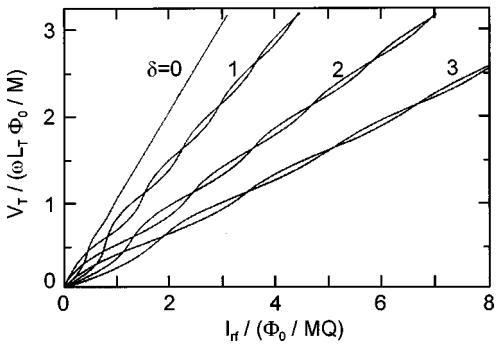

FIG. 7. Tank circuit voltage V_T vs rf drive current I_T for four values of the tuning parameter $\delta=[2(\omega_{\rm rf}-\omega_0)/\omega_0]Q$ and for $\Phi=0,\Phi_0/2$. Curves plotted for $\kappa^2 Q\beta_L'=\pi/2$ (Hansma, 1973).

In the presence of a static flux Φ and rf flux $\Phi_{\rm rf}\sin\omega_{\rm rf}t$, the current in the SQUID loop is

$$I = I_0\sin[(2\pi/\Phi_0)(\Phi+\Phi_{\rm rf}\sin\omega_{\rm rf}t)]$$
$$(2\pi LI_0 \ll \Phi_0). \tag{2.17}$$

The oscillating component of this current induces a current $I_i=-(M/Z)dI/dt$ into the tank circuit, where $Z=R_T+i[\omega_{\rm rf}(L_T-M^2/L)-1/\omega_{\rm rf}C_T]$ is its impedance; the inductance of the tank circuit is modified by the contribution $-M^2/L$ from the SQUID. If we assume that the rf frequency is near resonance and that Q is reasonably large, we can neglect all frequency components other than the fundamental. Expanding the right-hand side of Eq. (2.17) in terms of the Bessel function J_1, we find the induced current

$$I_i = \frac{2\kappa^2 QLI_0}{M(1+\delta^2)^{1/2}}\cos\left(\frac{2\pi\Phi}{\Phi_0}\right)J_1\left(\frac{2\pi\Phi_{\rm rf}}{\Phi_0}\right)\sin(\omega_{\rm rf}t-\theta). \tag{2.18}$$

Here, $\delta=2[(\omega_{\rm rf}-\omega_0)/\omega_0]Q$ is the normalized difference between the rf frequency and the tank-circuit resonant frequency ω_0, and $\theta=\tan^{-1}\delta+\pi/2$.

The rf flux applied to the SQUID is $MI_T\sin\omega_{\rm rf}t$, where I_T is the amplitude of the total current in the inductor which, in addition to the induced current given by Eq. (2.18), also contains a component of amplitude $QI_{\rm rf}/(1+\delta^2)^{1/2}$ produced by the external rf current. From Eq. (2.18) we see that the total current leads the induced current by a phase angle θ. The amplitudes of the total and external rf currents are related by

$$I_{\rm rf} = \frac{(1+\delta^2)^{1/2}}{Q}\left\{\left[\frac{2\kappa^2 QLI_0}{(1+\delta^2)^{1/2}M}\cos\left(\frac{2\pi\Phi}{\Phi_0}\right)\right.\right.$$
$$\left.\left.\times J_1\left(\frac{2\pi MI_T}{\Phi_0}\right)+I_T\cos\theta\right]^2+I_T^2\sin^2\theta\right\}^{1/2}. \tag{2.19}$$

Figure 7 shows plots of V_T vs $I_{\rm rf}$ for $\Phi=0$ and $\Phi_0/2$ for

four values of the tuning parameter δ. We see that the response is insensitive to the flux in the SQUID for $\delta=0$; thus the tank circuit for the nonhysteretic SQUID is operated off resonance. For a given value of δ, the response shows a series of oscillations as $I_{\rm rf}$ is increased, arising from the oscillations of the Bessel function. The maximum peak-to-peak modulation of V_T at fixed $I_{\rm rf}$ is of the order of $2\kappa^2 Q L I_0(\omega_{\rm rf} L_T/M)$, so that

$$V_\Phi \approx (2/\pi)\kappa^2 Q \beta_L' \omega_{\rm rf} L_T/M \approx (2/\pi)(\kappa^2 Q \beta_L')\omega_{\rm rf}(L_T/L)^{1/2}/\kappa. \quad (2.20)$$

This transfer function exceeds that of the hysteretic rf SQUID [Eq. (2.14)] by a factor of order $\kappa^2 Q\beta_L'$, which can be made larger than unity for the nonhysteretic case by choosing $\kappa^2 Q \gg 1$.

The intrinsic noise energy of low-T_c, nonhysteretic, rf SQUIDs has been calculated by several authors, and is approximately $3k_BT/(\beta_L')^2\omega_c$ (Likharev, 1986), where the drive frequency is set equal to $\omega_c = R/L$, the cutoff frequency of the SQUID. A noise energy as low as $20\hbar$ has been achieved by Kuzmin *et al.* (1985).

As a preamble to the discussion of nonhysteretic high-T_c SQUIDs, we note that Falco and Parker (1975) successfully observed flux modulation in an rf SQUID at 2 K with a supercurrent as low as 50 nA. The corresponding value of the noise parameter $\Gamma = 2\pi k_B T/I_0\Phi_0$ was about 1.7; at this high value, they were unable to observe any trace of supercurrent in an isolated junction. Thus it is evident that one can expect to operate an rf SQUID with substantially higher values of Γ than is the case for the dc SQUID (see Sec. II.C). Although this important fact has been known experimentally for many years, only very recently has the work of Chesca (1998) provided a quantitative explanation. In contrast to previous theories of the rf SQUID in which one regards thermal noise as a perturbation on a noise-free system, Chesca solves the Smoluchowski equation for the situation in which thermal fluctuations dominate. Thus both the signal produced by the SQUID and the noise are found in a unified calculation that yields analytical results. For the case $\beta_L' \leqslant 1$ and $\omega_{\rm rf} \ll R/L$, Chesca finds

$$\varepsilon \approx 3\Gamma^2\left(1+\frac{T_k}{T}\frac{1}{\kappa^2 Q}\frac{R/L}{\omega_{\rm rf}}\right)\frac{\exp(L/L_{\rm th}')}{L/L_{\rm th}'}\frac{k_B T L_{\rm th}'}{R}. \quad (2.21)$$

Here, $L_{\rm th}' = (\Phi_0/2\pi)^2/k_BT$ and T_k is the effective noise temperature of the tank circuit, including any contribution from the preamplifier. If one assumes $L/L_{\rm th}' = \beta_L'\Gamma \ll 1$ and that $\kappa^2 Q$ can be made sufficiently large that $(T_k/T)(R/\omega_{\rm rf}L)/\kappa^2 Q \ll 1$, Eq. (2.21) can be written in the alternative forms

$$\varepsilon \approx 3k_BT/(\beta_L')^2(R/L) \quad (2.22a)$$

$$\approx 3k_BT\Phi_0/2\pi\beta_L' I_0 R. \quad (2.22b)$$

Interestingly, Eq. (2.22a) is identical to the result found perturbatively for the rf SQUID for low values of Γ. The value for ε in Eq. (2.22b) is equal to $3/4\pi\beta_L'(1+\beta_L)$ times that for the dc SQUID in the limit $\Gamma\beta_L < 0.2$.

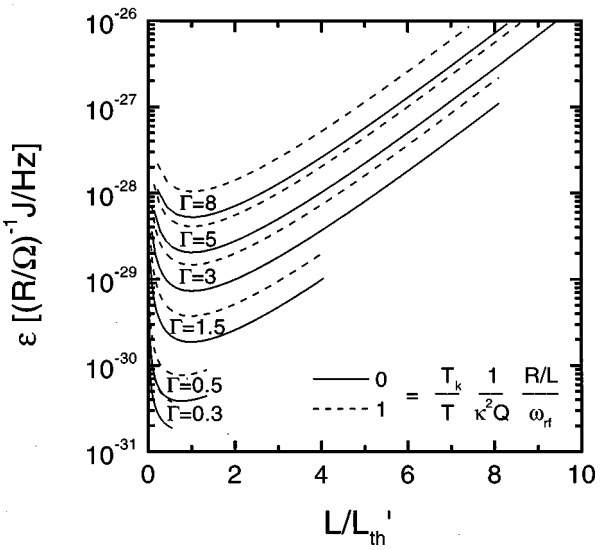

FIG. 8. ε vs $L/L_{\rm th}'$ for nonhysteretic rf SQUID at 77 K (Chesca, 1998).

Equation (2.21) is plotted in Fig. 8 for the two cases $(T_K/T)(1/\kappa^2 Q)(R/\omega L_{\rm rf}) = 0$ and 1, and for six values of Γ. One concludes from these plots that the optimal values are (Chesca, 1998)

$$\beta_L' = 1 \quad \text{if } \Gamma \leqslant 1, \quad (2.23a)$$

$$\beta_L' = 1/\Gamma \quad \text{if } \Gamma \geqslant 1. \quad (2.23b)$$

We note that for the lowest value of Γ plotted, 0.3, the curve is cut off at $\beta_L'\Gamma = L/L_{\rm th}' = 0.55$, at which value the noise energy approaches $10^{-31}\,{\rm JHz}^{-1}$ for $R = 1\,\Omega$. For the case $\Gamma \geqslant 1$, the noise energy is higher and the optimal SQUID inductance is approximately $L_{\rm th}' \approx 100\,{\rm pH}$ at 77 K. Again, this value is about two times higher than for the dc SQUID at 77 K. One consequence of this result is that one can expect to use rf SQUIDs with an area about two times higher than dc SQUIDs.

III. THIN FILMS: FABRICATION AND 1/*f* NOISE

In this section, we discuss issues related to the fabrication of epitaxial thin films for high-T_c SQUIDs and flux-coupling input circuits. Key requirements for the films are high crystalline quality and either elimination or efficient pinning of flux vortices, in order to achieve both good electrical transport properties and low levels of $1/f$ noise. For some structures, for example, multiturn flux transformers (Sec. VI.C) or multiloop magnetometers (Sec. VI.D), one requires two or more superconducting films separated by an insulating layer. Hence all layers must be of high crystalline quality. To achieve heteroepitaxial growth of such multilayer structures, it is essential that the various films have comparable lattice constants and thermal-expansion coefficients, that they are chemically compatible at the relatively high deposition temperatures, typically 700–800 °C, and that they can be deposited with sufficiently smooth surfaces to al-

low subsequent layers to grow with high structural and electrical integrity and without electrical shorts between them. Moreover, one must be able to pattern the films without introducing a significant deterioration in their properties.

A. Materials

Despite the wide variety of high-T_c compounds, work on SQUIDs has been mostly restricted to YBCO. This is largely because only YBCO films with their *c* axis normal to the substrate (''*c*-axis films'') have been shown to have sufficiently strong flux pinning at 77 K to ensure both high critical-current densities in the *ab* plane—several $10^6\,\mathrm{A\,cm^{-2}}$—and acceptably low levels of $1/f$ noise. Furthermore, because of the worldwide effort that has been focused on YBCO, its physical properties and growth mechanisms are well understood and high-quality thin films can be grown *in situ* by a variety of deposition techniques on a number of substrate materials. As a result, it seems unlikely that YBCO will be supplanted as the superconductor of choice, although $NdBa_2Cu_3O_{7-x}$ is worthy of consideration because of its superior stability.

There are a number of substrates suitable for growing high-quality YBCO films (for a discussion see Scheel *et al.*, 1991; Somekh and Barber, 1992; Braginski, 1993, 1996; Wellstood *et al.*, 1994; Phillips, 1996). To fabricate low-noise SQUIDs, one usually chooses substrates that are closely lattice matched to YBCO and have comparable thermal expansion coefficients, notably (100) $SrTiO_3$, $LaAlO_3$, and $NdGaO_3$, thus allowing the YBCO films to grow with a high degree of crystallographic perfection. In addition, MgO substrates are frequently used since they are relatively inexpensive and allow one to grow YBCO films with acceptable electrical properties.

B. Thin-film deposition

Among the many different techniques used to deposit YBCO *in situ* (for reviews, see Somekh and Barber, 1992; Phillips, 1993; Wellstood *et al.*, 1994), those most commonly applied to SQUID fabrication are pulsed laser deposition and sputtering, although a few groups have successfully used coevaporation. All of these techniques produce smooth YBCO films with excellent electrical properties. Typical YBCO films, 100–300 nm thick, grown on lattice-matched substrates such as $SrTiO_3$ (STO), have critical current densities at 77 K of $(2-5)\times10^6\,\mathrm{A\,cm^{-2}}$. The surface roughness of the best films, usually determined by atomic force microscopy, is below 10 nm and the half-width of the x-ray rocking curve (005 line) is typically 0.1–0.3°. The critical-current densities in such films are two orders of magnitude higher than in high-quality YBCO single crystals, indicating that a high density of defects, which provide strong pinning sites, must be present.

To deposit Ag or Au layers for contact pads, one can use thermal evaporation, electron-beam evaporation, sputtering, or ion-beam-assisted deposition, usually with the substrate at room temperature. To achieve a low metal/YBCO contact resistance ($<10^{-6}\,\Omega\,\mathrm{cm^2}$) one should deposit the metal layer either *in situ* or after only a brief exposure to air (Russek *et al.*, 1994, 1996). If the YBCO film is stored in air for any length of time or exposed to photoresist, low-energy Ar-ion-beam cleaning of the surface and/or postannealing in oxygen at 400–500 °C is necessary to achieve a low contact resistance.

C. Patterning

Patterning techniques that are well established in semiconductor and low-T_c superconductor technology are not necessarily applicable to YBCO thin films. One immediate problem is that contact of YBCO with water or water-soluble chemicals degrades the superconducting properties. Second, the use of dry-etching methods in a vacuum can lead to a significant heating of the sample and thus to oxygen loss at the edges. Given these limitations, however, a number of techniques have been used successfully to pattern YBCO films down to submicrometer dimensions without degrading their properties; for reviews, see Braginski (1993) and Wellstood *et al.* (1994).

Conventional photomasking followed by dry etching is the most widely used technique for patterning SQUID devices based on YBCO films or multilayers. However, sometimes special masks are used, especially for step-edge and ramp-edge junctions (Sec. IV) and for patterning submicrometer structures (Barth *et al.*, 1993; Schneider *et al.*, 1993; van der Harg *et al.*, 1995). Among dry-etching methods, the most commonly used is Ar-ion beam milling. To minimize damage to the YBCO, one restricts the beam energies to between 350 and 500 eV, the latter being the most common value, and the beam current density to below 1 $\mathrm{mA/cm^2}$. To reduce heating of the film, it is also important to cool the sample, either with water or particularly for submicrometer dimensions, preferably with liquid nitrogen. Alff *et al.* (1992) and Schneidewind *et al.* (1995) reported systematic studies of the effects of ion-beam voltage, current density and sample cooling on the dependence of the critical-current density on the linewidth of YBCO films. Generally, for high-quality, *c*-axis YBCO films, the edges are damaged over a length of much less than 1 μm provided the sample is water-cooled and the beam energy and current density do not exceed the values given above.

D. Multilayer processing

All multilayer structures for multiturn flux transformers, integrated magnetometers and multiloop SQUIDs involve a YBCO/insulator/YBCO trilayer. Of course, additional layers might be advantageous, for example, a superconducting ground plane. However, although integrated magnetometers with up to 15 epitaxial layers have been made (Lee *et al.*, 1991), it is difficult to maintain high crystalline quality throughout so many layers

as is required for low levels of $1/f$ noise. Thus we confine our attention to trilayers. The insulator is generally one of the substrate materials listed in Sec. III.A; the most widely used is $SrTiO_3$. As an alternative to the various insulating materials, $PrBa_2Cu_3O_{7-x}$ (PBCO) has been used in the fabrication of multiturn flux transformers (Keene *et al.*, 1993; Keene, Goodyear *et al.*, 1994).

An important issue related to the integrity of the insulator is the oxygen content of the lower YBCO film. To ensure proper oxygenation of a single YBCO film it is usually sufficient to vent the deposition chamber with 0.5–1 atm. O_2 and to cool the sample from the deposition temperature to room temperature in about 30 min. The use of this process after the deposition of a high-quality insulating layer on a YBCO film can result in a reduced transition temperature because the insulator inhibits the necessary oxygen diffusion (Humphreys *et al.*, 1991; Ludwig, Koelle *et al.*, 1995; Ockenfuß *et al.*, 1995). To reoxygenate the lower YBCO film fully, one can either increase the annealing time considerably (Ludwig, Koelle *et al.*, 1995) or perform the annealing in an oxygen plasma rather than in molecular O_2 (Yanamoto *et al.*, 1991; Humphreys *et al.*, 1991; Ockenfuß *et al.*, 1995).

In actual multilayer devices, the need to pattern each layer separately, usually with photolithographic processing, greatly complicates matters. Multiturn flux transformers, integrated magnetometers and multiloop SQUIDs all contain the basic elements of a superconducting interconnect technology: *crossovers* and *vias*. In these structures, one has to produce edges over which subsequent layers grow with high crystalline quality; in particular, the growth of YBCO over edges steeper than 45° results in grain boundaries and thus leads to a reduction in critical current (Jia *et al.*, 1991).

Various processes suitable for multilayer magnetometers were developed and have been extensively reviewed (Wellstood *et al.*, 1994; Braginski, 1996). In the process that was used to fabricate most of the low-noise multilayer magnetometers discussed in Secs. VI.C and VI.D, each layer is patterned by Ar-ion beam etching. To obtain the gently sloped edges on the lower layers, essential for the epitaxial growth of subsequent layers, one usually bakes the photoresist after development, yielding to a significant rounding of the edges (David *et al.*, 1994). The subsequent Ar-ion milling at an angle of typically 45–60° produces edges on the patterned film with ramp angles below 20°. Another key issue is the protection of the surface of the lower YBCO film, since photoresist attacks the YBCO surface thus degrading the growth of subsequent layers (Ludwig, Koelle *et al.*, 1995). To protect the YBCO, one commonly deposits an *in situ* $SrTiO_3$ layer, 20–50 nm thick, over the lower YBCO film, thus preventing its contact with photoresist (Missert *et al.*, 1993). Alternatively, a brief Ar-ion beam etch has been used to clean the surfaces before the deposition of the next layer (Keene, Goodyear *et al.*, 1994; Shen *et al.*, 1995). With these techniques, critical-current densities up to 3×10^6 A cm^{-2} for crossovers (Ludwig, Koelle *et al.*, 1995) and above 1×10^6 A cm^{-2} for vias (DiIorio, Yoshizumi, Yang, Maung, Zhang, and Power, 1993; Keene *et al.*, 1993) have been achieved in separate test structures at 77 K.

E. 1/*f* Noise in YBCO films

As we pointed out earlier, the main requirement for YBCO films used in SQUIDs is a low level of the magnetic flux noise generated by the thermally activated motion of flux vortices. To optimize the deposition process one should, in principle, measure the flux noise of each YBCO film. To our knowledge, such noise measurements have been performed only by the Berkeley group. As a simpler alternative, many groups measure the critical-current density j_c as an estimate of the flux pinning, but one must be careful in drawing conclusions about flux noise from measurements of j_c. These measurements are generally performed with strong driving forces applied by currents, and thus provide information on the pinning of the vortex lattice, that is, on the pinning *forces*. In contrast, flux noise measurements, performed in weak magnetic fields (below 10^{-4} T) reflect the dynamics of weakly interacting vortices in the superconducting sample and probe their pinning *energies*. For example, Ludwig, Koelle *et al.* (1995) found that *ex situ* YBCO/$SrTiO_3$/YBCO trilayers exhibited relatively high levels of flux noise despite the fact that similar test structures had high critical-current densities in both YBCO films. Furthermore, flux noise measurements on YBCO single crystals irradiated with protons or heavy ions indicated that protons proved to be more effective in reducing the flux noise while both produced comparable increases in critical-current density (Shaw *et al.*, 1996).

To study the flux noise in high-T_c thin films and single crystals, Ferrari *et al.* (1988, 1989, 1994) measured their fluctuating magnetization using a low-T_c, thin film SQUID in the shape of a 1-mm-square washer. The SQUID was operated in a flux-locked loop with a typical flux noise of $2\mu\Phi_0\,\mathrm{Hz}^{-1/2}$ at 1 Hz. The experiment was designed to allow tight inductive coupling between the SQUID, maintained at or near 4.2 K, and the sample, the temperature of which could be raised to above T_c. Subsequently, the availability of high-T_c SQUIDs with low levels of $1/f$ noise allowed the measurement of the flux noise of high-T_c films in liquid nitrogen more straightforwardly by mounting them directly on such a SQUID, patterned into a 0.5-mm-square washer, with a typical flux noise of $15\mu\Phi_0\,\mathrm{Hz}^{-1/2}$ at 1 Hz (Koelle *et al.*, 1993; Ludwig, Koelle *et al.*, 1995, Ludwig, Dantsker, Koelle, Kleiner, Miklich, and Clarke, 1995).

In their early work, Ferrari *et al.* (1988) found that the $1/f$ flux noise of a YBCO thin film decreases dramatically as the crystalline quality of the sample improves. For example, for a polycrystalline YBCO film they found a flux-noise power of $3\times10^{-4}\Phi_0^2$/Hz at 1 Hz and 40 K, whereas values below $10^{-10}\Phi_0^2$/Hz at 1 Hz and 77 K were obtained for high-quality epitaxial YBCO films (Shaw *et al.*, 1996). On the other hand, for YBCO single crystals, the flux-noise power at 1 Hz was more than a factor of 50 higher than the latter value, even after the

incorporation of artificial defects by proton irradiation (Shaw *et al.*, 1996). This result indicates that there must be a high density of effective, intrinsic pinning sites in high-quality (that is, magnetically quiet) epitaxial YBCO films, but unfortunately, little is known about their nature. Thus a film with low $1/f$ flux noise may have pinning sites with high activation energies or short hopping distances, or a combination of both; alternatively, the sample may simply contain fewer vortices. Studies in which various parameters controlling sample quality are systematically and independently varied are very much needed to shed light on these issues. Furthermore, the microstructural quality of patterned film edges may also be crucial, although its impact on $1/f$ noise has yet to be clarified.

The general tendencies observed for single YBCO films also apply to multilayers. Since the upper YBCO film in patterned YBCO/insulator/YBCO trilayers tends to be of poorer quality than a single YBCO film, its flux noise is generally higher. Nevertheless, Ludwig, Koelle *et al.* (1995) and Ludwig, Dantsker, Koelle, Kleiner, Miklich, and Clarke (1995) have demonstrated that a careful optimization of the multilayer fabrication process allows one to fabricate *ex situ* trilayers with low levels of $1/f$ flux noise.

Last, the level of $1/f$ noise in a given film generally increases strongly with the ambient magnetic field in which it is cooled unless its linewidth is made sufficiently narrow. These issues are deferred to Sec. IX.

IV. HIGH-T_C JOSEPHSON JUNCTIONS

The requirements for a successful junction technology include a nonhysteretic I-V characteristic, with properties close to the predictions of the RSJ model, a high I_0R product, controllable and reproducible parameters (I_0,R,C), high yield, high stability under room-temperature storage and thermal cycling, and low $1/f$ noise. These requirements are very well satisfied in low-T_c junctions by the Nb-Al_2O_3-Nb trilayer technology (Gurvitch *et al.*, 1983). Unfortunately, a comparable high-T_c technology does not yet exist, for the following reasons: First, in contrast to Nb, high-T_c materials require epitaxial growth, imposing severe constraints on the choice of materials and processing techniques. Second, again in contrast to Nb, the superconducting coherence length ξ is both short and highly anisotropic, typically 2 nm in the *ab*-plane and 0.2 nm in the *c*-axis direction. As a result, the properties of high-T_c materials are highly susceptible to structural and chemical changes on atomic length scales; in particular, the superconducting order parameter can be strongly suppressed at a superconductor-insulator interface, in turn reducing the I_0R product substantially (Deutscher and Müller, 1987). Thus the superconducting electrodes need to have perfect crystallinity, and a well-defined interface has to be achieved within a single unit cell. Third, the barrier materials are generally oxides close to a metal-insulator transition with a complex crystal structure and a strong sensitivity to defects on an atomic length scale. As a result, transport across the barrier is highly dependent on microstructural imperfections in the barrier and at its interface with the electrodes. Thus a well-defined barrier with high crystalline quality and homogeneity is required.

In the following we review those types of high-T_c junctions which have been most successfully used in SQUIDs. We divide them into two classes (Gross *et al.*, 1997): junctions with intrinsic interfaces and junctions with extrinsic interfaces. We do not discuss a third class, junctions without interfaces (weakened structures), since these have not been used widely in practical devices.

A. Junctions with intrinsic interfaces

The strong anisotropy of high-T_c superconductors with respect to both crystal structure and transport properties provides the basis for new types of weak links exploiting *intrinsic* interfaces and/or barriers. This new class of Josephson junctions, which has no analog in low-T_c superconductors, involves either the weak coupling in the *ab* plane between two superconducting grains with different orientations, the so-called grain-boundary junctions (GBJ's), or the intrinsic Josephson effect in the *c*-axis direction. While the feasibility of intrinsic Josephson junctions (Kleiner *et al.*, 1992; Kleiner and Müller, 1994) for SQUIDs has not been demonstrated, GBJ's were the basis of the first dc SQUIDs fabricated from polycrystalline thin films of YBCO (Koch *et al.*, 1987). Although grain sizes and orientations were uncontrolled, these devices provided the first evidence that high-T_c grain boundaries act as junctions and may be used in SQUIDs. Shortly after, junctions and dc SQUIDs were fabricated across single grain boundaries in epitaxial YBCO films on polycrystalline STO substrates (Tsuei *et al.*, 1989; Hagerhorst *et al.*, 1989); Subsequently, engineered GBJ's were developed, and the most important types are bicrystal, and step-edge GBJ's [Fig. 9(a) and (b)]. Although important historically, biepitaxial GBJ's (Char *et al.*, 1991) are no longer used for SQUIDs, because of their small I_0R products. For reviews on GBJ's see Gross (1994) and Gross *et al.* (1995).

1. Bicrystal grain-boundary junctions

The key to both the development of a useful high-T_c Josephson junction technology and the understanding of transport across grain boundaries was provided by the pioneering work at IBM, Yorktown Heights on bicrystal GBJ's (Chaudhari *et al.*, 1988; Dimos *et al.*, 1988; Mannhart *et al.*, 1988, Dimos *et al.*, 1990; Gross *et al.*, 1990a, 1990b, 1991). These junctions are fabricated by the epitaxial growth of a high-T_c thin film on a bicrystal substrate with a predetermined misorientation angle θ [Fig. 9(a)]. In contrast to other GBJ fabrication techniques, this method can be used to obtain arbitrary misorientation angles and geometries, such as [001] and [100] tilt or [100] twist grain boundaries (Dimos *et al.*, 1990), enabling a systematic study of transport across high-T_c grain boundaries. Their straightforward fabrication

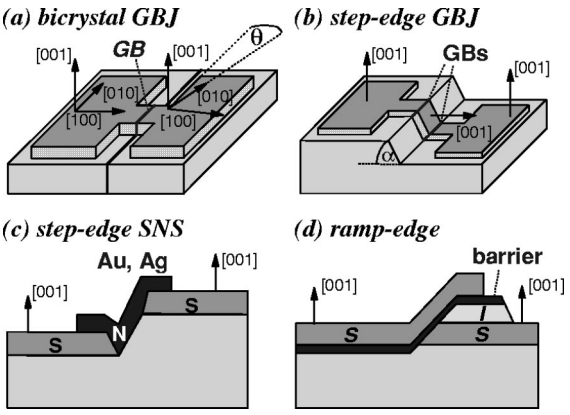

FIG. 9. Types of high-T_c Josephson junctions.

makes these junctions the most reliable and successful currently available, both for SQUIDs and more generally for any application which does not require many junctions at arbitrary positions on the substrate. Any substrate which supports the epitaxial growth of high-T_c films is suitable, including $SrTiO_3$ (Dimos *et al.*, 1988), YSZ (Ivanov *et al.*, 1991), Si (Chen *et al.*, 1991), $NdGaO_3$ (Quincey, 1994), MgO (Beck *et al.*, 1995), $LaAlO_3$ (Chen *et al.*, 1996), and *r* plane Al_2O_3 (Sapphire) (Vale *et al.*, 1997). Most work on bicrystal junctions has involved YBCO, but other superconductors have been investigated, including $Bi_2Sr_2CaCu_2O_8$ (Mayer *et al.*, 1993), $Tl_2Ba_2CaCu_2O_8$ (Kawasaki *et al.*, 1993), $HgBa_2CaCu_2O_6$ (Gupta *et al.*, 1994), and $La_{1.85}Sr_{0.15}CuO_4$ (Beck *et al.*, 1996).

Bicrystal junctions generally exhibit characteristics reasonably close to the RSJ model, provided θ exceeds a critical value, about 10° for YBCO (Dimos *et al.*, 1990; Gross, 1994). The critical-current density j_c for YBCO junctions decreases exponentially with increasing θ (Gross and Mayer, 1991; Ivanov *et al.*, 1991). This behavior is explained in part by the faceting of the grain boundary combined with *d*-wave pairing symmetry (Hilgenkamp *et al.*, 1996); however, it seems likely that a further contribution arises from an increase of the barrier thickness with increasing θ. For fixed θ, the critical-current density can be changed by more than one order of magnitude by appropriate annealing in oxygen (Kawasaki *et al.*, 1992), implying that the barrier thickness or height depends on oxygen content. Most SQUIDs have been made on 24° or 36° bicrystals, but recently 30° bicrystals have also become commercially available. At 77 K the $I_0R(j_c\rho_n)$ product of such junctions made from *c*-axis YBCO films on 24° bicrystals is typically 0.1–0.3 mV; comparable values have recently been reported on 30° bicrystals (Minotani, Kawakami *et al.*, 1997; Beyer *et al.*, 1998). The corresponding critical-current density j_c is of the order of $10^4\,A/cm^2$ at 77 K and the temperature-independent specific resistance-area product ρ_n is about $10^{-8}\,\Omega\,cm^2$. Although standard deviations in I_0R of around 20% have been reported for junctions on a given bicrystal (Miklich *et al.*, 1993), the parameters often vary much more widely because of variations in the quality of the bicrystal substrate (McDaniel *et al.*, 1997).

2. Step-edge grain-boundary junctions

The step-edge GBJ, which is also widely used, is based on the fact that an epitaxially grown, *c*-axis YBCO film changes its orientation at a steep step in the substrate or deposited dielectric [Fig. 9(b)]. This technique, initially realized by Simon *et al.* (1991), was subsequently refined by several groups (Herrmann *et al.*, 1991; Sun, Gallagher, Callegari *et al.*, 1993; Herrmann *et al.*, 1995; Pettiette-Hall *et al.*, 1995; Yi *et al.*, 1996). Common substrate materials are $SrTiO_3$ and $LaAlO_3$. For large step angles ($\alpha > 70°$) the two grain boundaries grow with different orientations, causing the lower junction to have a much lower critical-current density than the upper junction (Jia *et al.*, 1992). Thus, at least for currents not too far above I_0, the junction properties are determined solely by the lower grain boundary.

The substrate steps are aligned along major cubic axes of the substrate, and are usually patterned by standard lithography and Ar-ion milling so that their location can be chosen at will. This advantage over the bicrystal technique enables one to fabricate more complex circuits. Even for SQUIDs which require only one or two junctions, this flexibility in layout can be important, for example, for minimizing parasitic inductances.

It has been proposed that the grain boundaries formed at step edges behave as junctions because of their defect structure (Herrmann *et al.*, 1995), since 90° grain boundaries in planar films do not exhibit such behavior. Thus the properties of step-edge junctions depend strongly on the microstructure of the milled step and on the film-growth conditions, leading to greater spreads in parameters than for bicrystal junctions. The use of carbonlike diamond masks and very low milling rates improve the definition of the steps, and hence their reproducibility (Sun, Gallagher, Callegari *et al.*, 1993; Yi *et al.*, 1996). Dillmann *et al.* (1996) have used annealing processes to trim the parameters of their junctions. For a detailed review of the fabrication of step-edge junctions for SQUIDs, see Braginski (1996).

B. Junctions with extrinsic interfaces

This class of junctions involves a thin, deposited interlayer of insulating or normal material between two superconducting electrodes. Hence extrinsic interfaces are involved, and the control of their properties requires an advanced fabrication technology, usually involving the heteroepitaxial growth of high-T_c and interlayer materials. The transport and noise properties of these junctions are even less well understood than those for GBJ's. Although low-noise SQUIDs based on these junctions have been reported, the absence of reproducible fabrication processes has hindered their widespread use. Figures 9(c) and (d) illustrate two possible configurations:

the step-edge junction with a non-epitaxial noble-metal interlayer, and the ramp-edge junction with an epitaxially grown interlayer.

1. Step-edge SNS junctions

DiIorio *et al.* (1991), DiIorio, Yoshizumi, Yang, Maung, Zang, and Power (1993), and DiIorio *et al.* (1995) introduced the SNS junction illustrated in Fig. 9(c), and systematic studies of their properties have been carried out at NIST (Ono *et al.*, 1991, 1993; Rosenthal *et al.*, 1993; Reintsema *et al.*, 1995) and FZ Jülich (Grove *et al.*, 1996; Bode *et al.*, 1996). In principle, fabrication is simple: one cuts a steep step in the substrate, 50–100 nm high, using photolithography and Ar-ion milling, and deposits a high-T_c film directionally, so that the film does not grow on the step. Without breaking vacuum, one fills the gap by directional deposition of a Au or Ag layer, which makes contact to the a-b planes of the high-T_c films.

Very high I_0R products, up to 1 mV at 77 K, and high normal resistance, above 10 Ω for 4–8 μm widths, have been reported. However, the transport and noise properties are still unsettled issues. The I-V characteristics often exhibit excess current. The normal resistance appears to be determined by the boundary resistance at the SN interfaces, and various models for the transport have been suggested, for example, SINIS (Reintsema *et al.*, 1995) or ScNS (Bode *et al.*, 1996); c denotes point contacts at the SN interfaces. The major problem appears to be the lack of control of the interface properties which determine R and are most likely responsible for the large spreads in I_0. These difficulties have hindered the widespread application of this type of junction to SQUIDs.

2. Ramp-edge Josephson junctions

These junctions require the fabrication of an epitaxial trilayer with two superconducting electrodes separated by a thin barrier layer. Current transport is along the a-b planes of the c-axis oriented electrode films, taking advantage of the larger coherence length along this direction. One fabricates a ramp-edge junction [Fig. 9(d)] by first depositing a YBCO film and covering it with a thick, insulating film. Next, one patterns a ramp with a shallow angle (typically 10° to 20°) using ion milling or anisotropic wet etching, and finally deposits the barrier material and top electrode *in situ*. The top electrode effectively shields the magnetic-field component normal to the film surface. Hence ramp-edge junctions may offer an important advantage over planar GBJ's for operation in magnetically unshielded environments. Furthermore, ramp-edge junctions may be more robust against aging and thermal cycling compared to GBJ's since the barrier/interfaces are not directly exposed to the environment.

Gao *et al.* (1990, 1992) pioneered ramp-edge junctions with YBCO electrodes and a $PrBa_2Cu_3O_7$ barrier. Subsequently, many other barrier materials such as ruthenates or doped YBCO have been investigated (see, for example, Gross *et al.*, 1997 and references therein). The key requirement is a lower electrode with a smooth ramp edge of excellent crystalline quality to support the growth of a thin, homogenous barrier. Thus any damage caused by milling the ramp or by its exposure to air has to be healed prior to deposition of the barrier. The need to pattern the ramp with an *ex situ* process can be avoided by patterning the lower electrode with a microshadow mask (Strikovskiy and Engelhardt, 1996).

Ramp-edge junctions with Ca- or Co-doped YBCO barriers show behavior close to proximity effect coupling (Kleinsasser and Delin, 1995; Delin and Kleinsasser, 1996), with low or negligible interface resistance, but with junction resistances too low for SQUID applications. On the other hand, for ruthenate or PBCO barriers the junction resistance is dominated by interface resistance rather than the intrinsic barrier resistivity, and transport is explained via tunneling through localized states in the barrier or interface, which has a high defect density (Dömel *et al.*, 1995; Satoh *et al.*, 1995; Schilling, 1997). Using bromine etching to form the ramp, Faley, Poppe, Jia *et al.* (1995) fabricated a quasiplanar junction with PBC(Ga)O barriers that exhibited negligible interface resistance; hence the resistance of these junctions scaled with barrier thickness. Junctions 5 μm wide and with barriers 20 nm thick exhibited I-V characteristics close to that of the RSJ model with $I_0R \sim 200\,\mu$V and $R \sim 1\,\Omega$ at 77 K, making them good candidates for SQUIDs.

C. Discussion of high-T_c junctions

For most high-T_c junctions, one finds the following common properties:

(i) They are internally shunted and at 77 K produce I-V characteristics reasonably close to the RSJ model. The most common deviation from the RSJ characteristic is an excess supercurrent. Possible candidates for its origin are a nonsinusoidal current-phase relation (Ilichev *et al.*, 1998), superconducting shorts through the barrier, or Andreev reflection at the barrier interfaces (Alff *et al.*, 1998). At lower temperatures, that is, higher critical currents, the characteristics may become hysteretic, implying that even at 77 K β_c may not be too much below unity.

(ii) The critical-current density generally increases linearly with decreasing temperature, while, at least for GBJ's, the resistance-area product ρ_n is nearly independent of temperature (Gross, 1994).

(iii) The I_0R ($j_c\rho_n$) products are smaller than the gap voltage, typically below 300 μV at 77 K. Values of $j_c\rho_n$ up to about 1 mV at 77 K have been reported for some junctions, but always seem to be associated with large excess currents. Grain-boundary junctions (Gross, Chaudhari, Kawasaki *et al.*, 1990; Russek *et al.*, 1990; Hermann *et al.*, 1991) and junctions with artificial barriers show a scaling $j_c\rho_n \propto (j_c)^p$, where $p \approx 0.5$ over seven orders of

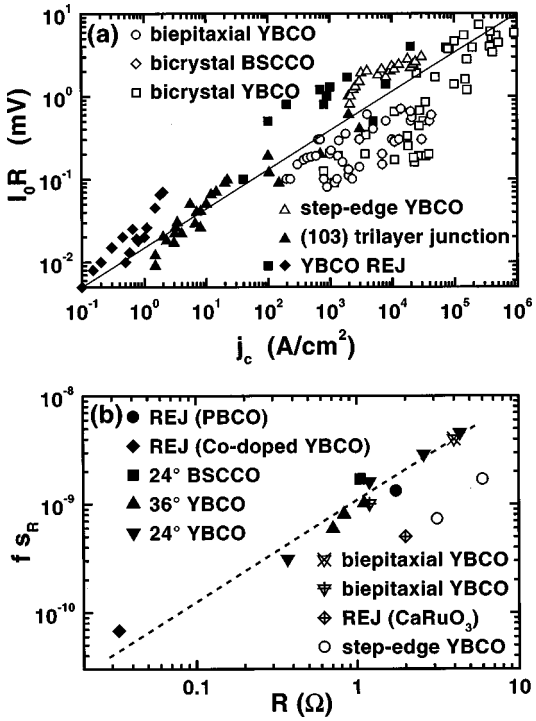

FIG. 10. Scaling behavior of various high-T_c Josephson junctions: (a) I_0R product vs critical current-density j_c at 4.2 K; a line with slope 0.5 has been drawn through the data (Gross *et al.*, 1997); (b) fs_R vs normal resistance R; the dashed line is a guide to the eye (Marx and Gross, 1997).

magnitude in j_c, as shown in Fig. 10(a) (Gross, 1994; Gross *et al.*, 1997, and references therein).

(iv) Most junctions exhibit large levels of low-frequency $1/f$ noise arising from fluctuations of the critical current and the junction resistance (Kawasaki *et al.*, 1992; Miklich *et al.*, 1992; Marx, Fath *et al.*, 1995). The normalized spectral densities $s_I \equiv S_{I_0}/I_0^2$ and $s_R \equiv S_R/R^2$ for critical-current and resistance fluctuations are temperature independent and proportional to the junction resistance (Marx and Gross, 1997), as shown in Fig. 10(b). Defining $S_{I_0}/I_0^2 = a^2/f$ one finds typically $a^2 \approx 10^{-8}\,R/\Omega$, which is about three orders of magnitude larger than for Nb junctions with shunt resistances of a few ohms (Foglietti *et al.*, 1986; Savo *et al.*, 1987). Furthermore, the relation $(s_I/s_R)^{1/2} \approx 1/(1\text{-}p)$ observed for GBJ's (Gross, 1994, Marx, Fath *et al.*, 1995) strongly suggests that the low-frequency noise and scaling of I_0R have the same microscopic origin.

The universal scaling of $j_c\rho_n$, s_I, and s_R is an important feature of high-T_c junctions because it may be the key to understanding their transport and noise properties and offers the possibility of adjusting important junction parameters for optimum SQUID performance. The fact that both GBJ's and junctions with artificial barriers have the same scaling suggests a common transport mechanism governed by thin interface layers. However, the details of this mechanism are still controversial. Since proximity effect coupling cannot explain the observed transport properties for the vast majority of junctions, several models have been proposed that include the effects of a boundary resistance between S and N layers (SNIS, SINIS) (Kupriyanov and Likharev, 1990) or of constrictions (ScNS, SNcNS) (Aminov *et al.*, 1996; Golubov and Kupriyanov, 1996). On the other hand, for grain-boundary junctions it has been proposed that resonant tunneling of quasiparticles via localized states in an insulating barrier acts as an intrinsic normal shunt (Gross and Mayer, 1991). This model, known as the intrinsically shunted junction model, naturally explains the low I_0R product in terms of an intrinsic shunt due to a high density of localized states. The universal scaling of I_0R with j_c suggests that the density of localized states is about the same in all junctions. The trapping and release of charge carriers in localized states lead to fluctuations in the local barrier height which cause I_0 and R to fluctuate with antiphase correlation (Marx, Alff *et al.*, 1995), thus explaining the high level of $1/f$ noise in junctions with a high density of localized states. The same scaling of I_0R with j_c is predicted by a channel model (Moeckly *et al.*, 1993) in which the Josephson current in GBJ's is restricted to narrow superconducting filaments in a weakly conducting medium. However, this model cannot account for the observed phase correlation of I_0 and R fluctuations, since the superconductive and resistive channels are spatially separated.

The scaling behavior described above has important consequences for the optimization of SQUIDs. At $T = 77\,\mathrm{K}$, j_c is typically $10^4\,\mathrm{A/cm^2}$ for 24° YBCO grain boundaries, corresponding to $I_0R \approx 100\,\mu\mathrm{V}$. Hence for junctions of width w and thickness $d \approx 200\,\mathrm{nm}$ critical currents of about $20\,\mu\mathrm{A}(w/\mu\mathrm{m})$ are typical. Thus to achieve $\beta_L = 1$ for an inductance $L \approx 50\,\mathrm{pH}$ one requires $w \sim 1\,\mu\mathrm{m}$, close to the minimum linewidth achievable with photolithography. Increasing I_0R with oxygen annealing or reducing the misorientation angle may not be very useful unless one can achieve submicron patterning without significant damage to the edges of the film. We note that for $p = 0.5$, an increase in I_0R by a factor of 3 requires an increase in j_c by an order of magnitude. An alternative to submicron patterning may be thinning of the film in the junction region; however, this approach is not applicable to all types of junctions, may be detrimental to the junction properties, and can contribute a significant kinetic inductance.

Clearly, it is highly desirable to have a lower critical-current density for the same I_0R product, but this would require reduction of the density of localized states which, in turn, would result in an increase of ρ_n for fixed j_c. Even if this goal could be achieved, since $\beta_c \propto j_c\rho_n^2 C_s$ increases with ρ_n^2 for fixed j_c and C_s, such junctions may become hysteretic at 77 K. In contrast, a change in $I_0R \propto j_c^{1/2}$ causes $j_c\rho_n^2$ to be constant and leaves β_c approximately unchanged (neglecting the change in the specific capacitance C_s with effective barrier thickness). Although junctions with high values of ρ_n are occasionally reported in the context of high performance

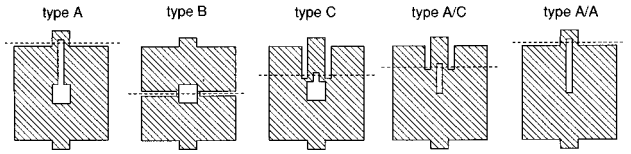

FIG. 11. Five configurations of planar dc SQUID fabricated at Berkeley. Dashed lines indicate the bicrystal boundary along which the junctions are formed. Outer dimension is typically $500\times500\ \mu m^2$.

dc SQUIDs (Lee *et al.*, 1995; Glyantsev *et al.*, 1996), detailed data on their transport characteristics have not been presented.

For the optimization of SQUIDs a detailed knowledge of the junction transport mechanism may not be necessary. However, control of the junction parameters is essential, and may only be possible if the transport mechanism is understood. This, in turn, may require the fabrication of junctions with well-defined interfaces and barriers. Such a technology is not yet at hand: spreads in I_0 and R are typically $\pm20\%$ on chip and usually much higher from chip to chip. Although these large spreads may be unacceptable for applications which require many junctions, they have not prevented the fabrication of low noise SQUIDs. Nevertheless, to allow a more systematic study of SQUID performance and to clarify discrepancies between experimental results and theory for high-T_c dc SQUIDs (Sec. V.C), a more reproducible technology is highly desirable. To complicate the issue, integrated SQUID magnetometers may require the incorporation of high-quality junctions into low-noise thin-film multilayers. The successful integration of a controllable, high-yield junction technology with a low-noise multilayer technology has still to be demonstrated.

V. dc SQUIDs

A. Practical devices

Early high-T_c dc SQUIDs were generally fabricated in the geometry of a square washer, following the most widely used configuration of low-T_c SQUIDs (Ketchen, 1981; Jaycox and Ketchen, 1981). Figure 11 shows a selection made at Berkeley. In these devices, it was implicitly assumed that ultimately the SQUIDs would be inductively coupled to flux transformers with planar, spiral input coils as is common practice with low-T_c magnetometers. Subsequently, various other magnetometer configurations emerged, in addition to the multiturn flux transformer (Sec. VI.C), and for reasons of minimizing the $1/f$ noise in ambient magnetic fields (Sec. IX.A) it is desirable to make SQUIDs with rather narrow linewidths. Thus a wide variety of SQUID configurations have been investigated, and we do not attempt to review them here; rather we shall describe some of the more useful types in Sec. VI in the context of magnetometers. Most SQUIDs are still made with either bicrystal or step-edge grain-boundary junctions, and these have yielded the highest performance to date.

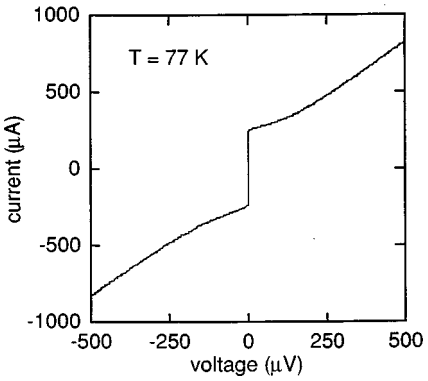

FIG. 12. I-V characteristics of bicrystal, type B dc SQUID at 77 K; $L=41$ pH, $I_0=120\ \mu$A, $R=1.28\ \Omega$.

With few exceptions, the SQUID is immersed directly in liquid nitrogen. To attenuate external magnetic-field fluctuations, above all the ubiquitous 50 or 60 Hz fields and their harmonics, one may surround either the dewar with a mu-metal shield or the SQUID with a high-T_c shield. Mu-metal shields have the advantage of reducing both the ambient static field and time-varying field substantially, while high-T_c shields generally offer greater attenuation of time-varying fields, but do not reduce the ambient field if they are cooled in it. Thus a combination of both types of shields is often desirable in evaluating the intrinsic noise of SQUIDs. It is also imperative to exclude radio-frequency interference, most commonly by running the measurement in a screened room.

Figure 12 shows a representative I-V characteristic for a YBCO SQUID, grown on a STO bicrystal, operated at 77 K. In Fig. 13 we have plotted the voltage V across the SQUID vs the applied flux Φ for a series of bias currents. As the current is increased, the amplitude of the oscillations increases smoothly to a maximum and then decreases. The SQUID is normally operated at the bias current that gives the maximum value of V_Φ.

B. Readout schemes

In virtually all applications, SQUIDs are operated in a flux-locked loop in which the voltage change across the

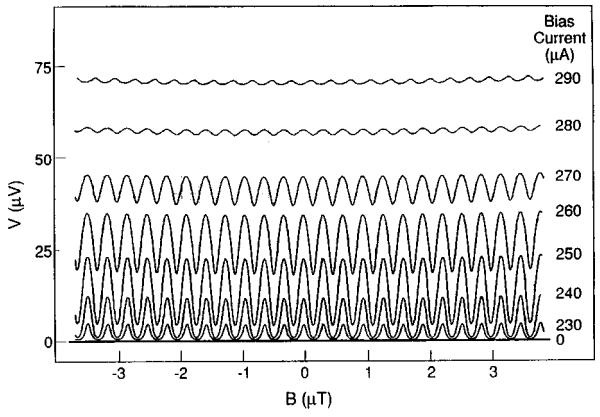

FIG. 13. V vs Φ for dc SQUID of Fig. 12 for seven values of bias current.

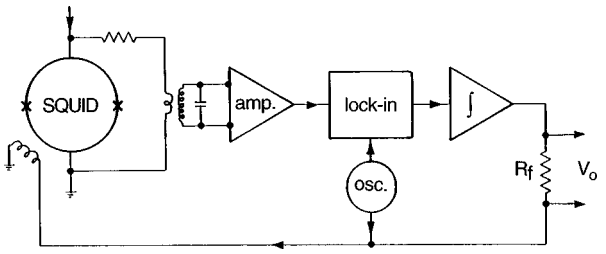

FIG. 14. Flux-locked loop for dc SQUID.

SQUID induced by an applied flux is amplified and fed back as an opposing flux. This feedback circuit linearizes the response of the SQUID, provides a straightforward means of measuring the intrinsic noise of the SQUID, and enables one to track inputs equivalent to many flux quanta. The input stage of the electronic circuitry is designed to add negligibly to the intrinsic noise of the SQUID. Drung (1996) has given a detailed review of a variety of schemes; here we review briefly the two most commonly used.

1. Flux modulation

In the widely used flux modulation scheme (Forgacs and Warnick, 1967), shown in Fig. 14, one applies a sinusoidal or square-wave flux modulation to the SQUID with a peak-to-peak amplitude of $\Phi_0/2$ and a frequency f_m of typically 100 kHz. The resulting alternating voltage across the SQUID is coupled to a room-temperature preamplifier via either a cooled LC series-resonant circuit (Clarke *et al.*, 1976) or a cooled transformer (Ketchen *et al.*, 1978). The voltage gain of either coupling circuit is usually chosen to transform the dynamic resistance of the SQUID at its operating point to the value required to optimize the noise temperature of the preamplifier. Since this noise temperature is typically a few kelvin, the preamplifier contributes negligible noise to a device operating at 77 K. After amplification, the signal is lock-in detected at the frequency f_m. If the quasistatic flux is $n\Phi_0$ (n is an integer), the V-Φ curve is symmetric about this local minimum and the voltage contains components only at the frequency $2f_m$. Thus the output of the lock-in detector is zero. On the other hand, if the flux is shifted away slightly from the local minimum, the voltage across the SQUID contains a component at frequency f_m and there will be an output from the lock-in detector. After integration (cf. Fig. 14), this signal is fed back as a current through a feedback resistor R_f to a coil inductively coupled to the SQUID; usually the same coil is used for both flux modulation and feedback. The flux fed back opposes the applied flux to keep the flux in the SQUID constant; the voltage developed across R_f is proportional to the applied flux. One can measure the intrinsic flux noise of the SQUID by connecting the output voltage to a spectrum analyzer in the absence of any input signal.

Ideally, the bandwidth for an optimized flux-locked loop extends to one half the modulation frequency. For unshielded applications in which the SQUID is exposed to the magnetic noise of the environment, a more important figure of merit is often the slew rate, that is, the maximum rate of change of flux that the system is able to track without losing lock. For an ideal single-pole integrator, the slew rate is $2\pi f_1\Phi_0/4$, where f_1 is the frequency at which the open-loop gain of the feedback loop falls to unity (Drung, 1996). A considerable improvement in the slew rate at low frequencies can be achieved by means of a two-pole integrator (Giffard, 1980; Wellstood *et al.*, 1984). Using a high-T_c SQUID with a 500-kHz flux modulation and a single-pole filter, Dantsker *et al.* (1994) obtained a slew rate of $10^5\,\Phi_0\,s^{-1}$ at 900 Hz. Recently, Koch *et al.* (1996) described a flux-locked loop with a modulation frequency of 16 MHz, using a resonant matching circuit with a superconducting, thin-film transformer to match the SQUID to the amplifier. The system had a closed-loop bandwidth exceeding 2.5 MHz and a slew rate greater than $10^6\,\Phi_0\,s^{-1}$ at frequencies up to 1 MHz. Subsequently, Penny *et al.* (1997) used a transmission-line transformer feeding a matched transmission line to couple the SQUID to the amplifier. With a low-T_c SQUID they achieved a bandwidth of 5 MHz, a slew rate of $1.9\times10^6\,\Phi_0\,s^{-1}$ at 200 Hz, and a flux noise of $5.5\mu\Phi_0\,Hz^{-1/2}$. The performance with high-T_c SQUIDs has not yet been reported.

A further issue of particular importance when the outputs of SQUIDs are subtracted to form electronic gradiometers (Sec. VIII.A) is the linearity of the flux-locked loop. To investigate the nonlinearity, Nichols *et al.* (1996) measured the harmonic generation using a high-T_c SQUID with 130-kHz flux modulation and a single-pole integrator. For input signals at frequencies up to 248 Hz and rms amplitudes up to 20 Φ_0, 2nd, 3rd, and 4th harmonics were each 115 dB below the fundamental. At higher frequencies the harmonic content began to increase because of the reduction in the open-loop gain. It was also shown that the amplitudes of the even harmonics depended critically on the amplitude of the 130-kHz flux modulation, becoming zero when the peak-to-peak value was precisely $\Phi_0/2$.

The slew rate and linearity that have been achieved are likely to be adequate for most applications in which the magnetometer is static. For situations in which the magnetometer is moved in the earth's magnetic field—for example, in towed systems—the demands are substantially higher, and the performance may or may not be adequate.

As will be shown later (Sec. V.D), fluctuations in the critical current and resistance of the junctions are a major source of $1/f$ noise in dc SQUIDs. Fortunately, their contributions can be greatly reduced by a number of schemes (Koch *et al.*, 1983; Foglietti *et al.*, 1986; Dössel *et al.*, 1991), which have been successfully applied to high-T_c SQUIDs (Koch *et al.*, 1992; Miklich *et al.*, 1993; Grundler, Eckart *et al.*, 1993). At the operating point of SQUIDs, the critical-current noise dominates the resistance noise and contributes $1/f$ noise in two ways. Fluctuations at frequencies $\ll f_m$ that are in phase at the two junctions give rise to a voltage noise across the SQUID that is eliminated by flux modulation at frequency f_m.

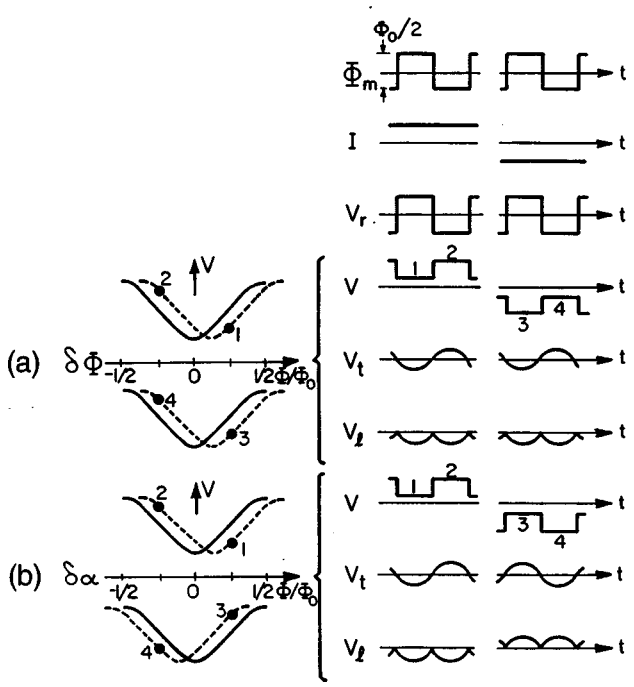

FIG. 15. Principle of bias-reversal scheme to reduce $1/f$ noise due to out-of-phase critical-current fluctuations. The left-hand column shows the V-Φ curves (solid lines), and the dashed lines indicate the effect of (a) an external flux change $\delta\Phi$ and (b) a flux change $\delta\alpha$ generated by out-of-phase critical-current fluctuations. The right-hand column shows, as a function of time t, (top to bottom) the flux modulation Φ_m, the bias current I, and the reference voltage V_r used to lock-in detect the signal from the SQUID; the next three rows are for an external flux change $\delta\Phi$, and show the voltage V across the SQUID, the voltage V_t across the secondary of the tuned transformer and the output V_l of the lock-in detector; the last three rows show the same voltages for an out-of-phase critical-current fluctuation (Koch *et al.*, 1983).

Fluctuations that are out-of-phase at the two junctions are equivalent to a flux noise that is not reduced by this scheme. Instead, one makes use of the fact that the apparent shift of the V-Φ characteristic along the flux axis changes polarity if one reverses the polarity of the bias current whereas the flux due to an input signal (or "flux noise") does not.

As an example of one of the bias-reversal schemes, we briefly describe that developed by Koch *et al.* (1983); the principle is illustrated in Fig. 15 and its implementation in Fig. 16. The SQUID is flux-modulated with a 100-kHz square wave of peak-to-peak amplitude $\Phi_m = \Phi_0/2$. Synchronously with the modulation, the bias current I through the SQUID is reversed, for example, at a frequency $f_r = 3.125$ kHz. The resistance bridge shown in Fig. 16 minimizes the 3.125 kHz switching transients across the transformer. Simultaneously with the bias reversal, a flux $\Phi_0/2$ is applied to the SQUID. In Figs. 15(a) and (b) we see that the bias reversal changes the sign of the voltage across the SQUID while the flux shift ensures that the sign of the flux-to-voltage transfer function remains the same. The transformer coupling the SQUID to the preamplifier is often tuned at the modulation frequency with a Q of about 3, so that any 100-kHz signals at the secondary are approximately sinusoidal.

We assume that the SQUID is operated in the usual flux-locked loop, with the output from the lock-in detector integrated and fed back to the SQUID (Fig. 16). Thus the 100-kHz signal across the SQUID consists of just the error signal. Suppose now that we apply a small external flux $\delta\Phi$ to the SQUID at a frequency well below f_r. The V-Φ curves are shifted as in Figs. 15(a), and the 100-kHz flux modulation switches the SQUID between the points 1 and 2 for positive bias and 3 and 4 for negative bias. As a function of time, the voltage V across

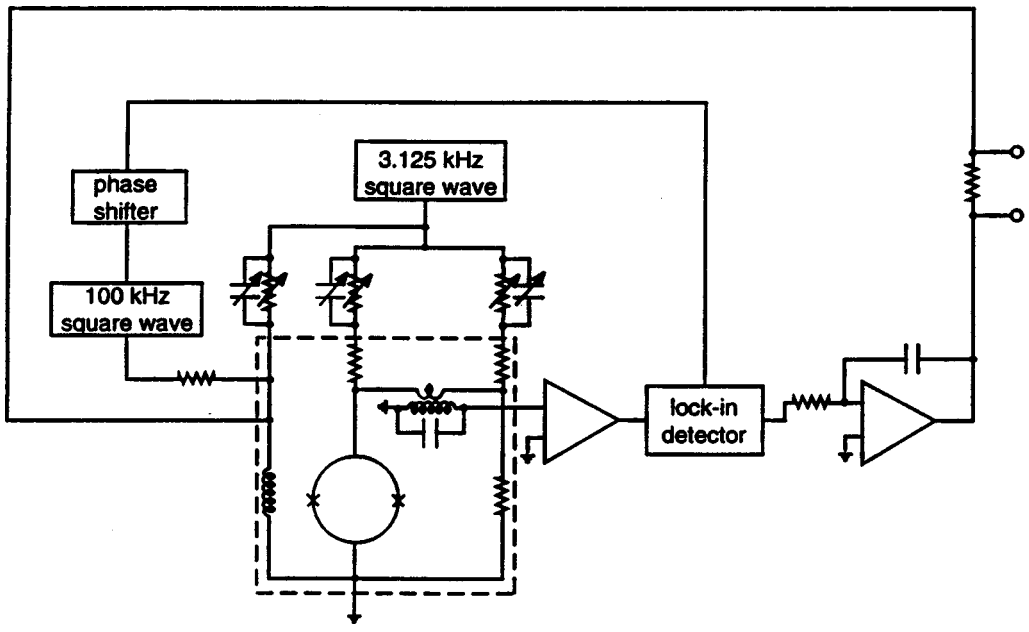

FIG. 16. Schematic for flux-locked loop with bias current reversal. Cryogenic components are enclosed in the dashed box (Koch *et al.*, 1983).

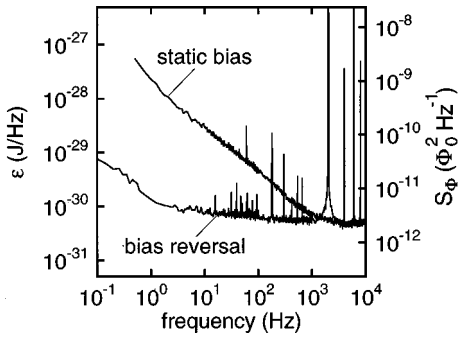

FIG. 17. Spectral density of flux noise of representative high-T_c dc SQUID with flux modulation and bias current reversal.

the SQUID is as shown in Fig. 15, and the signal across the tuned transformer V_t is at the fundamental frequency. When this signal is mixed with the reference voltage V_r, the output from the lock-in detector $V_{\not}$ will consist of a series of negative-going peaks for both polarities of the bias current. The average of this output produces a negative signal proportional to $\delta\Phi$ which is then used to cancel the flux applied to the SQUID. Thus, in the presence of bias reversal and flux shift, the SQUID responds to an applied flux in the usual way.

We consider now the effects of $1/f$ noise on the critical currents. The in-phase mode is eliminated by the 100-kHz flux modulation. Suppose, instead, we have an out-of-phase critical-current fluctuation at a frequency below f_r. Because the flux generated by this fluctuation *changes sign* when the bias current is reversed, the V-Φ curves are displaced in opposite directions. As a result, the voltage across the SQUID undergoes a phase change of π when the bias current is reversed, as shown in Fig. 15. Consequently, the voltage at the output of the lock-in due to the out-of-phase critical-current fluctuation changes sign each time the bias current is reversed, and the time average of the signal over periods much longer than $1/f_r$ is zero. Thus the $1/f$ noise due to both in-phase and out-of-phase critical-current fluctuations is eliminated by this scheme.

Figure 17 shows the spectral density of the flux noise of a representative SQUID operated with flux modulation and with and without bias reversal. Without bias reversal, $1/f$ noise is evident for frequencies below about 2 kHz. The application of bias reversal reduces the level of $1/f$ noise dramatically, by two orders of magnitude at 1 Hz, demonstrating that the $1/f$ noise indeed arose from critical-current fluctuations.

2. Direct readout

A "direct readout" scheme eliminates the need for a coupling network between the SQUID and the amplifier, and enables one to use particularly simple electronics for the flux-locked loop (Drung, 1994). In addition, it allows one to achieve bandwidths around 10 MHz relatively easily (Drung, 1996). The output of the current-biased SQUID is connected directly to one terminal of a low-noise, bipolar amplifier; an offset bias voltage is applied to the other terminal. After amplification, the signal is integrated and fed back via a resistor to a coil coupled to the SQUID. Since the preamplifier noise, typically 1 nV Hz$^{-1/2}$, usually dominates the SQUID noise, typically 0.1 nV Hz$^{-1/2}$ for low-T_c SQUIDs, it must be reduced to a tolerable level by increasing the transfer function. In the additional positive feedback (APF) scheme (Drung *et al.*, 1990) this increase is achieved by shunting the SQUID with an inductor L_a, with a mutual inductance M_a to the SQUID, in series with a resistor R_a. When the SQUID is current biased, a change in the voltage across the SQUID due to an applied flux generates a current through the shunting network and a flux in the SQUID. Thus the V-Φ characteristic becomes asymmetric, and the transfer function is enhanced by a factor $1/(1-G_a)$ in the region of positive feedback; here

$$G_a=[M_a+(\partial\Phi/\partial I)_V]V_\Phi/R_a \tag{5.1}$$

is the APF gain. The maximum slew rate is concomitantly reduced by a factor $(1-G_a)$. Thus for wideband systems G_a should be just high enough to make the effect of the preamplifier voltage noise negligible compared to the intrinsic SQUID noise. For a low-T_c SQUID and an effective APF gain of 0.57, a flux-locked bandwidth of 5 MHz was achieved with a white flux noise of 3.4 $\mu\Phi_0$ Hz$^{-1/2}$, corresponding to a magnetic-field noise of 1.6 fT Hz$^{-1/2}$. We note that the flux-to-current transfer coefficient of the SQUID at constant voltage, $(\partial\Phi/\partial I)_V$, is not affected by APF, so that the current noise of the amplifier may become important. If necessary, this contribution can be reduced by bias-current feedback (Drung and Koch, 1993).

To remove $1/f$ noise due to critical-current fluctuations, as for the flux-modulation scheme, one has to reverse the bias current (Drung, 1995); at the same time the bias voltage is reversed and a flux shift is applied to maintain the same polarity of the flux-to-voltage transfer function. Using this bias-reversal scheme, Ludwig *et al.* (1997) recently reported a modified, directly coupled flux-locked loop for high-T_c SQUIDs. Using a preamplifier with a voltage noise of 0.44 nV Hz$^{-1/2}$, their high-T_c SQUIDs could be operated without APF with a total rms white noise typically 20% higher than the intrinsic rms noise of the SQUID. For an optimum bias-reversal frequency of around 100 kHz, it was demonstrated that $1/f$ noise due to critical-current fluctuations can effectively be suppressed without increasing the white-noise level (Drung, Ludwig *et al.*, 1996; Drung, Dantsker *et al.*, 1996; Ludwig *et al.*, 1997). In addition, a maximum bandwidth of about 1 MHz and slew rates close to $10^6\Phi_0$/s were achieved.

C. White noise

In this section, we present data on the white noise measured by a number of groups: Biomagnetic Technologies, Inc., San Diego, Philips, Hamburg, University

of California, Berkeley, University of Hamburg, University of Jena, and University of Twente. The SQUIDs were made with either grain-boundary or SNS ramp-edge junctions. For the devices discussed, L ranged from 10 to 210 pH, and I_0R from below 10 μV to 300 μV. Although values of I_0R of 300 μV or larger are desirable, such values are generally achieved only with high values of I_0. As a result, β_L is often well above unity, and sometimes greater than 10. Values of β_L near unity were achieved only for I_0R below 200 μV. One should bear in mind that some of the estimated values of L are likely to be rather uncertain, because of both the intricate geometries of the SQUID loops and the possible contributions of kinetic inductance (Töpfer and Uhlmann, 1994; Hildebrandt and Uhlmann, 1995).

We now compare the measured results with the theoretical predictions of Sec. II.C. Similar comparisons have been made by Enpuku (1993) and Enpuku *et al.* (1993, 1994), Enpuku, Tokita *et al.* (1995), Keene *et al.* (1995), and Koch (1997). To give an overview of SQUIDs with widely varying parameters, it is convenient to present the results in terms of the dimensionless parameters Γ, β_L, and $\Gamma\beta_L$. For the devices discussed, Γ ranges from 0.004 to 1.8, β_L ranges from 0.12 to 65, and $\Gamma\beta_L$ ranges from 0.03 to 0.65; the majority of the values of $\Gamma\beta_L$ are above the desirable upper limit of 0.15.

We begin by recalling from Sec. II that $v_\phi(\beta_L;\Gamma\beta_L) = f(\beta_L)g(\Gamma\beta_L)$, with $f(\beta_L) = v_\phi(\beta_L;\Gamma\beta_L = \frac{1}{80})$ and $g(\Gamma\beta_L) = v_\phi(\beta_L;\Gamma\beta_L)/v_\phi(\beta_L;\Gamma\beta_L = \frac{1}{80})$. We find $v_\phi(\beta_L,\Gamma\beta_L)$ and $v_\phi(\beta_L,\Gamma\beta_L = \frac{1}{80})$ from Eqs. (2.5) and (2.6), respectively. In Figs. 18(a) and (b) the solid lines represent $v_\phi/f(\beta_L)$ and $v_\phi/g(\Gamma\beta_L)$ as functions of $\Gamma\beta_L$ and β_L, respectively. To compare the data with these predictions, we calculate the experimental values of $v_\phi/f(\beta_L)$ and $v_\phi/g(\Gamma\beta_L)$ and plot them as points in Fig. 18. The data show the same general trend as the theory, but relatively few points fall on or close to the predicted curves. Most of the data lie well below the predicted values, sometimes by as much as an order of magnitude. We note that not all authors measure the maximum value of V_Φ directly, for example, by applying a small oscillating flux, but instead measure the peak-to-peak voltage swing ΔV and assume $V_\Phi \approx \pi\Delta V/\Phi_0$. This estimate assumes that the voltage is sinusoidal in Φ, which is at best only an approximation.

We turn now to the dimensionless flux noise $s_\phi = S_\Phi(2\pi I_0R/\Phi_0) = s_v/v_\phi^2$. In the simulations, we saw that s_ϕ can be factorized as $s_\phi(\beta_L;\Gamma\beta_L) \approx f_\phi(\beta_L)g_\phi(\Gamma\beta_L)$, where we defined $f_\phi(\beta_L) = s_\phi(\beta_L;\Gamma\beta_L = \frac{1}{80})$ and $g_\phi(\Gamma\beta_L) = s_\phi(\beta_L;\Gamma\beta_L)/s_\phi(\beta_L;\Gamma\beta_L = \frac{1}{80})$. In Figs. 19(a) and (b) we plot s_ϕ/f_ϕ vs $\Gamma\beta_L$ and s_ϕ/g_ϕ vs β_L, respectively, together with the theoretical curves. In both cases the reduced noise power is as much as two orders of magnitude too high. One can explain this discrepancy only partly by the reduced value of the transfer function, which enters as v_ϕ^{-2}.

From Figs. 18 and 19 we see that the discrepancy between theory and experiment is roughly the same for all values of $\Gamma\beta_L$ and β_L. We also investigated whether

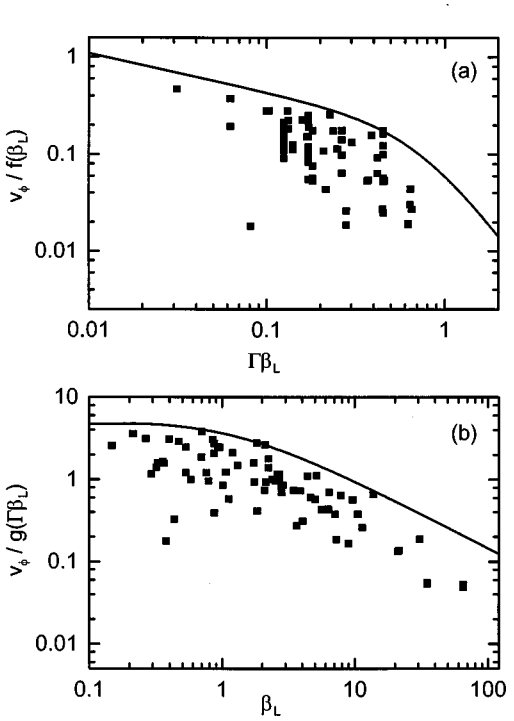

FIG. 18. Transfer function of dc SQUID: (a) Measured transfer function v_ϕ, normalized to the theoretical value $f(\beta_L)$, vs $\Gamma\beta_L$ for a wide selection of SQUIDs (solid squares); solid line corresponds to Eq. (2.5). (b) Measured transfer function normalized to the theoretical value $g(\Gamma\beta_L)$ vs β_L; solid line corresponds to Eq. (2.6).

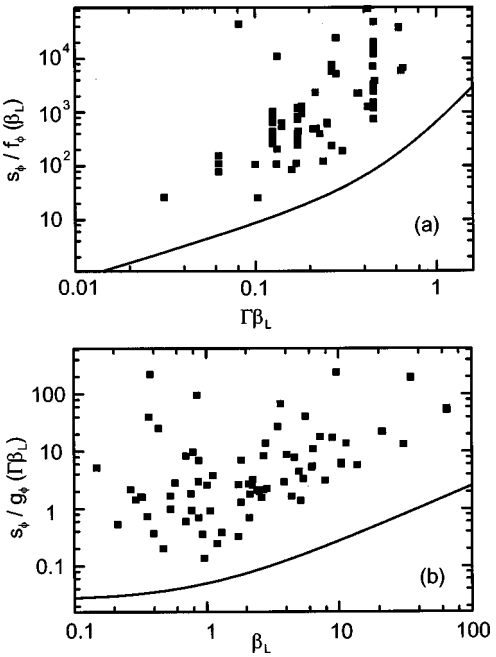

FIG. 19. Flux noise of dc SQUID: (a) Measured flux noise power, normalized to the theoretical value $f_\phi(\beta_L)$, vs $\Gamma\beta_L$ for the same SQUIDs as in Fig. 18 (solid squares); solid line corresponds to Eq. (2.8). (b) Measured flux noise power, normalized to the theoretical value $g_\phi(\Gamma\beta_L)$ vs β_L; solid line corresponds to Eq. (2.9).

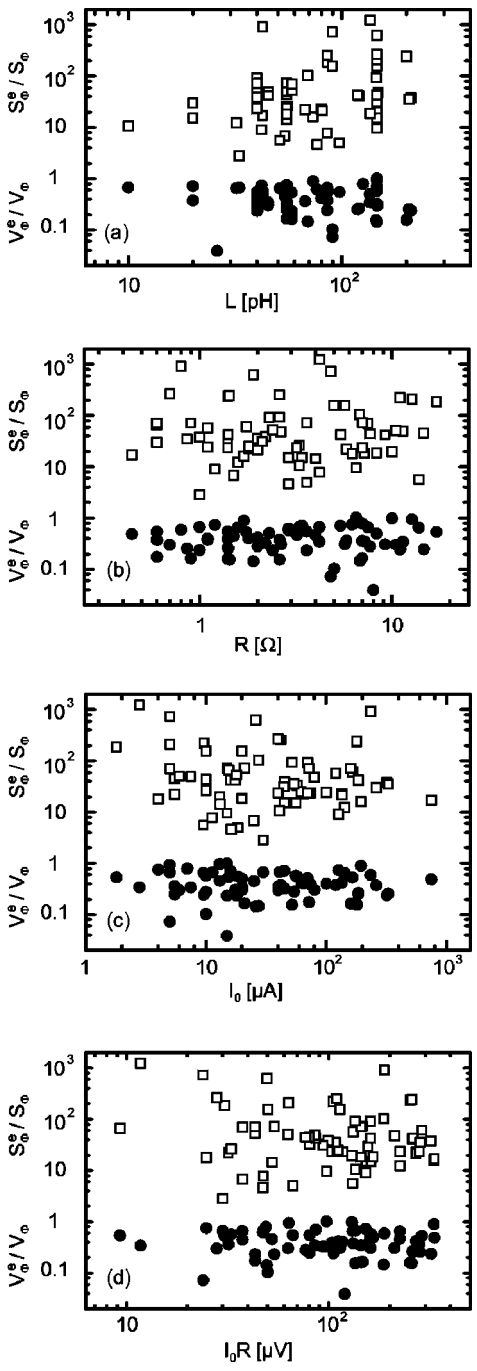

FIG. 20. For a wide selection of dc SQUIDs: ratio of measured and calculated transfer functions V_Φ^e/V_Φ (solid circles) and ratio of measured and calculated flux noise powers S_Φ^e/S_Φ (open squares) as a function of (a) SQUID inductance, (b) junction resistance, (c) junction critical current, and (d) I_0R.

systematic trends occur as functions of the absolute values of L, R, I_0, or I_0R by plotting V_Φ^e/V_Φ (solid circles) and S_Φ^e/S_Φ (open squares) versus these parameters in Fig. 20. The plots clearly show that there are no systematic trends throughout the ranges of parameters. However, for some devices V_Φ^e/V_Φ approaches unity; a similar result has been found by Koch (1997). Generally, the scatter in S_Φ^e/S_Φ is much greater than in V_Φ^e/V_Φ. We also calculated S_Φ by using the measured value V_Φ^e instead of using its predicted value. The scatter was reduced, but no systematic trends became apparent.

What are the possible reasons for the high values of white noise that are almost universally observed? One explanation is that some measurements may have been taken with improperly set bias conditions; however, this is an unlikely explanation for most of the data. Second, experience with low-T_c SQUIDs suggests that environmental noise and noise from the readout electronics are improbable explanations. A third possibility is that the SQUID inductances are significantly underestimated, for example, because of a higher than anticipated kinetic inductance. Enpuku, Tokita *et al.* (1995) show that actual inductance values, 1.4 to 2 times higher than the estimated values, would explain much of the discrepancy; however, for some 40 pH devices, the actual value would have to be as much as 4 times higher, which is unreasonable. For example, Lee *et al.* (1995) estimated that the kinetic inductance for their devices was about 15% of the geometric inductance. Thus this explanation seems somewhat unlikely. A fourth explanation (Foglietti *et al.*, 1995) is that the junctions have a current-phase relation that is far from sinusoidal and that excess critical currents would lead one to overestimate the value of I_0R obtained from the I-V characteristics. Since I_0R enters v_ϕ and s_ϕ as a normalization factor, the high value would lead one to overestimate v_ϕ in the theory, and underestimate s_ϕ. A fifth explanation for the observed discrepancies between theory and experiment could be the presence of resonances. While the model in Sec. II ignores parasitic effects, the large dielectric constant of the commonly used $SrTiO_3$ substrates results in a substantial spurious capacitance. Transmission-line resonances (Enpuku *et al.*, 1996), as well as capacitive feedback effects (Enpuku *et al.*, 1997), have been demonstrated to influence the SQUID performance significantly. These possibilities cannot be entirely ruled out since the published noise data for dc SQUIDs are rarely accompanied by detailed measurements of the I-V characteristics. However, the reasonably good fit of a least some I-V characteristics to the RSJ model (for example, Gross and Chaudhari, 1992), the dependence of the amplitude of Shapiro steps on microwave power, and the reasonably good quality diffraction patterns of the critical current in a magnetic field suggest that they are not strong candidates. Finally, an effective bath temperature of roughly 2 T could explain the results (Enpuku, 1993). A twofold increase in temperature would double the value of $\Gamma\beta_L$ and reduce $L_{\rm th}$ to 160 pH. Thus one would have to shift the data in Figs. 18(a) and 19(a) to the right by a factor of 2 to account for the higher noise. This higher temperature could arise from some nonequilibrium process in the junction, for example, random telegraph signals from flux motion at characteristic frequencies well above the measurement bandwidth. The resulting Lorentzian power spectra would be white below the hopping frequencies. To our knowledge, there is no experimental evidence to support this notion, but it would be worth-

while to extend the measurements to much higher frequencies to see whether or not the noise decreased.

Finally, we note that, although they are significantly above theoretical predictions, impressive levels of noise have been achieved at 77 K, for example, $1.4\,\mu\Phi_0\,\mathrm{Hz}^{-1/2}$ with $L=13$ pH (Kawasaki *et al.*, 1991) and $2.2\,\mu\Phi_0\,\mathrm{Hz}^{-1/2}$ with $L=51$ pH (Cantor *et al.*, 1995); the corresponding noise energies were about 3×10^{-31} JHz^{-1} and 2×10^{-31} JHz^{-1}, respectively.

D. Flicker (1/*f*) noise

For many applications, for example biomagnetism (Sec. X.A) and magnetotellurics (Sec. X.D), one requires the low level of noise to extend down to frequencies of 1 Hz or lower; if that were the case, high-T_c SQUIDs would be adequate for most purposes. Unfortunately, low-frequency 1/*f* noise, which is observed in low-T_c SQUIDs but is generally not a serious issue, is a severe problem in high-T_c SQUIDs and a great deal of effort has been expended in attempting to understand its origins and reduce its magnitude. Early high-T_c dc SQUIDs made from polycrystalline YBCO films (Koch *et al.*, 1989) exhibited large levels of 1/*f* noise, which increased the noise energy at 1 Hz to above $10^{-26}\,\mathrm{JHz}^{-1}$. Since that time, there have been dramatic reductions in the level of 1/*f* noise, and the 1/*f* corner frequency f_c (the frequency at which the extrapolated values of the white noise and 1/*f* noise intersect) has been reduced from ~1 kHz to ~1 Hz.

Work on low-T_c dc SQUIDs (Koch *et al.*, 1983) showed that there are generally two separate sources of 1/*f* noise. One arises from the motion of vortices in the body of the SQUID: even when the SQUID is cooled in zero field, some fraction of the vortices formed at T_c remain pinned at defects. The vortex hopping rate increases exponentially as the pinning energy is reduced, so that the microstructure of the film and the related pinning energies play an important role in determining the low-frequency noise (Ferrari *et al.*, 1994). As we have seen in Sec. III, the microstructural quality of films is particularly crucial. When the SQUID is cooled in a nonzero magnetic field, in general the additional vortices so formed create high noise levels (Sec. IX.A). Unfortunately, one cannot relate the magnitude of the 1/*f* noise to any other measurable physical quantity, so that a direct noise measurement is the only means of characterizing the quality of a given film. It is important to note that 1/*f* noise due to vortex motion cannot be reduced by any bias reversal scheme.

The second source of 1/*f* noise is fluctuations in the critical current of the junctions which, as we saw in Sec. IV.C, can attain high levels. These fluctuations contribute in two independent ways: an ''in-phase'' mode, in which the critical currents of the two junctions fluctuate in phase to produce a voltage across the SQUID, and an ''out-of-phase'' mode in which the two fluctuating critical currents produce a current around the SQUID loop. Resistance fluctuations also contribute 1/*f* noise. However, at the low voltages where SQUIDs are operated critical-current fluctuations dominate, and we shall not address resistance fluctuations further.

The first measurements of flux noise in high-T_c dc SQUIDs made from epitaxial YBCO films and with well-defined grain-boundary junctions were made by Gross *et al.* (1990a, 1990b). Measuring the voltage noise directly with a low-T_c SQUID preamplifier, they found similar levels of 1/*f* noise for both their SQUIDs and, after they had cut the loop, for the individual junctions. Furthermore, at temperatures well below T_c the 1/*f* voltage noise of the SQUIDs was constant, independent of V_Φ, providing strong evidence that in-phase critical-current fluctuations dominated the SQUID noise below 1 kHz. At temperatures just below T_c, however, they found that the 1/*f* noise power scaled with V_Φ^2, and attributed this to the rapid increase in the flux noise near T_c observed by Ferrari *et al.* (1989). Subsequently, Koch *et al.* (1992) measured the 1/*f* noise in bicrystal grain-boundary SQUIDs using flux modulation alone and also flux modulation combined with bias reversal. At 77 K, they found that bias reversal reduced the 1/*f* noise power by up to two orders of magnitude, demonstrating that critical-current fluctuations dominate the 1/*f* noise observed in SQUIDs with high-quality thin films, and that one needs to reduce both the in-phase and out-of-phase components.

In practice, the reduction of 1/*f* noise with bias reversal is optimized empirically, but nonetheless, there are predictions for the magnitudes of the in-phase and out-of-phase contributions (Koch *et al.*, 1983; Foglietti *et al.*, 1986). The in-phase mode produces a voltage noise with a spectral density $S_V\approx(\partial V/\partial I_0)^2 S_{I_0}/2\approx(V-IR_d)^2\times S_{I_0}/2I_0^2$, and the out-of-phase mode produces a term $S_v\approx L^2 S_{I_0}V_\Phi^2/2$. Here, R_d is the dynamic resistance. As mentioned in Sec. IV.C, one can write $s_I=S_{I_0}(f)/I_0^2\approx a^2/f$, where a is temperature independent and approximately equal to $10^{-4}(R/\Omega)^{1/2}$ for a wide variety of junctions. From these results, one can derive the approximate expressions

$$S_\Phi^{1/2}(\text{in-phase})\approx s_I^{1/2}|V-IR_d|/\sqrt{2}V_\Phi \approx(70\ \ \mu\Phi_0\,\mathrm{Hz}^{-1/2})10^4 a\zeta v_\phi^{-1}(f/\mathrm{Hz})^{-1/2}, \tag{5.2a}$$

where $\zeta=|V-IR_d|/I_0R\sim1$, and

$$S_\Phi^{1/2}(\text{out-of-phase})\approx s_I^{1/2}\beta_L\Phi_0/2\sqrt{2} \approx(35\ \ \mu\Phi_0\,\mathrm{Hz}^{-1/2})10^4 a\beta_L(f/\mathrm{Hz})^{-1/2}. \tag{5.2b}$$

For optimized values of high-T_c dc SQUIDs at 77 K, $\beta_L=1$, $\Gamma=0.2$, and $I_0R=100\,\mu\mathrm{V}$, we estimate a flux noise of about 200 (100) $\mu\Phi_0$ $\mathrm{Hz}^{-1/2}$ at 1 Hz for the in-phase (out-of-phase) contribution, substantially above measured levels of white noise. These estimates are in reasonable agreement with experimental observations, and emphasize the need for bias reversal with any high-T_c SQUID used for low-frequency measurements.

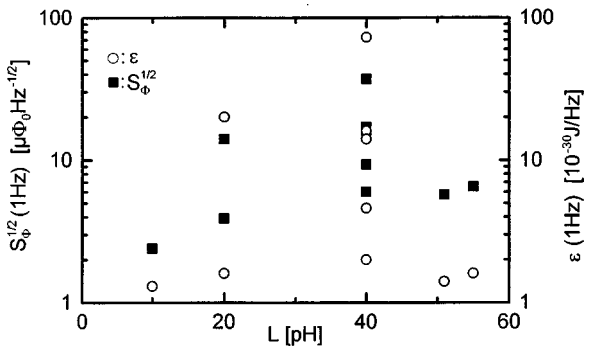

FIG. 21. $S_\Phi^{1/2}$ (1 Hz) and ε (1 Hz) of dc SQUIDs with various inductances, obtained at 77 K with flux modulation and bias reversal. (Data are from Koelle, Miklich, Ludwig *et al.*, 1993; Koelle, Miklich, Dantsker *et al.*, 1993; Koelle, Dantsker *et al.*, 1993; Miklich *et al.*, 1993; Cantor *et al.*, 1995; Lee *et al.*, 1995; Faley, Poppe, Urban *et al.*, 1995; Friedl *et al.*, 1992 and Grundler *et al.*, 1995).

We conclude this discussion with examples of $1/f$ noise in dc SQUIDs cooled in nominally zero magnetic field. In Fig. 21 we plot $S_\Phi^{1/2}(1\text{ Hz})$ and ε (1 Hz) for ten SQUIDs, with L between 10 and 55 pH, obtained with flux modulation and bias reversal. In the best devices, the noise energies approach $10^{-30}\,\mathrm{JHz}^{-1}$ at 1 Hz, a performance that is very adequate provided the SQUIDs can be coupled to appropriate pickup loops without further increases in the $1/f$ noise. However, as we discuss in Sec. IX.A, the level of $1/f$ noise in SQUIDs cooled in an ambient magnetic field such as that of the earth can be much higher than in zero field unless the linewidths are kept suitably narrow.

VI. dc SQUID MAGNETOMETERS

SQUIDs are mostly used as magnetometers or gradiometers. However, although SQUIDs are exquisitely sensitive to magnetic flux, their small area generally makes them relatively insensitive to magnetic field. An exception is the large square-washer design used for both dc and rf SQUIDs, which we discuss in Secs. VI.A and VII.A, respectively. Apart from these cases, one usually couples an additional superconducting structure to the SQUID to enhance its sensitivity to magnetic field; the magnetic-field noise is $S_B^{1/2}(f)=S_\Phi^{1/2}(f)/A_{\mathrm{eff}}$, where A_{eff} is the effective area of the magnetometer. Clearly, one endeavors to make A_{eff} as large as possible without increasing $S_\Phi(f)$ so as to produce high sensitivity to magnetic fields.

A. Square-washer designs

In this SQUID configuration (Ketchen 1981; Jaycox and Ketchen, 1981) a square washer with outer length D focuses flux into a square inner hole of length d. The effective area is dD (Ketchen *et al.*, 1985), and the inductance is $L_h=1.25\,\mu_0 d$ for $W=(D-d)/2>d$ (Jaycox and Ketchen, 1981). In practice, however, the incorporation of the two Josephson junctions into the SQUID loop modifies these expressions for A_{eff} and L. Five high-T_c dc SQUIDs grown on bicrystal substrates are shown in Fig. 11, and differ in the placement of the junctions intersecting the SQUID loop. In type A the junctions are outside the washer, and are thus far away from the region of strong field compression. The slit of length $l\approx W$ between the SQUID hole and the junctions can cause a significant increase in A_{eff} over the value dD, for example by a factor of 2.5 for $D=250\,\mu$m and $d=25\,\mu$m (Miklich *et al.*, 1993). More importantly, it increases the inductance by $L_{\mathrm{slit}}\approx(0.3-0.4\,l/\mu\mathrm{m})\,\mathrm{pH}$ (Wen, 1969). Thus, if one wishes to limit the total inductance to 40 pH, the maximum washer size is 200 μm even if there is no hole ($d=0$) as in type A/A. In contrast, for types B or C, the inductance is approximately L_h, independent of the washer size D. However, the effective area A_{eff} is significantly less than dD for $D\gg d$, because of the focusing of flux into the slits outside the SQUID loop (Miklich *et al.*, 1993; Tanaka *et al.*, 1994). The latter effect is minimized in type A/C: for example, for $D=500\,\mu$m and $L=40\,$pH one finds $A_{\mathrm{eff}}\approx 0.015\,\mathrm{mm}^2$, roughly a factor of two larger than for type B or C with the same values of D and L or for a 40-pH type A/A SQUID (Ludwig, Dantsker, Koelle, Kleiner, Miklich, Nemeth *et al.*, 1995).

A general calculation of the SQUID inductance and effective area requires a numerical treatment, for example solving the London equations for the specific geometry. Several groups have performed such calculations (Chang, 1981; Hosoya *et al.*, 1989; Sheen *et al.*, 1991; Töpfer, 1991; Uhlmann and Töpfer, 1992; Hildebrandt and Uhlmann, 1995). More simply, one can estimate the SQUID inductance by summing the inductance of the hole L_h the inductance of the slit L_{slit} which may be modeled as two coplanar striplines, and the inductance of the junction striplines $L_j=L_{j,g}+L_{j,k}$, which has a geometric and kinetic term. For a homogeneous current distribution the kinetic term is approximately $L_{j,k}\approx\mu_0(\lambda^2/t)2l_j/w$, where λ is the London penetration depth, t the film thickness, w the junction width and l_j the length of the junction striplines (Meservey and Tedrow, 1969). The contribution of L_j should be small, typically a few pH, if l_j/w is kept close to unity. This estimate of L should be accurate to within $\pm 10\%$.

For most dc SQUIDs with these geometries, the relatively small effective area implies that $S_B^{1/2}$ is inadequate for most applications. For example, with $A_{\mathrm{eff}}=0.015\,\mathrm{mm}^2$ and $S_\Phi^{1/2}=10\,\mu\Phi_0/\mathrm{Hz}^{-1/2}$ one finds $S_B^{1/2}=1.3\,\mathrm{pT/Hz}^{-1/2}$ well above the resolution of 10–100 $\mathrm{fT/Hz}^{-1/2}$ typically required. However, larger washers (Koelle, Miklich, Ludwig *et al.*, 1993; Tanaka *et al.*, 1994) have achieved a magnetic-field noise of about 150 $\mathrm{fT/Hz}^{1/2}$ at 1 kHz and 500 $\mathrm{fT/Hz}^{1/2}$ at 1 Hz with SQUID inductances of 40–100 pH and washers of 5–11 mm. Comparable performance has been achieved with flux-focusing plates of similar size coupled to washer SQUIDs $2\times 2\,\mathrm{mm}^2$ in size (Tanaka *et al.*, 1994; Itozaki *et al.*, 1996). The $1/f$ noise in these devices tends to be high, and in some cases the motion of vortices trapped in the washer limits the effectiveness of bias reversal in

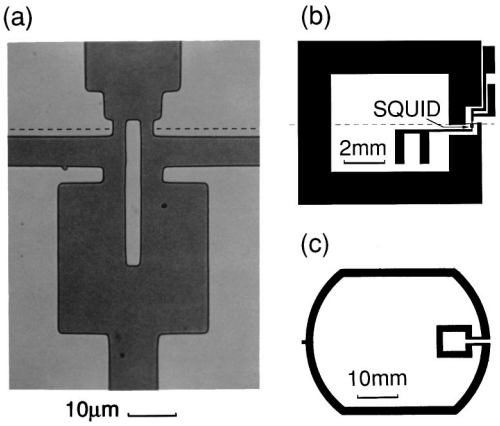

FIG. 22. Directly coupled magnetometer: (a) Photograph of 20 pH dc SQUID connected to the pickup loop shown in (b). Dashed line indicates grain boundary. (c) Configuration of single-layer YBCO flux transformer (Koelle, Miklich, Dantsker *et al.*, 1993).

reducing it (Koelle, Miklich, Ludwig *et al.*, 1993). Because of this limited performance, various alternative approaches for increasing the effective area have been pursued. There are two broad classes. The first is based on multilayer designs such as the flux transformer-coupled SQUID (Ketchen, 1981; Jaycox and Ketchen, 1981) (Sec. VI.C) or the fractional-turn SQUID (Zimmerman, 1971) (Sec. VI.D), which were successfully used for low-T_c magnetometers. However, the need for lower SQUID inductances and hence smaller SQUIDs for operation at 77 K has made optimum coupling of signal into the SQUID more challenging. Furthermore, multilayer high-T_c devices are more susceptible to excess $1/f$ noise and its reduction has been a major issue during the past years (Sec. III). As a result, single-layer designs have been developed which typically have less efficient coupling but benefit from straightforward fabrication, and lower levels of $1/f$ noise.

B. Directly coupled magnetometer

The directly coupled magnetometer (Matsuda *et al.*, 1991; Koelle, Miklich, Ludwig *et al.*, 1993) shown in Figs. 22(a) and (b) consists of a large pickup loop of inductance L_p and area A_p directly connected to the SQUID body of inductance $L \ll L_p$. A magnetic field B applied to the pickup loop induces a screening current $J = BA_p/L_p$, which in turn links a flux $(L-L_j)J$ to the SQUID. Here L_j is the parasitic inductance of the striplines incorporating the junctions, to which the current does not couple. The effective area is

$$A_{\rm eff} = (L-L_j)A_p/L_p \pm A_s, \tag{6.1}$$

where $A_s \ll A_{\rm eff}$ is the effective area of the bare SQUID. The sign of A_s depends on the relative senses of the SQUID and the pickup loop. Koelle, Miklich, Ludwig *et al.* (1993) investigated devices grown on STO bicrystals. In their best device, a 20 pH SQUID with $I_0 = 45\,\mu$A and $R = 3.4\,\Omega$ coupled to a 47 mm^2 pickup loop, they achieved a flux noise of 93 fT Hz$^{-1/2}$ at frequencies down to 1 Hz using bias reversal.

Subsequently, improvements in performance were achieved by reducing the large mismatch between L_p and L (Cantor *et al.*, 1995; Lee *et al.*, 1995). One can increase the ratio A_p/L_p by using a pickup loop with a large linewidth, $(d_1-d_2)/2$, where d_1 and d_2 are the outer and inner dimensions. In the limit $(d_1-d_2) > 2d_2$ in which $A_p = d_1 d_2$ and $L_p = 1.25\,\mu_0 d_2$, from Eq. (6.1) we find $A_{\rm eff} = 4d_1(L-L_j)/5\,\mu_0$; we have neglected A_s. Given the dependence of $S_\Phi(f)$ on L, I_0, and R discussed in Sec. II.C, one can then optimize $S_B(f)$.

Using Eq. (6.1) for $A_{\rm eff}$, together with Eqs. (2.8) and (2.9) over the ranges $0.01 < \Gamma\beta_L < 1$ and $0.4 < \beta_L < 5.6$, one finds

$$\frac{S_B^{1/2}}{(\text{fT Hz}^{-1/2})} = \frac{262\ \text{pH}}{L_{\rm th}} \frac{1}{(d_1/\text{mm})(L-L_j)/L_j} \times \left\{ \frac{1+\beta_L}{I_0R/\text{mV}} \left[\frac{80L}{L_{\rm th}} + \left(1 + \frac{4L}{L_{\rm th}} \right)^{4.1} - 1 \right] \right\}^{1/2}. \tag{6.2}$$

Clearly, $S_B^{1/2}$ scales with $1/d_1$. For a given value of L_j one can find a minimum in $S_B^{1/2}$ as a function of $L/L_{\rm th}$, which depends on I_0R and β_L. As mentioned in Sec. II.C, the noise can be optimized in different ways: one way is to keep $I_0R =$ constant and to vary I_0 by changing the junction area A_j. However, this is difficult to achieve for practical reasons, since large I_0R products are associated with high critical-current densities and hence the smallest values of I_0 are determined by the smallest linewidth that can be patterned. Alternatively, according to the scaling relation $I_0R \propto j_c^{1/2}$ found for many high-T_c junctions, one may keep I_0R^2 constant with fixed A_j and vary I_0, for example, by changing the oxygen content in grain-boundary junctions. In this case $(1+\beta_L)/(I_0R) \propto (1+\beta_L)/\beta_L^{1/2}$, which has a minimum at $\beta_L = 1$. The result of this optimization procedure is shown in Fig. 23 where we plot $S_B^{1/2}$ vs $L/L_{\rm th}$ for the stated values of I_0R, $L_{\rm th}$, L_j, d_1, and A_j and for six values of β_L ranging from 0.4 to 5.0. There is a shallow minimum at $L/L_{\rm th} \approx 0.3$, corresponding to $L \approx 100$ pH at 77 K. The dependence on β_L is weak, although $\beta_L = 1$ is optimum: the minimum magnetic-field noise varies from 11 to 13 fT Hz$^{-1/2}$ over the range of β_L plotted. Notice that the optimum value of $L/L_{\rm th}$, about 0.3, is rather higher than that for the lowest noise energy found in Sec. II.C. The reason is that the coupling efficiency between L_p and L increases more rapidly in this range than V_Φ decreases. In an earlier analysis based on the work of Enpuku, Tokita *et al.* (1995), Cantor (1996) found a shallow minimum in $S_B^{1/2}$ vs L corresponding to $S_B^{1/2} \approx 32$ fT Hz$^{-1/2}$ for $\beta_L = 1$, $d_1 = 9.3$ mm, $I_0R = 100\,\mu$V, and $L_j = 8.4$ pH; $S_B^{1/2}$ remained below 40 fT Hz$^{-1/2}$ for $30\,\text{pH} < L - L_j < 170\,\text{pH}$. This result differs somewhat from the prediction of Eq. (6.2) because Enpuku *et al.* find a faster reduction in V_Φ for $L/L_{\rm th} \gtrsim 0.4$ (Fig. 2).

The performance of directly coupled magnetometers with near optimum parameters can be appreciably bet-

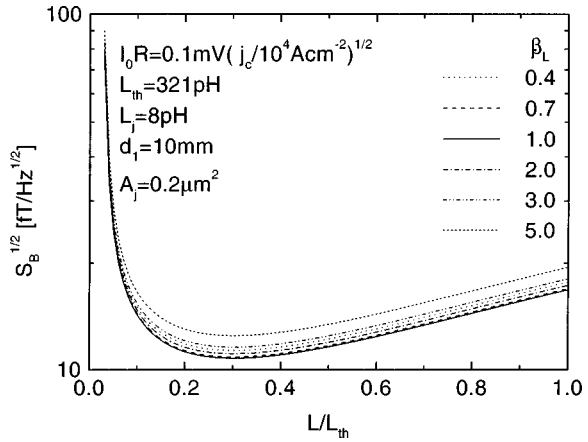

FIG. 23. Calculated rms magnetic-field resolution $S_B^{1/2}$ at 77 K vs normalized SQUID inductance $L/L_{\rm th}$ for directly coupled magnetometer in which the pick-up loop has an outer dimension $d_1=10$ mm. The curves were calculated for six values of β_L and fixed junction cross-section $A_j=0.2\,\mu\text{m}^2$ by varying j_c and hence $(I_0R)^2$.

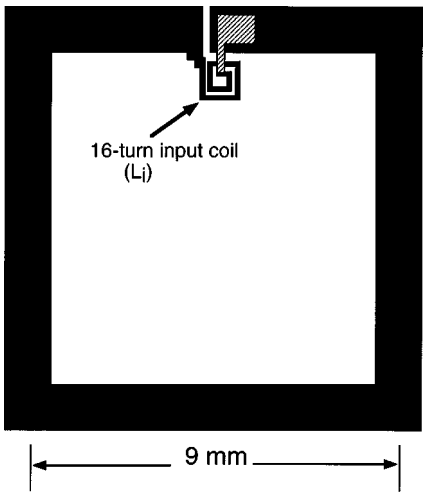

FIG. 25. Schematic layout of multilayer flux transformer (not to scale). Multiturn input coil (only two turns are shown) is either coupled to the SQUID in a flip-chip arrangement or deposited directly on top of it.

ter than that of the earlier devices. For $d_1=9.3$ mm, $d_2=3$ mm, and $L=50$ pH, Lee *et al.* (1995) and Cantor (1996) achieved best results of about 40 fT Hz$^{-1/2}$ at 1 kHz and 60 fT Hz$^{-1/2}$ at 1 Hz (with bias reversal). Using a 19×19 mm^2 pickup loop on a 20×20 mm^2 bicrystal, the same group achieved 14 fT Hz$^{-1/2}$ at 1 kHz and 26 fT Hz$^{-1/2}$ at 1 Hz (Fig. 24) (Cantor *et al.*, 1995). In similar work, Glyantsev *et al.* (1996) reported a noise level as low as 20 fT Hz$^{-1/2}$ at 1 kHz for a 150 pH SQUID coupled to a pickup loop with an outer diameter of 8 mm. However, they did not use bias reversal, and the noise was well above 100 fT Hz$^{-1/2}$ at 1 Hz. Recently, using an STO bicrystal with a 30° misorientation angle and a pickup loop with $d_1=9$ mm and $d_2=3$ mm, Beyer *et al.* (1998) obtained 23 fT Hz$^{-1/2}$ at 1 kHz and 67 fT Hz$^{-1/2}$ at 1 Hz. These values were achieved with bias reversal in the PTB magnetically shielded room; the noise at low frequencies was dominated by environmental noise.

To complete this section, we note that the effective area of the directly coupled magnetometer can be further increased by coupling it in a flip-chip arrangement to a single-layer flux transformer [Fig. 22(c)] on a separate substrate (Koelle, Miklich, Dantsker *et al.*, 1993). The small loop of the transformer (which is inductively coupled to the magnetometer pickup loop) has inductance $L_{\rm ti}$ and area $A_{\rm ti}$ and is in series with the large loop of inductance $L_{\rm tp}$ and area $A_{\rm tp}$. The effective area is

$$A_{\rm eff}\approx\frac{L-L_j}{L_p}\left(A_p+\frac{A_{\rm tp}\alpha_t(L_pL_{\rm ti})^{1/2}}{L_{\rm ti}+L_{\rm tp}}\right), \tag{6.3}$$

where α_t is the coupling coefficient between $L_{\rm ti}$ and L_p. For the devices shown in Fig. 22, the transformer yielded a gain of 3.4 and the magnetic-field noise improved to 31 fT Hz$^{-1/2}$ at 1 kHz and 39 fT Hz$^{-1/2}$ at 1 Hz.

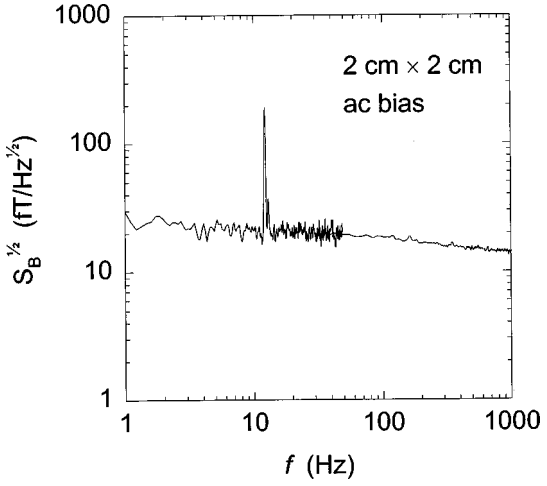

FIG. 24. Magnetic-field noise in a directly coupled magnetometer with bicrystal junctions and a 19×19 mm^2 pickup loop. The estimated inductance is 51 pH (Cantor *et al.*, 1995).

C. Flux transformer with multiturn input coil

The effective area of a SQUID may be efficiently enhanced by coupling it to a superconducting flux transformer with a multiturn input coil (Fig. 25). The transformer is a closed superconducting circuit consisting of a large-area pickup loop and a much smaller, multiturn input coil to couple flux into the SQUID. A magnetic field applied to the pickup loop induces a supercurrent that conserves the total magnetic flux and induces flux into the SQUID. The total effective area of the magnetometer is given by

$$A_{\rm eff}=A_pM_i/(L_i+L_p)\pm A_s\,, \tag{6.4}$$

where A_s is the effective area of the bare SQUID (including flux focusing, see Sec. VI.A), A_p and L_p are the area and inductance of the pickup loop, $M_i=\alpha(LL_i)^{1/2}$ is the mutual inductance between the SQUID inductance L and the input-coil inductance L_i, and α is the

coupling coefficient. The sign of A_s depends on the sense of the winding of the coil relative to the pickup loop. Assuming that α does not depend on L_i and L and making certain approximations (Martinis and Clarke, 1985), one finds the effective area is maximum when $L_i = L_p$:

$$A_{\text{eff}} = \alpha A_p (L/L_p)^{1/2}/2; \tag{6.5}$$

we have neglected A_s. In contrast to the directly coupled magnetometer (Sec. VI.B), the flux transfer into the SQUID can be optimized for a given value of L_p by varying the number of turns n on the input coil until $L_i = L_p$. For low-T_c SQUIDs integrated with multiturn input coils, the relations between M_i, L_i, L, and n (Ketchen, 1981) for the tightly coupled limit are usually in good agreement with experimental data (Jaycox and Ketchen, 1981). For high-T_c magnetometers on the other hand, there are only a few experimental studies on the coupling between the input coil and the SQUID (David *et al.*, 1995; Ludwig, Dantsker, Koelle, Kleiner, Miklich, Nemeth *et al.*, 1995; Kugai *et al.*, 1996), and the situation is less well understood. Ludwig, Dantsker, Koelle, Kleiner, Miklich, Nemeth *et al.* (1995) found that although α depends strongly on the SQUID design, being higher for type A/A and A/C than for type B and C devices (Fig. 11), it can be greater than 0.5 even for flip-chip magnetometers. Coupling the same transformer to different SQUID types, these authors showed that A_{eff} is proportional to A_s, that is, the magnetic-field gain is constant. According to Eq. (6.5), A_{eff} increases with increasing SQUID inductance L, but larger values of L do not necessarily produce lower magnetic-field noise. Using Eq. (6.5) one finds $S_B = 8(S_\Phi/2L)L_p/\alpha^2 A_p^2$, so that minimizing S_B with respect to L is equivalent to minimizing the noise energy $\varepsilon = S_\Phi/2L$. From Fig. 5 we know that for 77 K and $\beta_L = 1$, the (effective) SQUID inductance should not exceed 40–50 pH, although one should bear in mind that Eq. (6.5) is valid only so long as α is independent of L and L_i. We note also that the flux transformer reduces the effective SQUID inductance to $L[1-\alpha^2 L_i/(L_i + L_p)]$ (Zimmerman, 1971). However, this correction is small for $L_i = L_p$ and $\alpha \lesssim 0.5$.

1. Flip-chip magnetometers

The advantage of the flip-chip configuration over the integrated magnetometer is that problems related to the junction process can be separated from those related to the interconnect technology. One forms a flip-chip magnetometer by clamping the SQUID and the flux transformer chips together with either photoresist or a thin mylar sheet between them. The input coil and pickup loop of the transformer are usually patterned in one YBCO layer, and the crossover between the innermost turn of the coil and the pickup loop in the other. The first YBCO flux transformer with a multiturn input coil operating at 77 K was made by Wellstood *et al.* (1990) using shadow masks. The first multilayer flip-chip magnetometers were reported almost simultaneously by groups at Berkeley (Miklich *et al.*, 1991; Wellstood *et al.*, 1992) and IBM (Oh *et al.*, 1991). Since this early work, many groups have described the fabrication of multiturn flux transformers (Freltoft *et al.*, 1993; Hilgenkamp *et al.*, 1993) and the operation of flip-chip magnetometers at 77 K (Grundler, David *et al.*, 1993; Miklich *et al.*, 1993; Roas *et al.*, 1993; Keene, Goodyear *et al.*, 1994, Keene *et al.*, 1995; Dantsker *et al.*, 1995; Fife *et al.*, 1995; Ludwig, Koelle *et al.*, 1995; Scharnweber *et al.*, 1995; Schilling *et al.*, 1995; Kugai *et al.*, 1996).

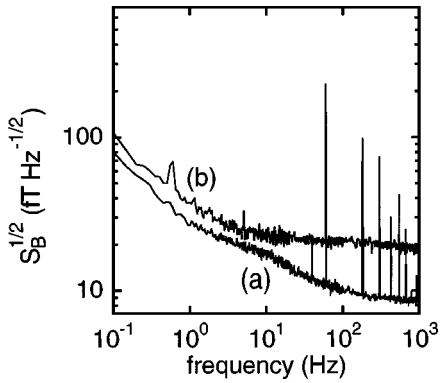

FIG. 26. Magnetic-field noise of (a) flip-chip magnetometer with a 9×9 mm^2 pickup loop and 16-turn input coil (Dantsker *et al.*, 1995), (b) the $\frac{1}{16}$-turn, 7-mm-diameter SQUID shown in Fig. 28 (Ludwig, Dantsker, Kleiner *et al.*, 1995).

The lowest magnetic-field noise was achieved by Dantsker *et al.* (1995), who used an 81 mm^2 pickup loop and a 16-turn input coil coupled to a 500 μm washer SQUID (type A/A in Fig. 11) with bicrystal junctions: 8.5 fT Hz$^{-1/2}$ at 1 kHz and 27 fT Hz$^{-1/2}$ at 1 Hz (Fig. 26). This performance depended critically on both the technology for fabricating multilayer structures with low levels of low-frequency flux noise and the use of a SQUID with a low flux noise. The uncoupled SQUID had a peak-to-peak modulation voltage $V_{pp} = 55\,\mu$V and a white flux noise of $7.3\,\mu\Phi_0$ Hz$^{-1/2}$. The flux transformer was aligned so that the crossover covered about 90% of the length of the SQUID slit, reducing the SQUID inductance from 70 to about 30 pH, close to the optimum. As a result, V_{pp} increased to 108 μV, and the flux noise decreased to $4.9\,\mu\Phi_0$ Hz$^{-1/2}$.

During the progressive reduction in $1/f$ magnetic-field noise from that in the first flip-chip magnetometer (Miklich *et al.*, 1991), 1.7 pT Hz$^{-1/2}$ at 1 Hz, to that reported by Dantsker *et al.* (1995), it was important to understand the sources of excess flux noise in these multilayer structures. According to the model of Ferrari *et al.* (1991) and Wellstood *et al.* (1991), there are two distinct mechanisms by which this noise is coupled into the SQUID. First, the SQUID senses directly the magnetic flux produced by a vortex moving in the YBCO films of the flux transformer ("direct noise"). Second, a vortex moving perpendicularly to a YBCO line induces a screening current in the transformer to conserve the total magnetic flux, coupling flux into the SQUID ("indirect noise"). Together with flux-noise measurements on various components of transformers, the model has been used to analyze sources of excess flux noise (Lud-

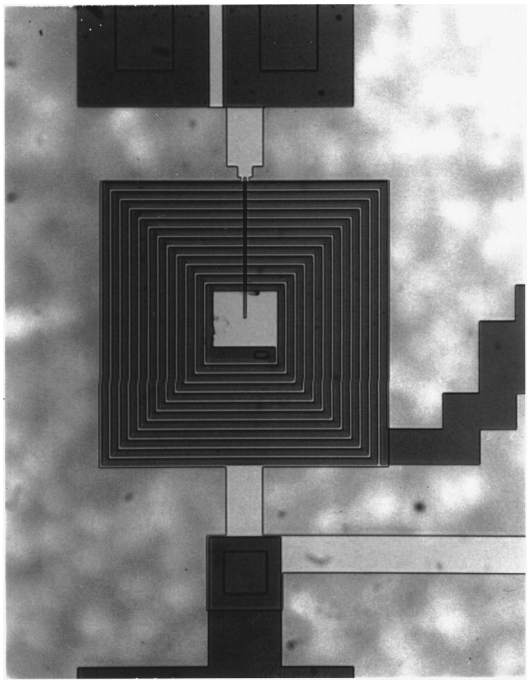

FIG. 27. Photograph of 12-turn input coil and SQUID of an integrated magnetometer with 500-μm SQUID washer located in lower YBCO layer. Bicrystal junctions are outside the washer.

wig, Koelle *et al.*, 1995; Ludwig, Dantsker, Koelle, Kleiner, Miklich, and Clarke, 1995), but it does not account for the degraded quality of YBCO films at the edges of crossovers and vias. To study the spatial distribution of critical-current densities and thus locate potential noise sources, several groups have successfully used such techniques as low-temperature scanning electron microscopy (Husemann *et al.*, 1993; Hollin *et al.*, 1994; Gerber *et al.*, 1996), low-temperature laser scanning microscopy (Sivakov *et al.*, 1994), magneto-optical imaging (Govorkov *et al.*, 1997) and scanning micro-Raman spectroscopy (Dieckmann *et al.*, 1996).

2. Integrated magnetometers

In an attempt to improve the inductive coupling between the SQUID and the input coil, several groups have integrated them on the same chip, thus reducing the spacing to the thickness of the insulating layer. Early monolithic SQUID magnetometers involving three YBCO layers and operating at 77 K (Lee *et al.*, 1991; DiIorio, Yoshizumi, Yang, Maung, and Power, 1993) exhibited large levels of low-frequency flux noise. As a result, attention turned to a simplified design requiring only two superconducting layers (Kromann *et al.*, 1993; Hilgenkamp *et al.*, 1994; David *et al.*, 1995; DiIorio *et al.*, 1995; Ludwig, Dantsker, Koelle, Kleiner, Miklich, Nemeth *et al.*, 1995; Shen *et al.*, 1995). In all cases, the insulator was $SrTiO_3$. The SQUID washer is used as either a crossunder or crossover for the flux transformer, obviating the need for an extra superconducting layer. The input coil and SQUID of such a magnetometer are shown in Fig. 27. The lowest magnetic-field noise was reported by Drung, Ludwig *et al.* (1996) using a magnetometer with 36° $SrTiO_3$ bicrystal junctions fabricated at NKT (Shen *et al.*, 1995), namely 9.7 fT Hz$^{-1/2}$ at 1 kHz and 53 fT Hz$^{-1/2}$ at 1 Hz. Whereas the effective area $A_{\rm eff}=1.72\,{\rm mm}^2$ for the $8.3\times8.6\,{\rm mm}^2$ pickup loop is comparable to that measured by others for their integrated devices, the SQUID parameters $R=9\ \Omega$ and $I_0=5.7\ \mu$A for an inductance of about 130 pH are close to optimum.

Despite this impressive performance, integrated magnetometers do have some disadvantages. One problem, reported by several groups, is that the V-Φ curves are often distorted by microwave resonances (Hilgenkamp *et al.*, 1994; Ludwig, Dantsker, Koelle, Kleiner, Miklich, Nemeth *et al.*, 1995; Drung, Ludwig *et al.*, 1996). Such resonances have not been reported for flip-chip magnetometers. These resonances in the input-coil-washer structure are well known from low-T_c devices to degrade the SQUID performance (Ryhänen *et al.*, 1989). Enpuku *et al.* (1997) and Minotani, Enpuku *et al.* (1997) recently reported the calculation of distorted V-Φ characteristics in good agreement with the data measured on high-T_c devices under the assumption that there is a parasitic capacitance between the input coil and the SQUID washer. Hilgenkamp *et al.* (1995) eliminated the resonances by means of a resistor between the SQUID and the input coil that shunted this parasitic capacitance. Another drawback is that the yield of high-performance integrated devices is well below that of flip-chip, multilayer devices. Finally, there is no compelling evidence that the coupling coefficient of integrated magnetometers is significantly higher than that for flip-chip devices (Ludwig, Dantsker, Koelle, Kleiner, Miklich, Nemeth *et al.*, 1995).

D. Multiloop magnetometer

An alternative multilayer approach to achieving large effective areas is the multiloop magnetometer or fractional-turn SQUID, originally proposed and demonstrated by Zimmerman (1971) with a machined niobium device. The essential idea is to connect N loops in parallel, thus reducing the total inductance to a level acceptable for a SQUID, while keeping the effective area large. Drung *et al.* (1990, 1991) developed sensitive multiloop SQUID magnetometers, based on their niobium thin-film technology; with eight parallel loops and a diameter of 7.2 mm these devices have a typical noise of 1.5 fT Hz$^{-1/2}$ down to a few Hz at 4.2 K. These devices have been used successfully for multichannel biomagnetic studies (Koch, Cantor *et al.*, 1991; Drung and Koch, 1993).

In the thin-film multiloop magnetometer, shown schematically in Fig. 28(a), N loops (for clarity, only four are drawn) are connected in parallel with the connection made at the center via coplanar lines. The two junctions connect the upper and lower superconducting films of the central trilayer. Compared with a flux-transformer-coupled magnetometer, the multiloop magnetometer

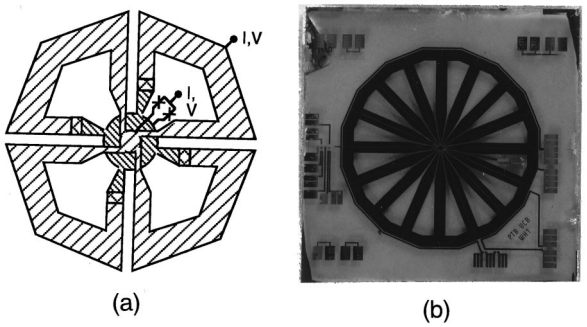

FIG. 28. Multiloop magnetometer: (a) Schematic layout of $\frac{1}{4}$-turn SQUID magnetometer. Cross-shaded regions indicate vias between upper and lower superconducting films. (b) Photograph of $\frac{1}{16}$-turn YBCO SQUID with outer diameter of 7 mm. Junctions are located close to the center (Ludwig, Dantsker, Kleiner *et al.*, 1995).

has the advantage that the current induced in each of the N loops when it is rotated in the earth's magnetic field is much smaller than that induced in a single loop of the same area. Furthermore, the device contains no closed superconducting loops, so that the maximum induced supercurrent is limited to the critical current of the junctions.

A comprehensive theory for thin-film multiloop SQUIDs and their performance at 77 K has been given by Drung *et al.* (1995). The effective area $A_{\rm eff}$ and inductance $L_{\rm eff}$ are given by

$$A_{\rm eff}=A_p/N-A_s \tag{6.6}$$

and

$$L_{\rm eff}=L_p/N^2+L_s/N+L_j. \tag{6.7}$$

Here, A_p and L_p are the area and inductance of the large, outer loop, A_s and L_s are the average area and inductance of one spoke of the cartwheel, and L_j is the parasitic inductance of the connections from the pickup loops to the junctions. Calculation of the magnetic-field noise and transfer function as a function of N, based on the simulations of Enpuku *et al.* (1993) for $V_\Phi(L)$ and $S_\Phi^{1/2}$, shows that the optimum value of N for a minimum magnetic-field noise increases strongly with the overall size. For a diameter of 7 mm, the optimum number of loops is 15 to 20, considerably more than typically used in the low-T_c case. Using these calculations, Drung *et al.* (1995) designed a high-T_c multiloop SQUID with 16 parallel loops and an outer diameter of 7 mm. They estimated $L_{\rm eff}=145$ pH, which is at the upper limit of acceptability for 77 K operation (Sec. II.C), and $A_{\rm eff}=1.77\,{\rm mm}^2$.

In the first practical realization of this magnetometer, Ludwig, Dantsker, Kleiner *et al.* (1995) used their YBCO-$SrTiO_3$-YBCO multilayer technology and bicrystal junctions to make the magnetometer shown in Fig. 28(b). Most of the area of the pickup loops is patterned in the upper YBCO film, and each loop makes contact to the lower YBCO layer in the center (cross-shaded region). The two 24° bicrystal junctions are located in the lower YBCO film and also make contact to the upper and lower YBCO films in the central trilayer region. A voltage modulation as high as 20 μV was observed despite the relatively high inductance, and resulted from the nearly ideal junction parameters, $I_0=13\,\mu$A and $R=10\,\Omega$. The effective area of 1.89 mm^2 was close to the predicted value. Using a flux-locked loop with 100 kHz flux modulation and bias reversal, the authors measured a magnetic-field noise of 18 fT Hz$^{-1/2}$ at 1 kHz and 37 fT Hz$^{-1/2}$ at 1 Hz (Fig. 26). Similar multiloop magnetometers based on the same design were subsequently made, using step-edge junctions (David *et al.*, 1996; Drung, Dantsker *et al.*, 1996) or PBCO ramp junctions (Reimer, Schilling *et al.*, 1995; Reimer, Ludwig *et al.*, 1995).

Two other high-T_c magnetometers involving multiloops differ from the design discussed above. Fife *et al.* (1995) coupled eight multiloop pickup coils with an outer diameter of 8.5 mm directly to a low-inductance washer SQUID with bicrystal junctions. The noise at 60 K with bias reversal was 100 fT Hz$^{-1/2}$ above 3 Hz. Scharnweber and Schilling (1996, 1997) recently reported an integrated magnetometer in which a flux transformer with a multiturn input coil and a multiloop pickup coil is inductively coupled to a low-inductance washer SQUID. For their best magnetometer, with four parallel loops 8.5 mm in diameter, at 77 K they measured a magnetic field noise of 44 fT Hz$^{-1/2}$ at 1 kHz with a static bias current and 100 fT Hz$^{-1/2}$ at 1 Hz with bias reversal.

E. Comparison of magnetometers

Given the plethora of magnetometer designs, which should one choose for a particular application? Of course, integrated, multilayer magnetometers—the multiturn flux transformer grown on a square washer SQUID or the fractional-turn SQUID—are very appealing and offer the highest sensitivity for a given area, at least in the white noise. Unfortunately, the currently low yield of junctions with acceptable values of I_0 and R means that the yield of integrated magnetometers with high performance is correspondingly low. Consequently, on a commercial basis their price is correspondingly high, probably too high for most real-world applications. Thus one should examine the alternatives, namely single-layer and flip-chip, multilayer magnetometers.

The directly coupled magnetometer is appealing in its simplicity, requiring only a single layer in a bicrystal or step-edge junction technology. Noise levels below 30 fT Hz$^{-1/2}$ have been achieved on $10\times10\,{\rm mm}^2$ bicrystals and below 20 fT Hz$^{-1/2}$ on $20\times20\,{\rm mm}^2$ bicrystals; however, the larger bicrystals are currently very expensive. Fortunately, provided one can avoid an increase in the low-frequency noise in the presence of the earth's magnetic field (Sec. IX), the performance of the magnetometers on the smaller chip is adequate for geophysics, and probably also for magnetocardiology. Nonetheless, despite the simplicity of fabricating these single-layer devices, one has to accept the fact that the chip-to-chip variability in the junction parameters currently ensures

that the yield of high-performance magnetometers is less than 100%. Even though substrates can be repolished and reused two or three times, the cost of manufacturing a single magnetometer with low noise is likely to remain higher than desirable.

An alternative philosophy is to fabricate (say) ten square-washer SQUIDs on a $10\times10\,\mathrm{mm}^2$ chip, select the best and dice the chip accordingly. Experience suggests that one should obtain several SQUIDs with low noise with this procedure. One then couples each of these selected devices to a multiturn flux transformer in a flip-chip arrangement. Thus one separates the fabrication of the single-layer SQUIDs from the multilayer process for the flux transformer. As a further step towards lowering the cost of flux transformers dramatically, one should develop processes for depositing them in quantity on two-inch or preferably four-inch wafers using coevaporation (Berberich *et al.*, 1994; Matijasevic *et al.*, 1997). If one could develop such large-scale processing for flux transformers, for the currently available junction technologies this approach would appear to be the most economical, and could be used for all applications.

VII. rf SQUIDs

Although there has been substantially more effort to develop high-T_c dc SQUIDs, progress with rf SQUIDs has been excellent. Several groups have investigated rf SQUIDs (for example, Zani *et al.*, 1991; Tinchev and Hinken, 1992; Tinchev, 1997) but since the most concentrated effort has been made at FZ, Jülich, we shall largely focus on their work. We note that the main body of this work preceded the theory of Chesca (1998), and that a great deal of progress was made on largely empirical grounds. Furthermore, it is difficult to measure the critical current of the junction precisely without opening the loop, so that in at least some of the devices reported it is not clear whether β_L' was greater or less than unity. It is possible that some of them were operated in a ''mixed mode'' in which the signal was produced by variations in both inductance and dissipation. For these reasons, it is often impracticable to compare the experimental results with theoretical predictions.

A. rf SQUIDs with lumped resonant circuits

The first rf SQUID magnetometers with high sensitivity (Zhang, Mück, Herrmann *et al.*, 1992; Zhang, Mück *et al.*, 1993) consisted of large YBCO square washers with step-edge, grain-boundary junctions [Fig. 29(a)], grown on $10\times10\,\mathrm{mm}^2$ $SrTiO_3$ substrates. The junctions were generally formed along the inner edge of the square washer to avoid the large parasitic inductance of the long slit. The SQUID was inductively coupled to the inductor of an LC tank circuit, which was resonant at 20 MHz in the early experiments. Subsequently, these authors increased the resonance frequency to about 150 MHz to increase the flux-to-voltage transfer coefficient and to reduce the level of white noise (see Sec. II). In addition to the rf excitation, the SQUID was flux modulated in the usual way and operated in a flux-locked loop. The SQUIDs could be operated in both the hysteretic and nonhysteretic modes. For example, Zhang, Mück, Herrmann *et al.* (1992) reported a transfer function greater than $40\,\mu\mathrm{V}/\Phi_0$ for SQUIDs in either mode, operated at 150 MHz.

Zhang, Mück *et al.* (1993) varied both the outer and inner dimensions (d_1 and d_2) of the square washer to find the optimum magnetic-field sensitivity. The effective area d_1d_2 increases with both d_1 and d_2, while the inductance L scales with d_2. Since $S_\Phi^{1/2}$ increases with L for both hysteretic and nonhysteretic modes, although with a different functional dependence, one expects to find a minimum. The optimum value, $170\,\mathrm{fT\,Hz}^{-1/2}$, occurred for $d_2\approx150\,\mu\mathrm{m}$, and corresponded to a flux noise of $7\times10^{-5}\,\Phi_0\,\mathrm{Hz}^{-1/2}$; the noise was white at frequencies down to 1 Hz. For larger inner dimensions the flux noise increased more rapidly than the effective area. At the time, this performance was the best obtained for a high-T_c magnetometer at 77 K.

There are several points to note about this result. First, the estimated inductance of this rf SQUID, about 240 pH, is larger than that of any useful dc SQUID. As a result, the effective area is substantially higher than for dc SQUIDs. In fact, the flux noise and noise energy of this rf SQUID are unremarkable by the standards of dc SQUIDs: it is the large effective area that produces the relatively low magnetic-field noise. The lack of $1/f$ noise is notable, and occurs for two reasons. In the first instance, as will be discussed in Sec. VII.C, the combination of rf and low-frequency flux modulation eliminates $1/f$ noise due to fluctuations in critical current. Of course, this scheme cannot reduce flux noise due to the motion of vortices in the square washer. Second, the relatively high level of white flux noise is now a virtue in that the $1/f$ knee is moved to a correspondingly low frequency.

Zhang, Mück *et al.* (1993) improved the performance of this device by coupling it to a flux concentrator, made of bulk YBCO, 43 mm in diameter. This magnetometer exhibited a white noise of $60\,\mathrm{fT\,Hz}^{-1/2}$ at frequencies down to about 5 Hz; the additional $1/f$ noise was due to flux noise in the concentrator. Subsequently, Zhang *et al.* (1994) fabricated single-layer rf SQUIDs with several directly coupled pickup loops, improving the noise to $120\,\mathrm{fT\,Hz}^{-1/2}$. They also fabricated a device in which the SQUID, in the form of a slit, was coupled to a $9\times9\,\mathrm{mm}^2$ pickup loop, and achieved $90\,\mathrm{fT\,Hz}^{-1/2}$ down to about 4 Hz. They achieved their best performance, however, by coupling a $8\times8\,\mathrm{mm}^2$ square washer SQUID with a $200\times200\,\mu\mathrm{m}$ hole to a single-layer flux transformer [inset, Fig. 30(a)] in a flip-chip arrangement. With a pickup loop of $40\times40\,\mathrm{mm}^2$ they achieved a magnetic-field noise of $24\,\mathrm{fT\,Hz}^{-1/2}$ at frequencies down to 0.5 Hz [Fig. 30(a)].

More recently, Ockenfuß *et al.* (1997) made a systematic study of thin-film, single-layer flux transformers. The flux transformers were deposited on either 1″ or 2″ diameter substrates. Each transformer in turn was

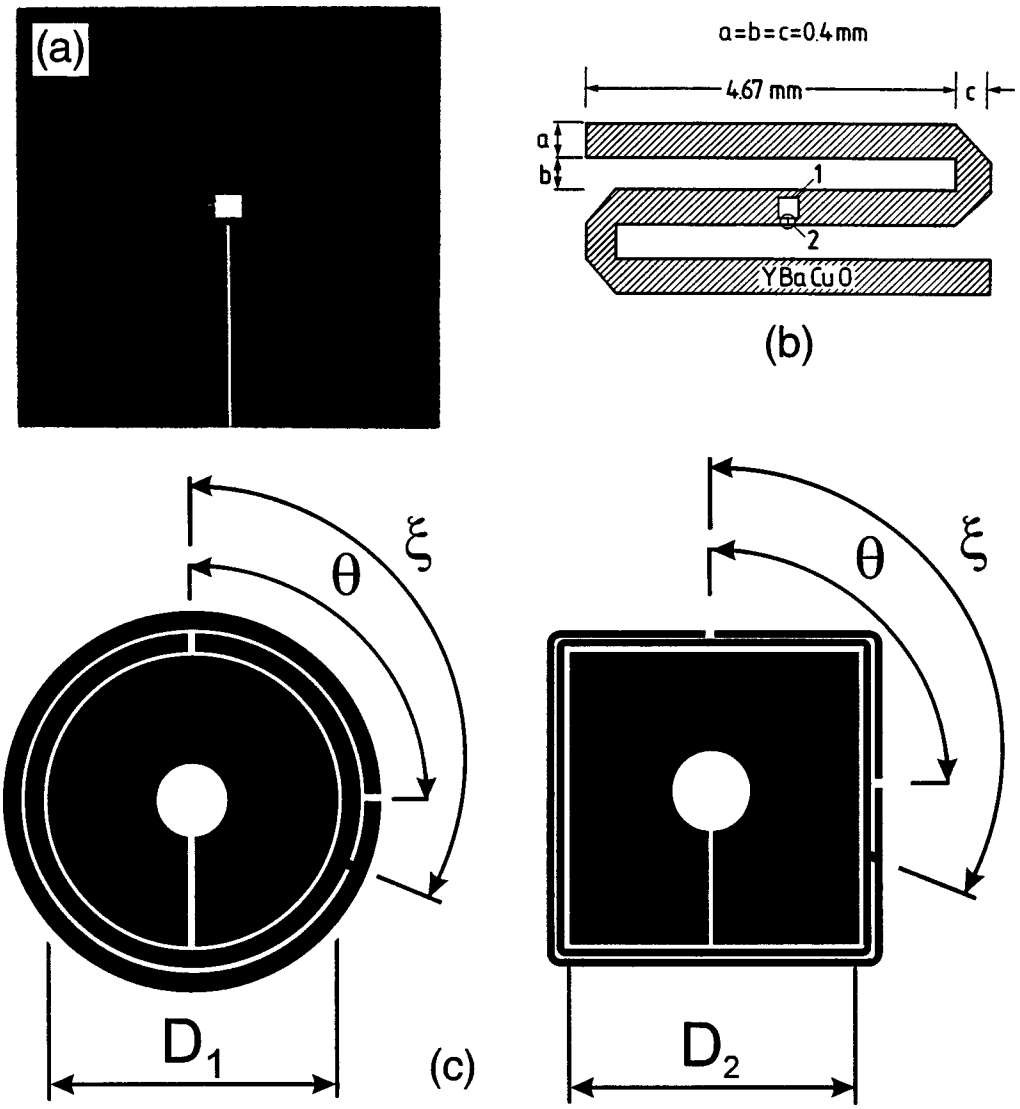

FIG. 29. Selection of rf SQUIDs from FZ, Jülich: (a) 6×6 mm^2 square-washer SQUID (Zhang, Mück, Hermann, *et al.*, 1993), (b) S-shaped microstrip SQUID (Zhang, Mück, Bode *et al.*, 1992), (c) coplanar microwave resonators (Zhang, Wolters *et al.*, 1997).

coupled in a flip-chip arrangement to an rf SQUID with a 200×200 μm^2 hole in an 8×8 mm^2 washer, operated at 200 MHz. The authors systematically reduced the width w_p of the pickup loop and measured the effective area and gain of the magnetometer. The maximum effective areas of 2.93 mm^2 and 4.94 mm^2 for the 1″ and 2″ transformers, respectively, were achieved for the maximum values of w_p, 8.2 and 19.0 mm; the corresponding magnetic field gains were 2.71 and 4.57. The magnetic-field noise above 10 Hz for these two cases was 52 fT Hz$^{-1/2}$ and 30 fT Hz$^{-1/2}$.

As a final remark, we note that all of the rf SQUIDs described above were at least somewhat undercoupled, that is, $\kappa^2Q<1$, so that the performance was less than optimum. Very recently, He *et al.* (1998) used a scheme in which they inductively coupled the lumped LC-resonant circuit to a coil that is connected to the 50 Ω transmission line supplying the rf signal. This approach, which was demonstrated at frequencies from 221 to 950 MHz, increases κ^2Q and reduces the flux noise compared with that obtained with conventional tank circuits.

B. rf SQUIDs with distributed element resonators

The devices described above involve lumped tank circuits consisting of a wire-wound coil and a capacitor. The flux noise achieved represents the limit of what can be achieved at 150–200 MHz. As is evident from Eq. (2.15), further reductions in noise require high-frequency operation, but it then becomes difficult to achieve the required high values of Q with lumped circuits. As a result, devices operating at higher frequencies have involved various kinds of microwave resonators (Daly *et al.*, 1991; Zhang, Mück, Bode *et al.*, 1992, Zhang *et al.*, 1995, Zhang, Soltner, Wolters *et al.*, 1997, Zhang, Zander *et al.*, 1997, Zhang, Wolters *et al.*, 1997; Hein *et al.*, 1995). Zhang, Mück, Bode *et al.* (1992) described an S-shaped microstrip resonator with the 100×100 μm^2 SQUID loop in its central region [Fig. 29(b)]; subsequently, the loop was reduced to 100×100 μm^2 (Mück, 1993), with the longer side parallel to the edge of the resonator. The microstrip was formed by placing the

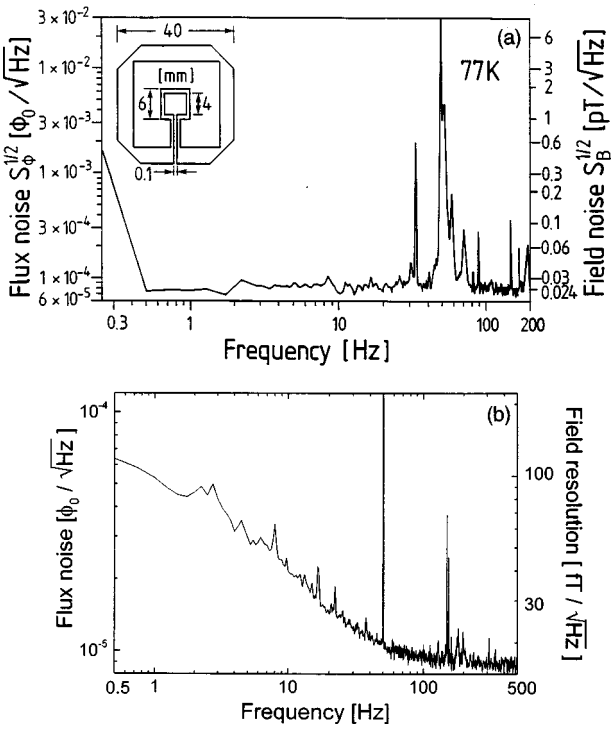

FIG. 30. Noise of rf SQUID magnetometers: (a) Magnetic flux and magnetic-field noise of 150-MHz SQUID with single-layer flux transformer with the configuration shown in the inset (Zhang *et al.*, 1994). (b) Magnetic-field noise of microwave resonator SQUID with 13-mm flux concentrator shown in Fig. 29(c) (Zhang, Wolters *et al.*, 1997).

0.5-mm-thick $LaAlO_3$ substrate on a copper groundplane, and coupled to the room-temperature electronics via a 50 Ω coaxial cable. At 3 GHz, the best of these devices yielded a flux noise of $1.6\times10^{-5}\,\Phi_0\,\text{Hz}^{-1/2}$, corresponding to a noise energy of about $6\times10^{-30}\,\text{JHz}^{-1}$. However, the small effective area of the SQUID resulted in a relatively high magnetic-field noise, about 1 $\text{pT Hz}^{-1/2}$.

Subsequently, Zhang and coworkers improved the magnetic-field sensitivity of microwave SQUIDs operating at about 1 GHz. In their first design, Zhang *et al.* (1995) used a stack of $10\times10\times1\,\text{mm}^3$ $SrTiO_3$ substrates, stacked face-to-face, as a dielectric resonator. The stack was placed above a $4\times4\,\text{mm}^2$ washer SQUID with a $60\times60\,\mu\text{m}^2$ inner hole. The stack was driven at resonance via a capacitively coupled line and the output voltage was also coupled out capacitively via a second line. With a frequency of 0.911 GHz and under optimum conditions, the flux noise was $10^{-5}\,\Phi_0\,\text{Hz}^{-1/2}$ and the magnetic-field noise was 105 $\text{fT Hz}^{-1/2}$; the latter noise was improved to 30 $\text{fT Hz}^{-1/2}$ by means of a single-layer flux transformer with a 22 mm pickup loop.

In a later design, Zhang, Soltner, Wolters *et al.* (1997) used an integrated resonator in which the circular rf SQUID was surrounded by a line, patterned in the same YBCO film, containing a gap that provided the capacitance necessary for the resonant circuit. The signal from the resonator was coupled out either capacitively or inductively; inductive coupling has the advantage that the coil can also be used for both flux modulation and flux feedback. At frequencies from 0.511 to 1.1 GHz typical values of Q were around 5000, so that the requirement $\kappa^2 Q \gtrsim 1$ was readily achievable. In the latest version of this device, Zhang, Zander *et al.* (1997) and Zang, Wolters *et al.* (1997) used the coplanar resonator designs shown in Fig. 29(c). Two coplanar lines surround the flux concentrator, which is coupled to the rf SQUID washer (2.5 or 3.5 mm in diameter) in a flip-chip configuration. The relative position of the gaps in the coplanar lines and the location of a short between them allows one to adjust the resonance frequency. For a SQUID with a $10\times500\,\mu\text{m}^2$ inner hole ($L\approx260\,\text{pH}$) coupled to a resonator with a 13-mm-diameter flux concentrator, Zhang, Wolters *et al.* (1997) obtained a white flux noise of $8.5\times10^{-6}\,\Phi_0\,\text{Hz}^{-1/2}$, corresponding to a noise energy of $6\times10^{-31}\,\text{JHz}^{-1}$ and a magnetic-field noise of 16 $\text{fT Hz}^{-1/2}$ [Fig. 30(b)]. The noise at 1 Hz, however, was substantially higher, about 100 $\text{fT Hz}^{-1/2}$, and most likely arose from the motion of vortices in the resonator. This configuration is particularly appealing in its simplicity, enabling one to design the device with appropriate parameters very straightforwardly and offering simple fabrication with a minimum of additional cryogenic components.

In a further step towards higher sensitivity, very recently Zhang *et al.* (1998) described a new design in which a multiturn flux transformer is integrated with the coplanar resonator. The pickup loop is connected to two coils, a multiturn coil to couple in low-frequency signals and a single-turn coil to couple in rf currents. A two-hole SQUID is coupled to these coils in a flip-chip configuration to form a magnetometer. The separation of rf and low-frequency currents is a key factor that enables the authors to achieve a high quality factor.

C. 1/*f* noise

In the rf SQUIDs described above the onset of 1/*f* noise generally occurs at a relatively low frequency—1 Hz or less—provided one uses a flux-locked loop. This low 1/*f* knee frequency is due in part to the fact that the white flux noise is generally higher than for dc SQUIDs, but the major reason is the action of the readout scheme in eliminating 1/*f* noise arising from critical-current fluctuations (Giffard, 1980; Mück, Heiden, and Clarke 1994). We first describe this effect for hysteretic SQUIDs.

We first consider the effect on $V_T^{(0)}$ [Eq. (2.11)] of a fluctuation δI_0 in I_0 at a frequency much less than $\omega_{\text{rf}}/2\pi$. The value of Φ_c is increased to $L(I_0+\delta I_0)$, so that the transitions from the $k=0$ state to the $+1$ and -1 states occur at the flux values $L(I_0+\delta I_0)$ and $-L(I_0+\delta I_0)$, respectively. As a result, $V_T^{(0)}$ is increased to

$$\tilde{V}_T^{(0)} = \omega_{\text{rf}} L_T(\Phi_c + L\,\delta I_0)/M. \tag{7.1}$$

We see that 1/*f* noise in the critical current results in a 1/*f* noise component in the demodulated rf voltage.

However, when the SQUID is flux modulated and operated in a flux-locked loop, the effect of critical-current fluctuations is greatly reduced. Consider the effect of an applied flux $\delta\Phi<\Phi_0/2$ on the characteristics shown in Fig. 6. The asymmetry introduced into the hysteresis loops causes the SQUID to make its transition from the $k=0$ to the $k=+1$ state at a lower rf flux, reducing the voltage across the tank circuit to

$$V_T^{(\delta)}=\omega_{\rm rf}L_T(\Phi_c-\delta\Phi)/M \quad (0<\delta\Phi<\Phi_0/2). \tag{7.2}$$

In the region DF of Fig. 6(c), the SQUID traverses only the $k=0\leftrightarrow k=+1$ hysteresis loop. Similarly, if we now change the flux to $-\delta\Phi$ ($|\delta\Phi|<\Phi_0/2$), the voltage is

$$V_T^{(-\delta)}=\omega_{\rm rf}L_T|(-\Phi_c+\delta\Phi)|/M \quad (-\Phi_0/2<\delta\Phi<0). \tag{7.3}$$

The SQUID now traverses only the $k=0\leftrightarrow k=-1$ hysteresis loop; the modulus sign in Eq. (7.3) reflects the fact that the detection of the peak value of the rf voltage is insensitive to whether the transition occurs on a positive or negative peak of the rf current. Suppose now that I_0 undergoes a slow fluctuation to a new value $I_0+\delta I_0$. The peak voltage across the tank circuit changes to

$$\tilde{V}_T^{(+\delta)}=\omega_{\rm rf}L_T(\Phi_c+L\,\delta I_0-\delta\Phi)/M \quad (0<\delta\Phi<\Phi_0/2) \tag{7.4}$$

and

$$\tilde{V}_T^{(-\delta)}=\omega_{\rm rf}L_T|-(\Phi_c+L\,\delta I_0)+\delta\Phi|/M \quad (-\Phi_0/2<\delta\Phi<0). \tag{7.5}$$

We see that the effect of a (say) positive fluctuation δI_0 is to increase $\tilde{V}_T$ uniformly for all values of applied flux; correspondingly, the demodulated voltage vs flux curve will be shifted uniformly to a higher voltage. However, when the usual modulating flux at frequency f_m with a peak-to-peak amplitude of $\Phi_0/2$ is applied to the SQUID, the amplitude of the resulting voltage at f_m is unaffected by this shift. Thus, when this signal is mixed down with the same frequency f_m, the resulting quasistatic output voltage is unaffected by fluctuations in the critical current. Any slow fluctuations in the amplitude of the rf driving current are similarly suppressed.

Mück, Heiden, and Clarke (1994) examined the $1/f$ noise in Nb rf SQUIDs operated in the hysteretic mode at 4.2 K. For a SQUID at 3 GHz, operated in a flux-locked loop with conventional flux modulation, they found that the flux noise was white at frequencies down to below 0.5 Hz. However, when they operated the SQUID open loop in the absence of flux modulation, the spectral density of the noise was $1/f$ at frequencies below about 1 kHz, and three orders of magnitude higher at 1 Hz than in the previous measurement. These results show very clearly that the conventional operating mode of the rf SQUID eliminates the effects of critical-current fluctuations.

In the case of nonhysteretic rf SQUIDs ($\beta_L'<1$), the critical current is small so that the amplitude of the $1/f$ noise fluctuations in the critical current, which scales as I_0, is also correspondingly low. This factor contributes to the low level of $1/f$ flux noise observed in these devices (Chesca, 1998). In addition, flux modulation suppresses $1/f$ flux noise due to critical-current fluctuations (Mück, Clarke, and Heiden, 1994). The value of the tank circuit voltage V_T is proportional to I_0 [Eq. (2.19)], but in addition V_Φ also depends on I_0 [Eq. (2.20)]. As a result, a fluctuation in I_0 results in not only a fluctuation in the component of V_T at the same frequency but also in the amplitude of the component at the flux modulation frequency. Since, however, the feedback loop is (ideally) sensitive only to the phase of the flux modulation, these amplitude fluctuations will not contribute to the output of the phase-sensitive detector. Thus critical-current fluctuations are suppressed by modulation and feedback as in the hysteretic mode.

VIII. GRADIOMETERS

In Sec. VI we described magnetometers with a white noise level below 10 fT $\mathrm{Hz}^{-1/2}$, a sensitivity adequate for most practical applications. However, in many of these applications—good examples are magnetocardiology and nondestructive evaluation—one needs to detect weak signals against a background of magnetic noise that is many orders of magnitude higher. In urban environments, the dominant source of noise is the 50 or 60 Hz signals, and a large number of harmonics, from power lines: peak-to-peak amplitudes can range from 20 nT to 1 μT. Additionally, traffic (trains, subways, cars) can cause even stronger disturbances. For this reason, most sensitive measurements with low-T_c magnetometers—particularly of biomagnetic signals—are currently made in a magnetically shielded room. However, except for enclosures, such as that at the PTB, Berlin, with very high levels of attenuation, most shielded rooms do not reduce the 50 or 60 Hz fields sufficiently, and one requires a gradiometer to discriminate against distant noise sources with small gradients in favor of nearby signal sources. The traditional low-T_c gradiometer is wound from niobium wire: two pickup loops wound in opposition and mounted on a common axis with a baseline (separation) of typically 0.1 m are connected in series with an input coil inductively coupled to a SQUID (Zimmerman and Frederick, 1971). Such a device measures the first-derivative axial gradient $\partial B_z/\partial z$. The addition of a third coil midway between the two loops results in a second-derivative gradiometer measuring $\partial^2 B_z/\partial z^2$. In the case of axial gradiometers, the separation of one pickup loop and the signal source is generally made rather less than the baseline, so that the instrument effectively detects the magnetic field from the source. Thin-film gradiometers have also been made, measuring either an axial gradient (Hoenig *et al.*, 1991) or more usually planar devices measuring an off-diagonal gradient of the form $\partial B_z/\partial x$ (Hämäläinen *et al.*, 1993).

Early wire-wound gradiometers were balanced by adjusting the positions of small, superconducting pellets, sometimes to an accuracy of 1 part in 10^6. (We define

"balance" as the ratio of the output of the SQUID when a uniform magnetic field is applied to the gradiometer to the output when the same field is applied to one pickup loop.) However, a myriad of interacting, mechanically adjusted components becomes impractical for more than a few channels. Current practice is to use magnetometers and first-derivative gradiometers for the software generation of second or third derivatives (Vrba, 1996).

The lack of suitable wire eliminates the wire-wound, high-T_c gradiometer as an option, and two alternative approaches have been adopted. The first is an electronic gradiometer made by subtracting the signals from separate magnetometers: the gradiometer can be axial or planar, and the baseline can be chosen at will. The second is a planar gradiometer with thin-film pickup loops.

A. Electronic subtraction gradiometers

A high-T_c, axial gradiometer was demonstrated by Tavrin *et al.* (1993a), who mounted two rf SQUIDs one above the other, each with a bulk flux focuser (Zhang, Mück, Herrmann *et al.*, 1992). One sensor was mounted rigidly while the plane inclination of the second, placed 60 mm above, could be adjusted from outside the cryostat to achieve a balance of about 1 part in 10^3. This system was used to measure magnetocardiograms (MCG) (Sec. X.A) in an unshielded environment, against a 50 Hz background of 1 to 20 nT, although the quality of the cardiograms was limited by $1/f$ noise in the magnetometers, about 1 pT $\mathrm{Hz}^{-1/2}$. Subsequently, Tavrin *et al.* (1994) added a third, vertically stacked sensor to form a second-derivative gradiometer. The lowest sensor was rigidly mounted, while the inclination of the other two, 60 and 120 mm above it, could be adjusted. The three channels, A, B, and C could be added electronically to generate two first-derivatives, $A-B$ and $B-C$, and the second derivative, $A-2B+C$. The system could be balanced to achieve a common mode rejection ratio of 1 part in 3000 and a gradient rejection of 1 part in 100. The magnetic-field noise referred to SQUID A or C was below 300 fT $\mathrm{Hz}^{-1/2}$. Once balanced, the unit required no readjustment after thermal cycling and after transporting it over long distances in the course of examining some 200 human subjects. A similar electronically formed axial gradiometer was recently reported by Borgmann *et al.* (1997) who used a set of adjustable superconducting plates, similar to those in early low-T_c gradiometers, to achieve the final balance. The authors achieved a balance better than 10^4 for uniform background fields and better than 200 for gradient fields. Electronic gradiometers have also been constructed with the magnetometers in the same plane (David *et al.*, 1997; ter Brake, Janssen *et al.*, 1997).

The balance of an electronic gradiometer is limited by the linearity of the flux-locked magnetometers and by the common mode rejection ratio of the subtraction system. In the presence of high background noise, the dynamic range and slew rate of the magnetometers may be challenged. None of these difficulties arises with superconducting gradiometers, which thus have an inherent advantage over electronic cancellation. However, the three-SQUID gradiometer (TSG) of Koch *et al.* (1993), shown in Fig. 31, also circumvents these problems by using electronic cancellation and subtraction. The center, reference magnetometer operates in a flux-locked loop and applies its output also to a coil coupled to each of the outer magnetometers. Thus the environmental noise at each of the two sensing magnetometers is greatly attenuated, reducing their linearity and slew-rate requirements. The signals from the outer two sensors are then subtracted to form a first-derivative gradiometer. Koch and co-workers demonstrated several versions of the TSG, with baselines of 0.1 to 0.25 m and using both low-T_c and high-T_c SQUIDs. The balance can be adjusted to about 1 part in 4000 by adjusting the feedback currents with room-temperature resistors. A key advantage of this approach is that any noise generated by the central sensor is applied equally to the two outer magnetometers and eliminated in the subtraction. As a result, one can use less sensitive SQUIDs to generate the canceling fields or even a total-field magnetometer, such as a flux gate, which can be used to cancel not only the fluctuating fields but also the static field. However, one difficulty with most flux gates is that their bandwidth is typically limited to 100 Hz, so that they cannot be used to cancel harmonics of the 50 or 60 Hz signal. In their original publication, Koch *et al.* reported a white gradient noise of 6 pT m^{-1} $\mathrm{Hz}^{-1/2}$ for SQUIDs with 3×3 mm^2 flux-focusing washers. For a baseline of 0.1 m, this result corresponds to a magnetic-field noise of 600 fT $\mathrm{Hz}^{-1/2}$ referred to one sensor.

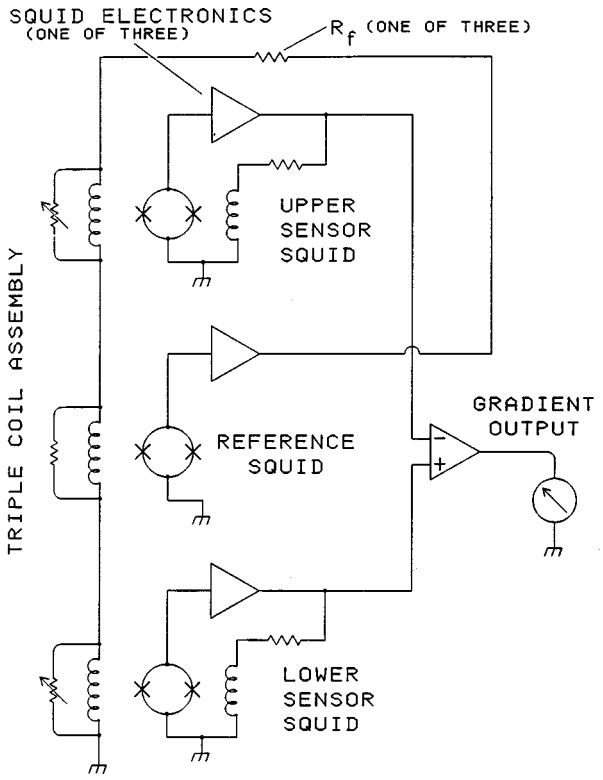

FIG. 31. Configuration of three-SQUID gradiometer (Koch *et al.*, 1993).

B. Gradiometric flux transformers

Electronic subtraction enables one to choose an arbitrary baseline and to adjust the balance externally. Experience with low-T_c devices, however, shows that it is notoriously difficult to operate such systems in the harsh environment of a laboratory or a hospital and to achieve an adequate signal-to-noise ratio for clinical applications. Low-T_c systems intended for unshielded operation invariably have a gradiometric flux transformer to bear the brunt of the large level of background noise; even then, an adequate signal-to-noise ratio in unfavorable situations may not be possible (Vrba, 1996). Thus there are strong incentives to develop high-T_c equivalents, albeit in planar geometries. An early gradiometer fabricated from a YBCO-STO-YBCO multilayer (Eidelloth *et al.*, 1991) employed a multiturn input coil coupled to two pickup loops of opposite senses in the same plane. The baseline was about 5 mm. The multiturn coil was coupled to a square-washer SQUID in a flip-chip arrangement. At the time, multilayer technology was still in its infancy and the device exhibited substantial levels of $1/f$ noise. The best reported gradient noise at 10 Hz was 400 $\mathrm{pT\,m^{-1}\,Hz^{-1/2}}$. A similar flip-chip gradiometer with improved $1/f$ noise was reported later by Keene, Chew *et al.* (1994). However, both gradiometers exhibited poor balance because of the unbalanced SQUID. The balance was improved by two orders of magnitude to about 1 part in 1000 by means of gradiometrically configured SQUIDs (Keene, Chew *et al.*, 1994; Keene *et al.*, 1995).

An alternative gradiometer configuration (Ketchen *et al.*, 1978) consists of two pickup loops in parallel with a SQUID measuring the current induced along the common line [(Fig. 32(a)]. This configuration has the disadvantage that large supercurrents are induced around the perimeter when the device is rotated in an ambient field. Knappe *et al.* (1992), Zakosarenko *et al.* (1994), Daalmans *et al.* (1995), Schultze, Stolz *et al.* (1997), Schmidl, Wunderlich, Dörrer, Specht *et al.* (1997) and Dörrer *et al.* (1997) have all made single-layer, first-derivative gradiometers of this kind, using dc SQUIDs with either step-edge or bicrystal junctions. The baselines are limited by the size of the substrate to about 5 mm, and the best gradient sensitivities are about 50 $\mathrm{pT\,m^{-1}\,Hz^{-1/2}}$. All the dc SQUID-based gradiometers described above have the disadvantage that the SQUID itself has a nonzero response to magnetic field, producing an intrinsic imbalance. This problem is circumvented in the rf SQUID-based gradiometer by Zhang, Soltner, Krause *et al.* (1997), resembling the configuration of Fig. 32(a), with a single, step-edge junction intersecting the central strip. This structure is a re-creation of the Nb "two-hole" rf SQUID (Zimmerman *et al.*, 1970). The device had a baseline of about 5 mm and was balanced to 1 part in 1000. The gradient field noise was about 100 $\mathrm{pT\,m^{-1}\,Hz^{-1/2}}$ above 10 Hz. One of these gradiometers was used to perform eddy-current measurements of cracks in aluminum in an unshielded environment.

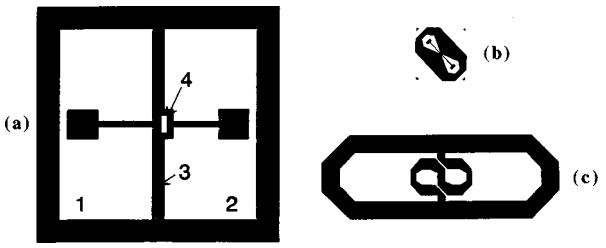

FIG. 32. Gradiometers: (a) Principle of single-layer, planar gradiometer with parallel inductances 1 and 2. A gradient $\partial B_z/\partial_x$ induces a current in the central strip 3 that links flux to the SQUID 4 (Daalmans, 1995). (b) First-derivative planar gradiometer on a $10\times10\,\mathrm{mm^2}$ chip that is coupled to (c) the gradiometric structure on a two-inch substrate (Faley *et al.*, 1997).

Several attempts have been made to extend the baseline using single-layer gradiometers in a flip-chip arrangement (Daalmans, 1995; Faley *et al.*, 1997). The concept is illustrated in Figs. 32(b) and (c) (Faley *et al.*, 1997), which shows a dc SQUID with quasiplanar PBCO junctions on a $10\times10\,\mathrm{mm^2}$ chip that is inductively coupled to a gradiometric flux transformer on a 50 mm substrate. The central strip in the transformer is intended to reduce the inductance and pickup area of the SQUID by screening. The baseline was 20 mm, the balance about 1 part in 1800 and the noise 5 $\mathrm{pT\,m^{-1}\,Hz^{-1/2}}$ at 1 kHz. A comparable sensitivity was reported by Daalmans (1995).

It should be noted that all the single-layer, thin-film gradiometers lose substantial sensitivity because the inductances of the pickup loops are mismatched to the input coil coupling them to the SQUID. This drawback, together with the relatively short baseline of even the largest devices (20 mm) implies that none of them is practicable for applications such as magnetocardiology. However, as demonstrated already, they may be well-suited to nondestructive evaluation (NDE). To achieve high enough sensitivity and a long enough baseline for magnetocardiology with this approach would require a multiturn input coil fabricated on a substrate at least 50 mm and preferably 100 mm in length. This somewhat daunting prospect has yet to be tackled.

A new approach to single-layer, thin-film gradiometers was recently demonstrated by Dantsker, Froehlich *et al.* (1997) who fabricated the asymmetric, planar gradiometer shown schematically in Fig. 33(a). The gradiometer consists of a directly coupled SQUID magnetometer with a pickup loop of inductance L_m and area A_m, and a superconducting flux transformer with an input loop of inductance L_i and area A_i connected to a pickup loop of inductance L_p and area A_p. The mutual inductance between the magnetometer and input loop is $M_i=\alpha(L_mL_i)^{1/2}$. With a suitable choice of these parameters, one attains the balance condition

$$\alpha=[A_m/(A_p+A_i)](L_p+L_i)/(L_iL_m)^{1/2} \tag{8.1}$$

for which the directly coupled magnetometer produces zero response to a uniform magnetic field B_z. On the other hand, a magnetic field δB_z applied only to the

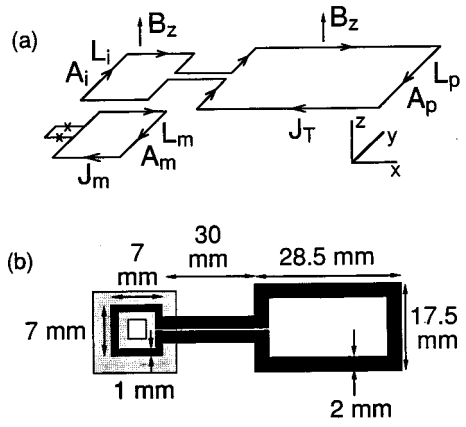

FIG. 33. Configuration of asymmetric, planar gradiometer coupled to a directly coupled magnetometer: (a) schematic, (b) experimental (shaded square represents magnetometer) (Dantsker, Froehlich *et al.*, 1997).

magnetometer and the input loop induces a current $\delta J_m = \eta \delta B_z A_m / L_m$ in the magnetometer loop, where

$$\eta = [L_p/L_i + 1 - \alpha(L_m/L_i)^{1/2} A_i/A_m]/(L_p/L_i + 1 - \alpha^2) \tag{8.2}$$

represents the screening effect of the flux transformer.

The physical configuration of the gradiometer is shown in Fig. 33(b). The single-layer directly coupled magnetometer was patterned in a 150-nm-thick YBCO film laser-deposited on a $10 \times 10\,\mathrm{mm}^2$ $SrTiO_3$ bicrystal. The outer and inner dimensions of the magnetometer loop are 10 and 2 mm, respectively, yielding an estimated inductance $L_m = 4$ nH and area $A_m = 20$ mm^2. The flux transformer was fabricated from a 260-nm-thick YBCO film coevaporated on a 100 mm *r*-plane sapphire wafer. For these dimensions, balance is predicted to occur for $\alpha = 0.43 \pm 0.04$. The corresponding value $\eta = 0.95$ implies that the flux transformer reduces the intrinsic sensitivity of the magnetometer by only 5%. The baseline—the separation between the midpoints of the two loops—is 48 mm.

The gradiometer was balanced by sliding the flux transformer over the magnetometer, immersed in liquid nitrogen, thereby varying the coupling coefficient α. A balance of about 1 part in 3000 was achieved with respect to magnetic fields perpendicular to the plane of the gradiometer, while the intrinsic balance with respect to in-plane fields was about 1 part in 1400. Operated in an unshielded environment, the gradiometer reduced the 60 Hz peak by a factor of 1600 compared with the bare magnetometer.

This approach to gradiometers has several advantages. The fact that the intrinsic magnetic-field sensitivity of the magnetometer is reduced by only a few percent by the presence of the transformer is particularly appealing for high-T_c devices, for which resolution is at a premium. It should not be necessary to use particularly high quality films, since vortex motion in a flux transformer with a relatively large area and inductance does not contribute significantly to the overall $1/f$ magnetic-field noise (Koelle, Miklich, Dantsker *et al.*, 1993). The general principle can be extended to other derivatives of the magnetic field: for example, the addition of a second, identical pickup loop on the opposite side of the input loop would produce a gradiometer sensitive to $\partial^2 B_z / \partial x^2$. The high degree of balance and long baseline make this gradiometer eminently suitable for multichannel arrays for biomagnetic measurements. However, it would be impracticable to balance these gradiometers mechanically—a more realistic approach might be to mount the transformer permanently on the magnetometer and to achieve the final balance by laser trimming.

Finally, which of these gradiometers should one use? Currently, the two major applications are biomagnetism and NDE (Secs. X.A and X.B). For NDE, one generally does not require particularly high sensitivity, and a relatively compact, single-layer gradiometer with a baseline of 5–10 mm is likely to be adequate. For biomagnetism, the situation is more complex. Good results have been achieved with electronic subtraction of magnetometers, but limitations of slew rate, linearity and CMRR present difficulties for unshielded operation. Still, this approach is the only one that can measure an axial gradient. For the immediate future, at least, gradiometric flux transformers are limited to planar configurations. Ideally, one would like to fabricate a long-baseline gradiometer with a multiturn, multilayer input coil, with an inductance to match that of the pick-up loops, inductively coupled to the SQUID. In practice, the cost of manufacturing such structures on large substrates—say, four inch—is likely to be prohibitive. The best alternative would seem to be the asymmetric, planar gradiometer, provided it can be balanced adequately without recourse to mechanical adjustment.

IX. SQUID'S IN UNSHIELDED ENVIRONMENTS

Sections VI and VII illustrate the low levels of magnetic flux and field noise achieved with high-T_c SQUIDs and magnetometers. All these results, however, were obtained with the devices cooled and operated inside magnetic shields which attenuate the ambient static and time-varying fields by large factors. In this section, we discuss the operation of high-T_c SQUIDs in the ambient environment, without magnetic shielding, as is essential for some applications. For example, it is obviously impractical to shield an airplane wing undergoing nondestructive evaluation. In the case of geophysical applications, one measures fluctuating magnetic fields generated either naturally or by man-made sources, and has no option other than to operate the magnetometer unshielded. In biomagnetic measurements, magnetically-shielded rooms large enough to enclose a patient and multiple SQUID sensors are commercially available and have been widely used with low-T_c SQUIDs, but their price—as high as \$0.5 M—adds substantially to the overall cost of the system. This is particularly true for systems with a relatively small number of channels, for example, for magnetocardiology, and the elimination of the MSR would do much to make such techniques more financially accessible.

A SQUID exposed to the ambient environment is adversely affected by a variety of sources. These can be categorized into sources that are extrinsic—arising directly from the environment—and sources that are intrinsic to the SQUID. Examples of environmental noise sources are nearby power lines (typical amplitudes are 20 nT–1 μT at 50 or 60 Hz), computer displays (40 to 80 Hz), lasers, elevators, and automobiles. These extrinsic noise sources and their harmonics and intermodulation products obscure the signal of interest such as a magnetocardiogram, and their reduction requires gradiometers (Sec. VIII) or active cancellation. One possible intrinsic effect is the reduction of the critical current, resulting in a decrease in the transfer function and an increase in the white noise. For example, Miklich *et al.* (1994) found that the critical current of their 3-μm-wide bicrystal junctions decreased by 15% when they were cooled in a 100 μT field. However, this problem can be largely eliminated by reducing the width of the junctions: Dantsker, Tanaka, and Clarke (1997) found an insignificant reduction in the critical current of 1-μm-wide junctions cooled in 130 μT. We note that ramp-edge junctions are intrinsically shielded and also suffer a negligible critical current reduction in comparable fields (Faley, Poppe, Urban *et al.*, 1995).

A. 1/*f* noise

The low-frequency flux noise power of most high-T_c SQUIDs increases when they are cooled in the earth's field, by as much as a factor of 50. This increase is caused by the thermally activated hopping of weakly pinned vortices which penetrate the YBCO film during cooling. Ferrari *et al.* (1994) used a low-T_c dc SQUID to measure the noise in YBCO films cooled in static fields B_0 and found that at low frequencies $S_\Phi(f)$ scaled as $1/f$ for cooling fields above a few μT. Furthermore, $S_\Phi(f)$ scaled linearly with B_0 [Fig. 34(a)], as expected for the uncorrelated hopping of vortices since $S_\Phi(f)$ is expected to be proportional to the number of vortices and hence to B_0. Miklich *et al.* (1994) found similar increases for a dc SQUID [Fig. 34(b)] and a directly coupled magnetometer, although $S_\Phi(f)$ did not always scale linearly with B_0. Other authors (Faley, Poppe, Urban *et al.*, 1995; Tanaka *et al.*, 1995; Glyantsev *et al.*, 1996) confirmed these findings, in SQUIDs, and Keene *et al.* (1996) found that the low-frequency noise of their planar gradiometers increased substantially for cooling fields above 15 μT. The flux noise for the SQUID in Fig. 34(b) at $B_0 = 50\,\mu$T is about $200\,\mu\Phi_0/\mathrm{Hz}^{-1/2}$ at 1 Hz. Even coupled to the best flux transformer described in Sec. VI.C, this excess noise would limit the magnetic-field resolution to about 400 $\mathrm{fT/Hz}^{1/2}$, an order of magnitude greater than that of the most sensitive sensors in zero field. Recently, however, Schmidt *et al.* (1996) showed that the flux noise in one of their directly coupled magnetometers, about $10\,\mu\Phi_0\,\mathrm{Hz}^{-1/2}$ at 1 Hz, was nearly independent of magnetic field up to 100 μT, but gave no details of the fabrication process or geometry.

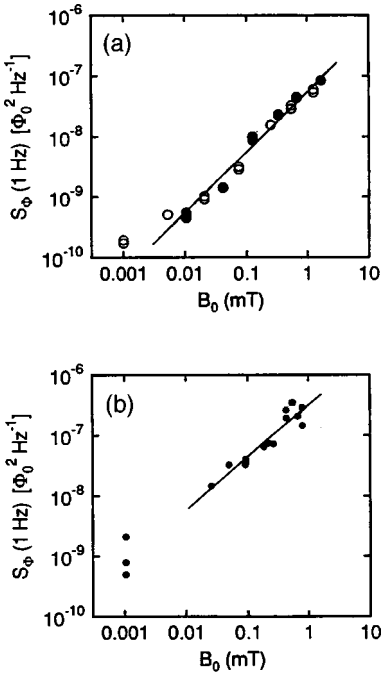

FIG. 34. Flux noise S_Φ (1 Hz) vs cooling field B_0: (a) for a YBCO film at 77 K, measured with a low-T_c SQUID. Filled and open circles indicate reversed direction of B_0, line is least-squares fit. (b) for YBCO dc SQUID with bicrystal junctions and 250-μm washer, measured with bias reversal (Miklich *et al.*, 1994).

Reduction of the excess $1/f$ noise in SQUIDs operated in unshielded environments is clearly essential. One must eliminate either the motion or the presence of flux vortices, and we now examine the approaches that have been investigated.

To reduce the motion of a given density of vortices, one has to create strong pinning sites. Shaw *et al.* (1996) showed that proton or heavy-ion irradiation of single crystals of YBCO not only increased the critical-current density but also reduced the $1/f$ noise substantially. However, the critical-current densities were still substantially lower and the $1/f$ noise in ambient fields still substantially higher than the values in thin films. Furthermore, heavy-ion irradiation at doses up to the level at which T_c starts to degrade does not increase the critical current of thin films that already have high critical-current densities (Barbour *et al.*, 1992), implying that pinning in these films as grown is already close to optimum. Thus it seems unlikely that this approach will materially reduce the level of $1/f$ noise in thin YBCO films cooled in an ambient magnetic field.

One method of eliminating the excess $1/f$ noise is to cancel the static field that causes it. For medical applications, some groups, for example Aarnink *et al.* (1995), have used a three-axis flux-gate magnetometer as a reference sensor that controls the current through three orthogonal sets of cancellation coils surrounding the dewar. This technique can reduce the ambient field to about 1%, but the flux-gate magnetometers themselves generate excess noise. This noise can be reduced if one

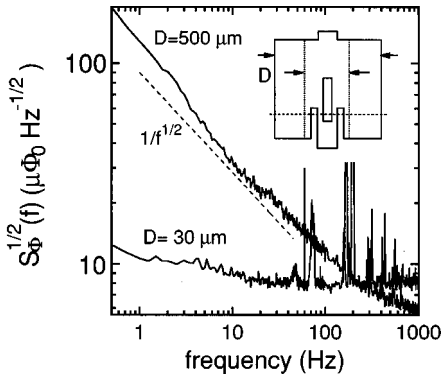

FIG. 35. $S_\Phi^{1/2}(f)$ for dc SQUID shown in the inset cooled in a field of 24 μT. Upper trace is for device with outer dimension $D=500\,\mu$m, lower trace is after repatterning to a width $D=30\,\mu$m (dotted lines). Inset not to scale. Dashed line indicates grain boundary (Dantsker *et al.*, 1996).

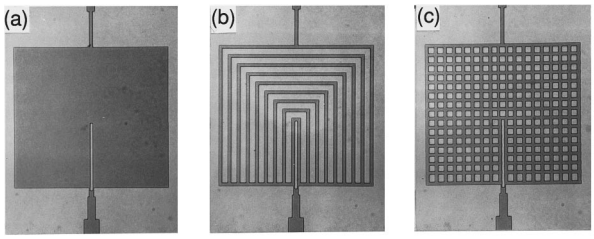

FIG. 36. Photographs of (a) a solid, thin-film dc SQUID, (b) a SQUID with eight slots and (c) with 248 holes. The outer dimensions of each device are 186 μm$\times$204 μm (Dantsker, Tanaka, and Clarke, 1997).

uses SQUID gradiometers. A simpler and perhaps more practical version of this method is the three-SQUID gradiometer (Koch *et al.*, 1993, see Sec. VIII.A) with the reference SQUID replaced with a flux-gate magnetometer. Of course, none of these methods is appropriate for geophysical measurements in which one is interested in fluctuations in the ambient magnetic field.

The most practical method of eliminating the excess $1/f$ noise is to design the superconducting components of the magnetometer so that flux vortices do not enter. For a film of width w cooled in a perpendicular field B_0, Clem(1996) has shown that it is energetically unfavorable for flux to penetrate provided $w\leqslant(\pi\Phi_0/4B_0)^{1/2}$. Dantsker *et al.* (1996) studied the $1/f$ noise produced by SQUIDs with various film widths as a function of the magnetic field in which they were cooled. The upper trace of Fig. 35 is the flux noise $S_\Phi{}^{1/2}(f)$ of a square-washer bicrystal SQUID with outer dimensions of 500 μm and a slit 100 μm long and 4 μm wide, cooled in 24 μT. The observed $1/f$ spectrum is typical for such devices. The SQUID was subsequently repatterned to reduce the outer dimension to 30 μm and the linewidth to 13 μm, as indicated by dotted lines in the inset. The lower trace shows that the low-frequency noise is dramatically lower, by two orders of magnitude in power at 1 Hz. Similar measurements on SQUIDs with linewidths ranging from 4 to 13 μm showed that the flux noise at 1 Hz, typically $8-20\,\mu\Phi_0\,\mathrm{Hz}^{-1/2}$, was independent of the cooling field up to a threshold B_T, above which the noise increased rapidly, indicating that vortices begin to penetrate the film. Although B_T increased with decreasing linewidth, the increase was slower than Clem's model predicts. For example, in the first batch of devices B_T was about 33 μT for $w=4\,\mu$m, a field about three times less than the predicted value $\pi\Phi_0/4w^2\approx100\,\mu$T. It was suggested that poor-quality edges, which offer low-energy sites where vortices tend to nucleate, were the most likely cause of the lower threshold. However, subsequent work (see below) showed that threshold fields of over 100 μT could be achieved with more carefully patterned edges. We note that edges should be vertical to give the highest threshold field, a requirement that is the antithesis of the smoothly beveled edges needed for multilayer structures.

We now discuss the implications of this result to directly coupled magnetometers in which we use a SQUID with a narrow linewidth. We show that the pickup loop is expected to add negligible $1/f$ noise even though its linewidth is often several millimeters wide and thus the film is penetrated by vortices even in low cooling fields. The motion of the vortices generates screening currents which couple an indirect flux noise $S_\Phi^{\mathrm{in}}(f)$ to the SQUID. For a square pickup loop of outer and inner dimension d_1 and d_2 and inductance L_p, this indirect noise is given by (Dantsker *et al.*, 1996)

$$S_\Phi^{\mathrm{in}}(f)\approx S_\Phi^U(f)\alpha_d^2(L/L_p)^2(d_1+d_2)/(d_1-d_2). \qquad (9.1)$$

Here, $S_\Phi^U(f)$ is the spectral density of the flux noise of an unpatterned YBCO film measured by a SQUID placed directly over it, typically $10^{-9}\,\Phi_0{}^2/\mathrm{Hz}$ at 1 Hz for high-quality films cooled in $B_0=50\,\mu$T (Ferrari *et al.*, 1994). Taking the typical values $L\approx20\,$pH, $\alpha_d\approx1$ and $L_p\approx5\,$nH for a magnetometer pickup loop with $d_1\approx10$ mm and $d_2\approx2$ mm, we find S_Φ^{in} (1 Hz)$\approx10^{-14}\,\Phi_0^2/\mathrm{Hz}$. This value is several orders of magnitude below the flux noise of the SQUID (for example, Fig. 35). The best directly coupled magnetometers on a $10\times10\,\mathrm{mm}^2$ substrate have a noise of about $50\,\mathrm{fT\,Hz}^{-1/2}$ (Lee *et al.* 1995; Beyer *et al.*, 1998), and with appropriate SQUID design it should be possible to achieve this result in the earth's field at frequencies down to (say) 1 Hz. This would be adequate for most geophysical applications.

We turn next to a discussion of multilayer devices. In the case of the multiloop magnetometer (Sec. VI.D), at least in principle, it should be possible to reduce all the linewidths to (say) 4 μm, so that the $1/f$ noise should not increase in ambient fields up to about 100 μT. For a square-washer SQUID coupled to a multiturn flux transformer, however, it is clearly out of the question to reduce the outer dimensions of the SQUID. Dantsker, Tanaka, and Clarke (1997) tackled this problem using SQUIDs with the configurations shown in Figs. 36(b) and (c). Once again, the key is to maintain narrow linewidths. In the first design [Fig. 36(b)] the SQUID washer is interpenetrated by eight slots, each 8 μm wide, separating nine YBCO strips, each 4 μm wide. In the second design [Fig. 36(c)] 248 holes, each $8\times8\,\mu$m, di-

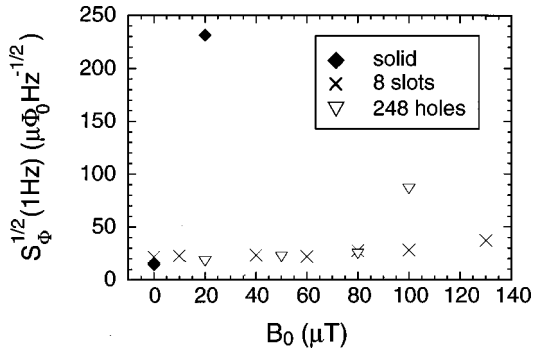

FIG. 37. $S_\Phi^{1/2}$ (1 Hz) vs cooling field B_0 for the three SQUIDs shown in Fig. 36 (Dantsker, Tanaka, and Clarke, 1997).

vide the washer into a grid of 4-μm-wide lines. Figure 37 compares $S_\Phi{}^{1/2}$(1 Hz) for three devices made on a single chip in the configurations of Fig. 36, cooled in static magnetic fields B_0. The noise of the solid SQUID increases rapidly with B_0, much like the device in Fig. 34(b). The SQUID with slots, on the other hand, shows no significant increase in the noise for fields up to at least 100 μT. At 130 μT the noise has increased somewhat, suggesting that vortex entry occurred just below this field. For the device with 248 holes $S_\Phi{}^{1/2}$ (1 Hz) also shows no increase for cooling fields up to at least 80 μT. Furthermore, measurements of the mutual inductance M_i between each of the SQUIDs in Fig. 36 and a seven-turn input coil revealed that the presence of slots or holes reduces M_i by no more than 14%. Since the flux noise generated by the pickup loop is expected to be unimportant, these results suggest that it should be possible to operate magnetometers with multiturn input coils in the earth's magnetic field with no increase in $1/f$ noise.

However, it should be stressed that when a device is moved in an ambient magnetic field, the induced supercurrents are very likely to generate vortices and increase the noise. For example, Keene *et al.* (1996) rotated a planar gradiometer in static fields as high as 70 μT and measured a monotonic increase in the $1/f$ noise as they turned the device through 90°; furthermore they observed large random telegraph signals (RTS) over some narrow angular ranges. Thus, after any such devices are moved in a static field, it is likely to be necessary to raise their temperature briefly above T_c to release the induced currents.

Earlier, Koch *et al.* (1995) had investigated the effect of cooling a directly coupled magnetometer inside a magnetic shield which they subsequently removed, exposing the device to an ambient field. They showed that the current generated in the pickup loop by the field caused vortices to enter the material. Exposure to a field of 50 μT, for example, caused a substantial increase in the level of $1/f$ noise. We note that, according to our discussion concerning Eq. (9.1), the density of vortices generated by these currents must far exceed the density produced by the ambient field itself. If this were not the case, the $1/f$ noise contribution of the loop would be negligible. Koch *et al.* (1995) demonstrated that this flux entry and ensuing $1/f$ noise could be prevented by means of a "flux dam"—a weak link in the pickup loop that limits the circulating current to its critical current. With the flux dam in place, exposing the magnetometer to 50 μT after a zero-field cool resulted in a considerably smaller increase in the $1/f$ noise. More recently, Milliken, Brown, and Koch (1997) reported a directly coupled magnetometer containing a flux dam in which the noise of several hundred fT Hz$^{-1/2}$ at 1 Hz did not increase significantly when the device was exposed to fields as high as 34 μT following a zero-field cool. Thus for magnetometers that are subject to being moved, the lowest levels of $1/f$ noise are likely to be achieved with a combination of narrow linewidths and a flux dam.

B. Hysteresis

Magnetic hysteresis in a SQUID-based instrument manifests itself as a shift of the voltage-flux characteristics along the flux axis after the magnetic field is cycled. This effect is undesirable if one wishes to keep track of the absolute value of the magnetic field or to measure gradients in large fluctuating background fields. Magnetic hysteresis is observed for low-T_c and high-T_c SQUIDs and is related to vortex entry and pinning near the edges of thin films (Koch *et al.*, 1989; Sun *et al.*, 1992; Sun, Gallagher, and Koch, 1993; Sun *et al.*, 1994; Clem *et al.*, 1993; Purpura *et al.*, 1993; Keene *et al.*, 1996). The degree of hysteresis is expressed by the hysteresis parameter $h=\delta\Phi/\Delta\Phi$, where $\delta\Phi$ is the flux error caused by sweeping the applied flux between $\pm\Delta\Phi$. For integrated thin-film low-T_c gradiometers operated at 4.2 K in the ambient magnetic field, a magnetic hysteresis as low as 10^{-9}–10^{-11} (Koch, Ketchen *et al.*, 1991) has been measured. Initial studies on high-T_c dc SQUIDs based on polycrystalline films showed high levels of nonlinear hysteresis (Foglietti *et al.*, 1989; Koch *et al.*, 1989). For grain-boundary dc SQUIDs involving epitaxial YBCO films on bicrystals, Gross and Chaudhari (1992) reported $h<10^{-6}$ at 77 K for $\Delta\Phi\leqslant\Phi_0$.

Sun and co-workers made systematic studies of the hysteresis in low-T_c and high-T_c dc SQUIDs using cycling fields ranging from 10 μT to 1 mT peak to peak. In each case they found both time-independent and time-dependent hysteresis. The time-independent hysteresis appeared above a threshold field of a few hundred microtesla. The threshold field had a similar temperature dependence to the critical-current density of the thin films, suggesting a relation between this hysteresis and flux pinning. Sun *et al.* (1994) developed a quantitative model involving the Lorentz force on vortices due to screening currents, the surface barrier to flux entry, and the pinning force of defects in the superconducting film. Within this model they showed that the observed threshold field corresponds to the value at which the Lorentz force equals the sum of the surface barrier and the pinning force. Since the screening currents and hence the Lorentz force on a vortex are maximum at the edges of the film and decay into film, the vortices are swept into the film until the Lorentz force becomes smaller than

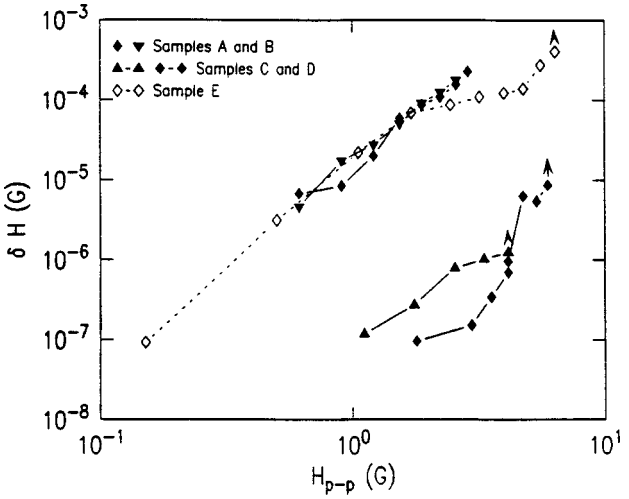

FIG. 38. Hysteresis of YBCO dc SQUIDs with a 240-μm square washer. Lower traces are for devices prepared with higher edge quality and show a significant reduction in hysteresis (Sun *et al.*, 1994).

the pinning force. The distance over which the vortices penetrate into the washer and the ensuing degree of hysteresis are predicted to depend crucially on the local pinning force near the film edges, in agreement with the dramatic reduction of the hysteresis achieved by improving the quality of the film edges (Sun, Gallagher, Callegari *et al.*, 1993). This improvement is illustrated in Fig. 38. Clearly, to obtain small hysteresis one requires a high average critical-current density in the films. However, the hysteresis is dominated by the local properties close to the edges: for example, a single grain boundary cutting across the edge of a SQUID washer increased the hysteresis by several orders of magnitude (Sun *et al.*, 1994). Keene *et al.* (1996) made similar measurements of hysteresis in a gradiometric, high-T_c SQUID coupled to a gradiometric flux transformer with multiturn input coils. For cycling fields up to 70 μT, the hysteresis parameter averaged 3×10^{-6}. When the measurements were repeated on the SQUID without the flux transformer, the hysteresis was little changed for cycling fields below 40 μT but increased dramatically for higher fields. The authors attribute this behavior to the pinning of the radial motion of vortices in the SQUID by the input coils. It is particularly important to note that high edge-pinning forces are a key to producing low levels of both $1/f$ noise and hysteresis, and imply steep film edges. This requirement is, unfortunately, not compatible with the need for gently sloping edges on all but the last film of a multilayer structure.

C. rf interference

Environmental rf fields may have a major effect on SQUIDs. In their simulations, Koch *et al.* (1994) coupled rf signals to dc SQUIDs as both a flux and a bias current, via the input and output circuitry of the SQUID. They showed that rf interference distorts the V-Φ characteristic by both reducing its amplitude and creating an asymmetry about the $\Phi_0/2$ point. The first effect increases the white noise of the SQUID but, when conventional flux modulation is used, does not create a shift in the output of the flux-locked loop. The second effect can lead to a large increase in the level of low-frequency noise; however Koch and co-workers showed that this problem can largely be eliminated by using bias current reversal.

One can often effectively eliminate rf interference by means of appropriate shielding. However, this may not be possible in certain situations, notably for systems that are required to move in the earth's field; such motion induces eddy currents in the shield. In these situations, the combined use of flux modulation and bias reversal greatly reduces the effects of rf interference. Koch *et al.* (1994) emphasize that the rf coupling is reduced by making the superconducting structure small so as to decrease their antenna gain and, especially, by making the input and output circuits and the SQUID itself as balanced as possible. A high degree of balance prevents common mode rf fields, which have no effect on the SQUID, from creating differential signals that couple to the current and flux biases.

D. Temperature fluctuations

The effects of temperature fluctuations or drifts on the output of a high-T_c SQUID have been largely ignored until recently. However, these effects can be substantial (Milliken, Koch *et al.*, 1997; ter Brake *et al.*, 1997). Such fluctuations can be induced, for example, by changes in the ambient pressure above the liquid nitrogen bath. A change in temperature modifies the penetration depth and hence the effective sensing area of a SQUID, producing a flux change in the presence of an ambient magnetic field. For typical devices in the earth's magnetic field, the change in flux can be as high as $0.5\,\Phi_0/\mathrm{K}$. To achieve a noise level of (say) $10\,\mu\Phi_0\,\mathrm{Hz}^{-1/2}$ with this temperature coefficient would require a temperature stability of a few tens of $\mu\mathrm{K\,Hz}^{-1/2}$ at frequencies above 1 Hz. The effect of temperature fluctuations can be reduced by appropriate design of the SQUID and flux transformer, stabilizing the ambient pressure, providing a long thermal time constant between the bath and the device, and reducing the ambient field. These are complicated issues that require further attention.

X. APPLICATIONS

The first practical measurement with a high-T_c SQUID was probably the use of a bulk rf SQUID by Likhachev *et al.* (1990) to detect the magnetocardiogram of a human subject. Since then, as the sensitivity of SQUIDs has progressively improved, the range of applications has grown rapidly. Currently, there is most interest in magnetocardiology and, to a lesser extent, magnetoencephalography, nondestructive evaluation (NDE), and SQUID "microscopes." Geophysical instrumentation is receiving growing attention and appears to

have an important future. We shall review each of these topics in turn. Of the various other applications, we mention just two. One is the SQUID picovoltmeter, in which the voltage to be measured is coupled in series with a resistor and a multiturn, single-layer film that is inductively coupled to a directly coupled magnetometer (Miklich *et al.*, 1995; Faley *et al.*, 1997). The other is the spinner magnetometer, in which a geophysical sample is rotated, typically at 10 rev/sec, just below the bottom of a dewar containing a high-T_c SQUID (Tinchev, 1997). The resulting oscillating magnetic field enables one to determine the static magnetization of the sample.

A. Biomagnetism

Biomagnetism refers quite generally to the measurement of magnetic fields produced by any living organism but, apart from experiments on magnetotactic bacteria mentioned in Sec. X.C, it appears that high-T_c magnetometers have been used only to detect signals from the human body. These fields range from several tens of picotesla from the human heart down to a few tens of femtotesla from the spinal cord (Wikswo, 1995). The majority of the commercial low-T_c SQUIDs ever made are employed in multichannel systems for magnetoencephalography (MEG)—measurements of signals from the human brain. This application demands a magnetic-field resolution of a few $\mathrm{fT\,Hz^{-1/2}}$ at frequencies down to about 1 Hz. As discussed in Sec. VI, the best high-T_c SQUID magnetometers have a white noise below 10 $\mathrm{fT\,Hz^{-1/2}}$, but at 1 Hz the noise is about a factor of 3 higher. Thus high-T_c magnetometers are not yet quite good enough for clinical MEG, although there have been several demonstrations of neuromagnetic measurements (Zhang, Tavrin *et al.*, 1993; DiIorio *et al.*, 1995; Curio *et al.*, 1996; Drung, Ludwig *et al.*, 1996). On the other hand, the requirements for magnetocardiology (MCG)—measurements of signals from the human heart—are somewhat more relaxed, and as a result most biomagnetic measurements with high-T_c SQUIDs have focused on this application.

Although the peak signal amplitudes in MCG are several tens of picotesla, there is fine structure of clinical interest with a mean amplitude of about 2 pT (David *et al.*, 1997). The base-to-peak amplitude of a biomagnetic signal to be identified in a single measurement in a bandwidth Δf is given by $B_p = c_R S_B^{1/2} (\Delta f)^{1/2}$. The crest factor c_R is determined by the probability that an observed magnetic field is signal rather than noise, and a value of about 4 is used under the assumption that the noise is white throughout the measurement bandwidth (Ott, 1988). Thus for the typical values $\Delta f = 200\,\mathrm{Hz}$ and $B_p = 2\,\mathrm{pT}$, the sensor should have a noise below 35 $\mathrm{fT\,Hz^{-1/2}}$. Although magnetocardiograms measurements have been obtained by a number of groups to illustrate the performance of their magnetometers, only a few such recordings, obtained in a well-shielded environment, are of sufficient quality to yield diagnostically useful information. The best data were obtained in the magnetically shielded room of the PTB in Berlin with

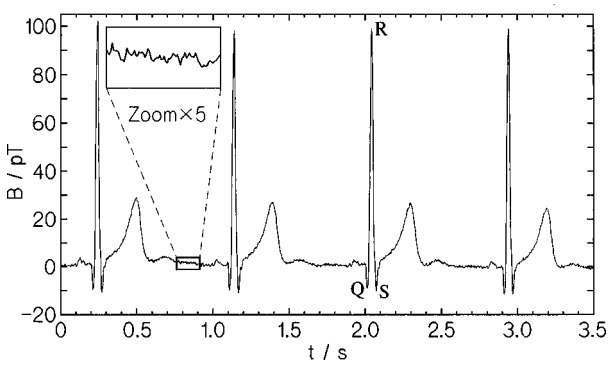

FIG. 39. Real-time trace of magnetocardiogram recorded with NKT integrated magnetometer in magnetically shielded room at PTB in Berlin. The measurement was performed in a bandwidth of 0.016–200 Hz without power line filter. Inset illustrates very low peak-to-peak noise (Drung, Ludwig *et al.*, 1996).

several kinds of multilayer magnetometers (Drung, Ludwig *et al.*, 1996; Drung, Dantsker *et al.*, 1996). The highest signal-to-noise ratio was obtained with an integrated magnetometer involving a multiturn input coil, fabricated at NKT, which had a noise of 10 $\mathrm{fT\,Hz^{-1/2}}$ at 1 kHz and 53 $\mathrm{fT\,Hz^{-1/2}}$ at 1 Hz (Drung, Ludwig *et al.*, 1996). An unfiltered, real-time MCG measurement with this device is illustrated in Fig. 39. The measurement bandwidth was 200 Hz, resulting in a base-to-peak noise amplitude of 0.75 pT and a signal-to-noise ratio of 130 for the peak value. The latter value is considered acceptable for MCG with low-T_c systems. The sensitivity of this particular high-T_c magnetometer was adequate to detect wide-band MEG signals produced by both the central and peripheral nervous systems, with amplitudes of 100 fT or less (Curio *et al.*, 1996; Drung, Ludwig *et al.*, 1996).

Subsequently, Burghoff *et al.* (1996) used a high-T_c rf SQUID magnetometer in the Berlin shielded room to record the MCG of both a healthy subject and a subject with arrhythmia. The noise of the sensor was 35–40 $\mathrm{fT\,Hz^{-1/2}}$ at 200 Hz. To assess the performance of the high-T_c magnetometer, the PTB 37-channel, low-T_c system (Koch, Cantor *et al.*, 1991) was used as a reference. Although the rms noise of the high-T_c sensor was a factor of 4 higher than the low-T_c sensors, one half of this disadvantage was regained from the shorter distance between the high-T_c magnetometer and the thorax. The ability to place high-T_c SQUIDs closer to the signal source clearly relaxes their sensitivity requirement somewhat compared with their low-T_c counterparts. A further potential advantage of liquid nitrogen-cooled sensors is that the cryogenic package can be made quite compact. Schilling *et al.* (1996) measured a MCG with a cryostat containing only 0.1 liter of liquid nitrogen.

The systems we have just described have only a single channel. However, most applications require a multichannel system to enable one to map fields from the heart at different locations. The most elaborate high-T_c systems have been built at the Superconducting Sensor Laboratory in Japan: 4 channels (Tanaka *et al.*, 1994), 16 channels (Itozaki *et al.*, 1994), and 32 channels (Itozaki

et al., 1996). Their sensors were 5-mm-washer dc SQUIDs with a noise of 70–250 $\mathrm{fT\,Hz^{-1/2}}$ at 1 kHz and 300–800 $\mathrm{fT\,Hz^{-1/2}}$ at 1 Hz; to protect them from moisture, the SQUIDs were sealed in an epoxy resin package. The 32 SQUIDs were in a flat 6×6 array, with each corner location unoccupied, with 40 mm separation. Magnetocardiogram recordings were obtained in a small magnetic shield, with inner dimensions $0.8\times0.8\times2\ \mathrm{m^3}$. Although the noise specifications did not fulfill the requirements listed earlier, Itozaki and co-workers were able to obtain magnetocardiac isofield contour maps of the *R, S*, and *T* waves.

To our knowledge, the only multichannel system using multilayer technology is the four-channel system of DiIorio *et al.* (1995), who used integrated, multiturn magnetometers. The noise levels were 70 $\mathrm{fT\,Hz^{-1/2}}$ at 1 kHz and 280 $\mathrm{fT\,Hz^{-1/2}}$ at 1 Hz. These authors obtained both MCG's and MEG's in a magnetically shielded room.

All the systems described so far involved magnetometers, and can thus be used only in a magnetically shielded room, which, as pointed out in Sec. IX, is expensive. If one hopes to see SQUIDs in widespread use, one is required not only to replace liquid ^{4}He with liquid N_2 but also to eliminate the need for expensive shielding. This requirement has driven extensive development of gradiometers: since the separation of the sensor and the source is only a few tens of millimeters, even high-order gradiometers behave as magnetometers for the signal source, provided the baseline is sufficiently long (Vrba, 1996).

Tavrin *et al.* (1994) and Borgmann *et al.* (1997) used second-order electronic gradiometers to record good-quality MCG's in unshielded environments. However, the bandwidth was only 0–30 Hz, which is insufficient for some of the high-frequency information of clinical interest. Weidl *et al.* (1997) used a single-layer, planar gradiometer with a 4-mm baseline to record MCG's in an unshielded environment with a bandwidth of 250 Hz. The *R* peak was just resolved in a real-time trace. The authors demonstrated that the signal-to-noise ratio could be significantly improved by averaging, by using notch filters, and by triggering the recording with the peak of the electrocardiogram (Seidel *et al.*, 1997).

Progress towards the development of multichannel systems for unshielded operation has been reported by Woeltgens *et al.* (1997), David *et al.* (1997), ter Brake, Janssen *et al.* (1997), and ter Brake, Karunanithi *et al.* (1997). David *et al.* fabricated a nine-channel system based on directly coupled dc SQUID magnetometers, each of which was enclosed in a fiberglass module to protect it from moisture. Each module contained a resistive heater so that the SQUID could be driven into the normal state to release trapped magnetic flux. To reduce the environmental noise David *et al.* (1997) used a copper coil around the dewar as a reference magnetometer that fed compensating currents into a coil surrounding the planar magnetometer array. They also used digital subtraction to form first-derivative gradiometers. The combination of these techniques reduced the noise at 30 Hz from about 30 $\mathrm{pT\,Hz^{-1/2}}$ to about 1 $\mathrm{pT\,Hz^{-1/2}}$ for each channel, an order of magnitude above the intrinsic noise of the sensors. This performance made it possible to obtain contour maps after 80 averages, with the aid of a template matching technique. Compensating the component of the earth's static magnetic field perpendicular to the plane of the magnetometers did not reduce the noise any further. The excess noise was believed to arise from gradients in the environmental noise or the motion of vortices in the YBCO films. The latter effect could presumably be eliminated by reducing the linewidths of the superconducting films sufficiently (Sec. IX.A).

Ter Brake, Janssen *et al.* (1997), and ter Brake, Karunanithi *et al.* (1997) made a similar seven-channel system, also encapsulating their directly coupled magnetometers to exclude moisture. They used groups of three neighboring magnetometers in the planar array to form electronic first- and second-order gradiometers. Noise rejection was limited to about 2% by lack of planarity and by variations in the transfer functions of the individual SQUIDs, which resulted in varying gains and phase shifts in the flux-locked loops.

The five-channel system of Woeltgens *et al.* (1997) makes use of the TSG (Koch *et al.*, 1993). Three magnetometers were stacked in the *z* direction to form the TSG, and two more magnetometers were used to cancel residual *x* and *y* components of the noise. In addition, the outputs from a three-axis flux-gate magnetometer were coupled to three sets of external coils to provide active noise cancellation. The lowest noise achieved was about 400 $\mathrm{fT\,Hz^{-1/2}}$ at 1 Hz (Koch, 1997).

We have seen that single-channel, multilayer magnetometers operating in a magnetically shielded environment have sufficient resolution to obtain clinically meaningful MCG's. Packages to protect the sensors and to enable excess flux to be expelled have been developed. However, no multichannel system has yet been demonstrated that even approaches the performance of the best single-channel devices, suggesting that such high-T_c sensors are not yet routinely available. With regard to unshielded systems, a good deal of progress has been made, but substantially more will have to be made before the noise levels approach that of high-T_c directly coupled magnetometers, about 100 $\mathrm{fT\,Hz^{-1/2}}$, let alone the much lower noise levels of low-T_c systems. One might hope some of the recent progress reported in Secs. VIII and IX will lead to lower noise in unshielded systems in the near future.

B. Nondestructive evaluation

Nondestructive evaluation (NDE) is the noninvasive identification of structural or material flaws in a specimen. Examples are the imaging of surface and subsurface cracks or pits due to corrosion or fatigue in aging aircraft and reinforcing rods in concrete structures (Wikswo, 1995). While there is a variety of acoustic, thermal, and electromagnetic techniques currently used in NDE, these methods are often not entirely adequate for de-

tecting flaws at an early enough stage, usually because of a lack of spatial or depth resolution.

An important application of high-T_c SQUIDs in NDE is to replace induction coils in eddy-current imaging, a widely used method for the detection of subsurface damage in metallic structures such as aircraft (Wikswo, 1995). In this technique, one applies an alternating magnetic field produced by a drive coil and lock-in detects the fields generated by the induced eddy currents in the structure. The eddy currents are diverted by structural flaws resulting in distortions of the magnetic field. Since the eddy currents flow over a skin depth, which is inversely proportional to the square root of the frequency, deep defects require correspondingly low frequencies. Thus the flat frequency response of SQUIDs is a distinct advantage over the response of coils which falls off with decreasing frequency. Furthermore, high-T_c SQUIDs are distinctly preferable to low-T_c SQUIDs because their associated dewars or cryocoolers can be lighter and more compact. The insertion of SQUIDs into the NDE market is largely contingent on one's ability to retain high sensitivity in a mobile unit capable of operating in the magnetically unfriendly environment of an aircraft maintenance hangar or a factory.

Demonstrations of eddy-current NDE using high-T_c SQUIDs have been reported by a number of groups, especially during the past two years. Both dc and rf SQUIDs have been used in a variety of magnetometer and gradiometer configurations. The drive coil is mounted on the cryostat and typically has a double-D configuration to minimize the excitation field at the SQUID, which is mounted at the point where the field changes sign. For most realistic applications, one scans the SQUID and drive coil over the sample.

In one such system Tavrin *et al.* (1995) used an electronic SQUID gradiometer consisting of two high-T_c SQUIDs in a dewar of liquid nitrogen suspended over a sample that was scanned linearly at about 7 mm/s in an unshielded laboratory environment. The authors successfully imaged a series of slots cut into a copper plate as well as a 6-mm hole in a 1-mm-thick sheet of aluminum situated beneath two additional sheets of the same material. In a similar unshielded system Carr *et al.* (1977) used an electronic gradiometer consisting of two dc SQUIDs that was scanned above three 3-mm-thick layers of aircraft-grade aluminum held together by rivets and containing simulated defects 2–4 mm long radiating from the rivet centers in all three layers. Excitation fields were applied at two discrete frequencies and the resulting signals were lock-in detected and subtracted in an appropriate manner to distinguish the defects in the deeper layer from those in the surface layer.

In a step towards practical development of this technology, Hohmann *et al.* (1997) reported NDE measurements of structures in an unshielded environment using dc and rf SQUID-based magnetometers and monolithic gradiometers cooled by a commercial Joule-Thomson cryocooler. Either the sample or the sensor was scanned on a mobile x-y stage; the latter mode was aimed at investigating the possibility of a mobile SQUID system. Among the flaws analyzed were a corrosion pit and a simulated fatigue crack in an aluminum sheet; both were hidden underneath four intact 1.5-mm-thick aluminum plates. Figure 40 shows the image of a corrosion pit detected at a drive frequency of 20 Hz with the cryocooler in motion.

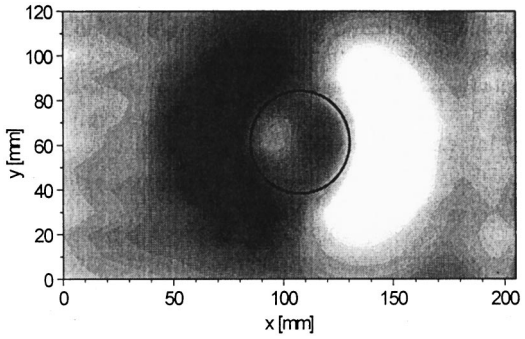

FIG. 40. Eddy-current image of a corrosion pit in an aluminum sheet ($1.5\times200\times400$ mm) situated beneath four aluminum sheets of equal size (Hohmann *et al.*, 1997).

Kreutzbruck, Tröll *et al.* (1997), Mück *et al.* (1997), and Kreutzbruck *et al.* (1998) developed two NDE systems, one with the sensors cooled by liquid nitrogen and the other with them cooled by a miniature Stirling refrigerator, which chills neon gas to about 50 K. Each system contained up to four rf SQUIDs operated at 3 GHz, with a noise of about 1 pT $\mathrm{Hz}^{-1/2}$ above 1 Hz and a high slew rate and dynamic range to allow unshielded operation. This group reported an impressive demonstration of one of their systems in an aircraft hangar to detect flaws in felloes that were rotated close to the dewar at 6–20 rpm. The felloe consists of a hollow steel cylinder containing six ferromagnetic steel bars, at 60° intervals, for heat dissipation, and three venting holes, 10 mm in diameter, at 120° intervals. Thus, in searching for cracks in the felloe, it is necessary to distinguish their signature from the signals produced by the bars and holes. Figure 41 shows the amplitude and phase of the magnetic field detected by the SQUID as the felloe is rotated through 360°. A 4-mm-long crack is easily distinguished from the periodic signals from the bars and holes. The authors developed an algorithm that combines the amplitude and phase data to make the periodic signals vanish, leaving a prominent signal from the crack [Fig. 41(c)]. Similar work has been reported by Krause *et al.* (1997), who tested aircraft wheels with a mobile SQUID system in the Lufthansa maintenance facility at Frankfurt airport. Although still at the prototype stage, these techniques have considerable promise as an NDE tool for the aircraft industry.

Historically, much of the early research on NDE with low-T_c SQUIDs was concerned with the detection of magnetic fields generated by specimens containing magnetized components (Donaldson *et al.*, 1990; Banchet *et al.*, 1995), and several groups are now using high-T_c devices for this approach. Schmidl, Wunderlich, Dörrer, Specht, Linzen *et al.* (1997) and Kasai *et al.*

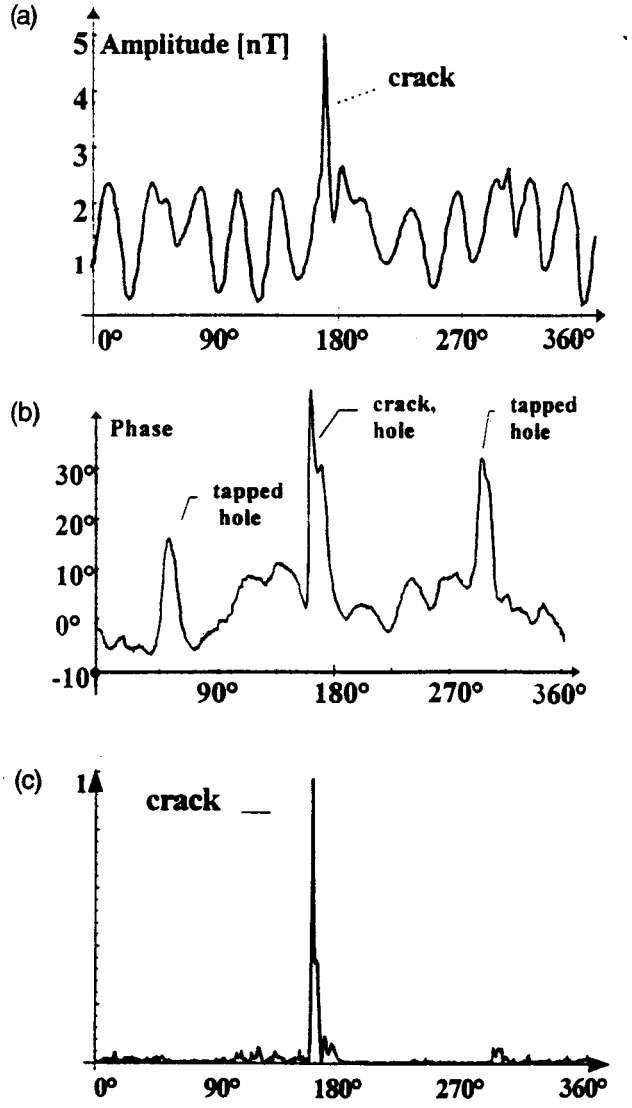

FIG. 41. Crack detection in an aircraft felloe: (a) Amplitude and (b) phase of gradiometer signal produced by eddy currents during one rotation of the felloe. The crack is indicated. The periodic signal is due to ferromagnetic steel bars located in the felloe at 60° intervals and three tapped holes at 120° intervals. (c) Result of algorithm to suppress signals from the steel bars and holes. (Mück *et al.*, 1997).

(1997) used a planar dc SQUID gradiometer and a magnetometer, respectively, to scan samples of steel to explore the correlation between mechanical stress and magnetic-field distribution. The latter group imaged the magnetic field contours resulting from different degrees of residual stress in the material. This method is a unique probe of the mechanical or thermal stress to which a sample has been subjected. We have recently become aware of work by Tavrin *et al.* (1999), under contract with a manufacturer of turbine engines. These authors detect ferrous inclusions in the disks of turbine engine rotors using a high-T_c, second-order electronic SQUID gradiometer in an unshielded environment. This work represents an important step beyond "proof-of-concept" in introducing high-T_c SQUIDs into the NDE market. In a very different application Nagaishi *et al.* (1997) used a high-T_c dc SQUID magnetometer to detect fine magnetic particles in a rapidly moving copper wire. In their arrangement, the nitrogen-cooled SQUID was surrounded by a magnetic shield and the wire was pulled through holes in the shield about 15 mm below the SQUID at speeds of 10 to 500 m/min. Iron particles as small as 50 μm in diameter were detected. The goal of this technique is to locate impurities that make the wire brittle, causing it to break.

Although some of the measurements we have just described are at the prototype stage, there have been impressive demonstrations on aircraft components. Fortunately, these techniques do not require the highest sensitivity, since the Nyquist noise generated by the sample can be on the order of 1 $\mathrm{pT\,Hz^{-1/2}}$. This noise level is much lower than that of coils conventionally used for eddy current NDE. Thus, although some development remains, the future of NDE based on high-T_c SQUIDs is very promising indeed.

C. Scanning SQUID microscopy

Magnetic microscopes based on low-T_c dc SQUIDs have been used to image static magnetic fields with a combination of high field and spatial resolution (for example, Mathai *et al.*, 1993; Vu and Van Harlingen, 1993; Tsuei *et al.*, 1994). This development led, shortly afterwards, to the development of high-T_c SQUID microscopes (Black *et al.*, 1993; Black, 1995; Lee *et al.*, 1996, 1997), in which the sample may be at either 77 K or at room temperature. Most often, the sample is scanned over the SQUID in a two-dimensional raster to produce an image. The scanning stage, made from nonmagnetic composite material, is driven by threaded rods turned by stepper motors. The frequency at which the image is obtained ranges from near zero, where one simply measures the static magnetic field produced by the sample, to beyond 1 GHz.

Figure 42 shows a microscope in which the sample is maintained at room temperature. The SQUID is mounted in vacuum at the upper end of a sapphire rod, the lower end of which is cooled by liquid nitrogen. Superinsulation surrounding the rod ensures that the temperature gradient along it is negligible. The SQUID is separated from room temperature and atmospheric pressure by a window, which may be either a 75-μm-thick sapphire disk or a 3-μm-thick Si_xN_y window fabricated on a Si chip. In the first case, the SQUID-to-sample separation is typically 150 μm, whereas in the latter, the separation can be as low as 15 μm. The entire system is surrounded by a mu-metal shield to exclude spurious magnetic field fluctuations, and the SQUID is operated in a flux-locked loop.

A novel application of the microscope, in which the sample is held fixed, is the detection of the motion of magnetotactic bacteria (Lee *et al.*, 1997). Each bacterium contains a series of magnetite particles giving it a magnetic moment of about $5\times10^{-16}\,\mathrm{A\,cm^2}$. As an example of such measurements, Fig. 43 shows the spectral density of the magnetic-field fluctuations produced by an

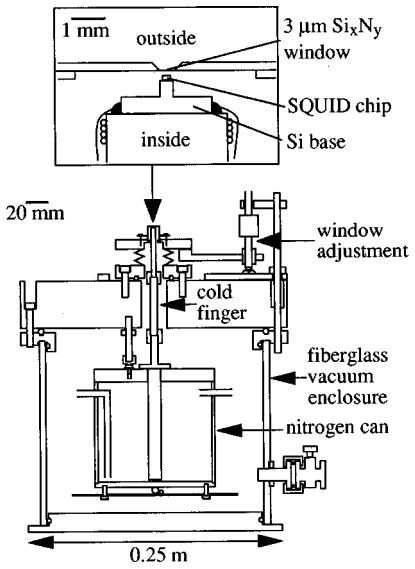

FIG. 42. Sectional side view of scanning SQUID microscope, without X-Y scanner (Chemla *et al.*, 1997).

ensemble of dead bacteria in water. The bacteria undergo Brownian rotation, producing a Lorentzian power spectrum of the form $1/[1+(\omega\tau_0)^2]$, where $\tau_0 = \alpha_r/k_BT$ is the characteristic rotation time of the bacteria and α_r is the rotational damping coefficient. The fitted value of τ_0, 15.9 s, is in good accord with predictions assuming a bacterial diameter of 1 μm and a length of 4 μm. Measurements underway include the dynamics of living bacteria (Chemla *et al.*, 1997), the effects of an applied magnetic field, and the migration of bacteria through porous media.

We turn now to higher-frequency operation. In the frequency range from 1 kHz to 1 MHz, Black *et al.* (1994) operated the SQUID open loop and used a drive coil to apply a sinusoidal magnetic field to induce eddy currents in the sample and modulate the flux in the SQUID. The magnetic response of the sample is determined by measuring the amplitude and phase of the output from the SQUID: the out-of-phase component corresponds to the eddy current in the sample. This approach resembles the eddy current technique described in Sec. X.B, but enables one to operate at substantially higher frequencies.

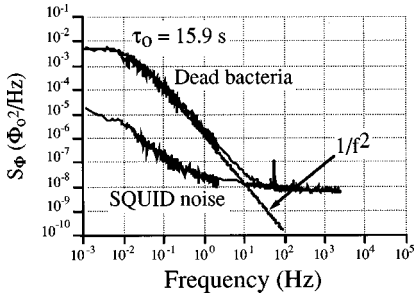

FIG. 43. Spectral density of dead magnetotactic bacteria with fitted Lorentzian (solid line). Lower power spectrum represents the SQUID noise (Lee *et al.*, 1997).

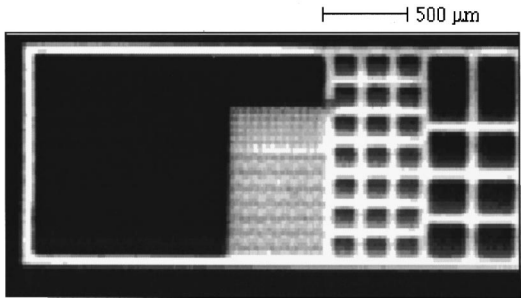

FIG. 44. Image of patterned thin film of Cu scanned over SQUID with 9 GHz Josephson frequency (Black *et al.*, 1995).

Black *et al.* (1995b, 1995) extended the imaging frequency from 1 MHz to 1 GHz by applying a rf field to the sample, which, in turn, couples an rf flux Φ_{rf} into the SQUID. The rf flux smoothes out the V-Φ curve of the SQUID, reducing the modulation depth. Thus, when the SQUID is also flux-modulated at a low frequency, $f_m = 25\,\mathrm{kHz}$, one can show that the modulation depth is given by

$$V(\Phi_{rf}) = V_0 J_0(2\pi\Phi_{rf}/\Phi_0), \tag{10.1}$$

where V_0 is the value with no rf field and J_0 is the zero-order Bessel function of the first kind. Equation (10.1) can be inverted to find Φ_{rf} provided it is sufficiently small. This technique was used to image a wire in the shape of a meander pattern.

For frequencies higher than 1 GHz, one can use the SQUID itself as the source of the field excitation (Black *et al.*, 1995a, 1995). The oscillating magnetic fields at the Josephson frequency corresponding to the bias voltage induce eddy currents in the nearby sample which couple fields back into the SQUID. The essential effect is to reduce the inductance of the SQUID, thereby increasing the voltage modulation depth measured at low frequencies. Thus by monitoring the modulation depth as the sample is scanned over the SQUID one can obtain images at microwave frequencies. Figure 44 shows an image of a 500-nm-thick Cu film that had been patterned into a series of grids of various sizes. The SQUID was 40 μm from the grid, and the Josephson frequency was about 9 GHz. The brightest regions correspond to an increase in modulation depth of about 2%.

In concluding this section, we note that the best scanning SQUID microscopes with cold samples have a spatial resolution of perhaps 5 μm, while those with room-temperature samples have a resolution that is more like 30–50 μm. A recent innovation (Pitzius *et al.*, 1997), however, has dramatically improved the spatial resolution for cold samples, albeit at the price of magnetic-field sensitivity. These authors use a soft magnetic tip to focus the flux from the sample into the SQUID, and were able to achieve a spatial resolution of the order of 0.1 μm. A similar principle has been used by Tavrin and Siegel (1997) to examine room-temperature samples.

D. Geophysics

A particularly appealing application of high-T_c SQUID magnetometers is in geophysical surveying

(Clarke, 1983), for example, magnetotellurics, controlled-source electromagnetics, and cross-borehole sounding. In magnetotellurics, one measures simultaneously the fluctuating horizontal components of the electric and magnetic fields at the earth's surface; these fluctuating fields originate in the magnetosphere and ionosphere. From these frequency-dependent fields one calculates the impedance tensor of the ground and hence estimates the spatial variation of the resistivity of the ground. Frequencies of interest are typically 10^{-3}–10^{2} Hz, and the corresponding skin depths, assuming a resistivity of 10 Ωm, are 50 km to 150 m. To eliminate the effects of local noise sources, one cross-correlates the fluctuating fields with those measured with a remote reference magnetometer 5–10 km away. Applications of magnetotellurics include surveying for oil and gas, and locating subsurface fault lines. In controlled-source electromagnetics, one uses a transmitter to supply large current or magnetic pulses to the ground, and determines the magnetic response. The naturally occurring fluctuating fields are now a source of noise, and a remote magnetometer is used to cancel them. In cross-borehole sounding, a receiver in one borehole is used to detect magnetic pulses from a transmitter in a second borehole. From the real and imaginary parts of the received signal one deduces the susceptibility of the ground between the two boreholes, and models the porosity.

Currently, these magnetic measurements are made with induction coils. In fact, in the late 1970s and early 1980s, low-T_c SQUID magnetometers were used very successfully in magnetotellurics (Clarke *et al.*, 1983) and exploited commercially. However, the inconvenience of using liquid helium, particularly in remote areas of the world, coupled with the drop in the price of oil which severely curtailed oil prospecting, led to the abandonment of cryogenic sensors. The advent of liquid nitrogen-cooled magnetometers, on the other hand, has renewed interest in this application. Below about 1 Hz, the spectral density of the noise in coils increases as $1/f^3$, whereas that of SQUIDs increases as $1/f$, giving the latter magnetometer a substantial advantage at low frequencies. Furthermore, coils for use below 1 Hz can be as long as 1.5 m, and the deployment of three such coils orthogonally, buried in the ground for stability, is a tedious undertaking. Thus a three-axis high-T_c magnetometer in a compact dewar with a long hold time becomes very competitive.

Dantsker *et al.* (1994) constructed a three-axis magnetometer based on directly coupled magnetometers, and showed that it had sufficient slew rate for use in the field. Wang *et al.* (1997) reported preliminary experiments using a high-T_c magnetometer for magnetotellurics and transient electromagnetics. Matzander *et al.* (1997) deployed a system with a white noise of 200 $\mathrm{fT\,Hz^{-1/2}}$ and a $1/f$ knee of 10 Hz, and used it successfully to demonstrate controlled-source electromagnetic measurements. A system for shallow borehole sounding is under development (Drung *et al.*, 1997; Radic *et al.*, 1997).

What sensitivity does one require, for example, for magnetotellurics? A white noise of 20–30 $\mathrm{fT\,Hz^{-1/2}}$ and a $1/f$ knee of 1 Hz would be competitive; needless to say, these noise levels must be attained with the magnetometer operating in the earth's magnetic field, so that elimination of low-frequency noise due to vortex motion is imperative (Sec. IX.A). The fabrication of such a system is eased by the fact that there are no tight space constraints, and one could almost certainly use single-layer components, for example, a dc or rf SQUID coupled to a large-area flux transformer in a flip-chip arrangement.

XI. CONCLUDING REMARKS

The performance of high-T_c dc and rf SQUIDs and of magnetometers based upon them has progressed to the point where, in principle, it is adequate for many practical applications. One notable exception is magnetoencephalography, where the magnetic-field noise of a few $\mathrm{fT\,Hz^{-1/2}}$ at frequencies down to below 1 Hz routinely achieved with low-T_c devices is still somewhat beyond the reach of their high-T_c counterparts. What, then, are the major issues remaining in the fabrication and operation of the high-T_c devices and what are the most likely uses of them in the next few years?

Many groups can routinely deposit high-quality thin films of YBCO with low levels of $1/f$ flux noise in zero magnetic field. Very few, however, have anything like the same capability to deposit a YBCO-STO-YBCO structure, with each layer patterned to form a flux transformer, with guaranteed electrical integrity let alone low levels of $1/f$ noise. The multilayer magnetometers with the lowest white magnetic-field noise all exhibit $1/f$ noise at 1 Hz, even when cooled in zero magnetic field. Since unpatterned trilayers can be made with negligible excess noise, the noise in patterned structures is presumably associated with edges. It is likely—but not assured—that sufficiently careful engineering of these edges, perhaps accompanied by more transmission electron microscopy, will reduce the flux noise power at 1 Hz by the required order of magnitude. With regard to junctions, despite enormous progress with artificial barriers, the workhorse for SQUIDs remains the grain-boundary junction. Even bicrystal grain-boundary junctions are not entirely routine: although one often can produce, say, a dozen SQUIDs on a bicrystal that all exhibit quantum interference, not all of them have optimum characteristics and correspondingly low noise. The degree of irreproducibility represents the variability in the bicrystal substrates, and it is not obvious that a great deal of improvement can be made. Thus the field still awaits the invention of a new junction technology that offers both high yield and high I_0R product. For the moment, at least from an economic standpoint, the best philosophy is probably to fabricate relatively large numbers of SQUIDs, select the best, and couple them to a suitable input circuit in a flip-chip arrangement.

Most research has been focused on dc SQUIDs, probably because their performance at 4.2 K has been much superior to rf SQUIDs. However, the advantage

of the dc SQUID over the rf SQUID at 77 K is much narrower, in part because one can use a somewhat larger inductance for the latter so that the effective area and intrinsic magnetic-field sensitivity are higher. To date, magnetometers based on dc SQUIDs have achieved lower noise than those of comparable size based on rf SQUIDs, particularly at low frequencies. However, this advantage has been due largely to the use of multilayer flux transformers coupled to dc SQUIDs, and may not persist now that such transformers are being used with rf SQUIDs. On the other hand, the fact that the white noise in dc SQUIDs is generally higher than predicted remains an important issue. If this problem is eventually resolved, for example, by the introduction of a more ''perfect'' type of junction, the performance of dc SQUIDs may well improve substantially. Furthermore, the possibility of significant crosstalk between rf SQUIDs in a multichannel system may prove to be a significant challenge. Thus the question of whether to choose dc or rf SQUIDs is still open, and may ultimately depend on the application at hand.

We have emphasized issues of operating SQUIDs in an unshielded environment. The fact that the $1/f$ noise can increase dramatically when a high-T_c SQUID is cooled in the earth's field is peculiar to high-T_c superconductors: because they are operated at much lower temperatures and have much higher flux-pinning energies, low-T_c SQUIDs do not suffer from this drawback. Hopefully, the introduction of narrow linewidths has solved the problem for high-T_c devices cooled in a static field, although this has yet to be demonstrated for a SQUID coupled to a multilayer, multiturn flux transformer. The use of a ''flux dam'' offers the possibility of maintaining low $1/f$ noise even after the ambient field is changed. In common with low-T_c SQUIDs, for most applications the operation of high-T_c SQUIDs without shielding generally raises the issue of ambient magnetic-field noise. The solution—the gradiometer—is the same for both techniques. However, 4.2 K systems have an inexpensive ''low tech'' approach based on niobium wire that is not available to 77 K systems. In high-T_c systems, the current options are to subtract the outputs of two or more magnetometers or to make planar, thin-film gradiometers. The former approach requires no new thin-film components and can be easily implemented with diagonal or off-diagonal first- or second-order gradients, arbitrarily long baselines, and in ingenious configurations such as the three-SQUID gradiometer. The thin-film gradiometers have the advantage of substantial rejection of uniform magnetic-field noise—say, by three orders of magnitude—by a passive, linear, noise-free device. It is straightforward to make gradiometers with short-baselines—a few millimeters—that are very adequate for nondestructive evaluation. On the other hand, a baseline of, say, 50 mm is more of a challenge. Single-layer, symmetric flux transformers have been used successfully but lose sensitivity because the inductance of their large-area pickup loops cannot be matched to the much lower inductance of the SQUID. The solution, of course, is to use multiturn input coils, but the cost of making multilayer structures on large substrates is likely to be prohibitive. An alternative solution is the asymmetric gradiometer which requires only a single-layer flux transformer and does not significantly reduce the intrinsic sensitivity of the magnetometer to which it is coupled. The choice of gradiometers is another area that remains to be resolved.

Turning briefly to applications of high-T_c SQUIDs, we have seen impressive demonstrations of both MEG and MCG. However, as already noted, the sensitivity of high-T_c sensors is marginal for the former systems and while these systems are confined to relatively few centers and to a magnetically shielded room, the cost and higher boil-off rate of liquid ^{4}He are not overriding issues. On the other hand, one might hope that MCG will become a more widespread modality over the next few years, for example, in the assessment of damage to heart muscle following a cardiac infarction, for the diagnosis of heart arrhythmia and for locating the source of certain kinds of arrhythmia. Here, the benefits of liquid nitrogen as a cryogen—or indeed of a cryocooler in the longer term—combined with unshielded operation are highly desirable. Although clinical trials on large numbers of patients have yet to be performed, MCG currently appears to be the largest potential application of high-T_c SQUIDs. Whether or not this field materializes depends not only on the development of suitable, low-noise gradiometers for unshielded operations but also on the availability of funding for suitable trials.

A second application, nondestructive evaluation (NDE), is the one where the most ''real world'' progress has been made, for example, for the evaluation of aircraft components. Techniques involving both eddy currents and remanent magnetization have been successfully implemented. This is an area in which the ultimate sensitivity of SQUIDs is not required—generally 1 $\mathrm{pT\,Hz^{-1/2}}$ is more than sufficient—and in which short-baseline gradiometers are adequate. The ability of the SQUID to operate in a static field and over a very wide range of frequencies gives an advantage over flux-gate magnetometers, and the fact that the sensitivity is maintained at arbitrarily low frequencies offers a distinct advantage over coils. This area seems poised for rapid growth.

Novel ''SQUID microscopes'' can be used in either a scanning or a static mode. The potential of these microscopes for biology is intriguing. One novel example is in immunoassay (Kötitz *et al.*, 1997). Here, one labels an antibody with a tiny magnetic particle and exposes it to an appropriate antigen in the solid phase. The binding of the antibody with the antigen is detected by means of the remanent magnetization imparted to the immobilized particle. Another potential use of the microscope is to detect low-frequency nuclear magnetic resonance (NMR) and nuclear quadrupole resonance of room-temperature samples, for example, NMR of hyperpolarized ^{129}Xe (TonThat *et al.*, 1997).

The use of high-T_c SQUIDs in geophysics is ''straightforward'' now that low levels of $1/f$ noise can be realized in the earth's magnetic field. One should not

underestimate the sensitivity of commercially available coils in these applications, but since the space constraints on a three-axis magnetometer are not severe, one should be able to achieve 10 fT $Hz^{-1/2}$ at 1 Hz, with a $1/f^{1/2}$ increase at lower frequencies, using a single-layer flux transformer. Such a system, packaged with suitably rugged dewar and electronics, would be very competitive for low-frequency applications at the earth's surface. In the longer term, the use of SQUID magnetometers for cross-borehole sounding would offer a distinct advantage over coils.

What will it take to foster this wide range of applications? Currently, most of these techniques continue to be practiced by people who are experts in SQUIDs and, indeed, who have made the devices themselves. Clearly, this situation must change if high-T_c SQUIDs are to be widely deployed. This change will require not only more user-friendly packaging but also lower pricing. Lower costs imply larger-scale manufacturing, and it is to be hoped that one or more companies will soon see fit to adopt the necessary processing technologies. However, one should recognize that the total system price is often dominated by the cost of the cryogenics, be it liquid nitrogen or a cryocooler. This additional expense must be justified in terms of improved performance compared with competing technologies if SQUID-based instruments are to be widely adopted.

Note added in proof. Chesca (1998b, 1999) developed an analytic theory for dc SQUIDs operating in the presence of large thermal fluctuations, similar to his approach for rf SQUIDs. This work is based on solving the two-dimensional Fokker-Planck equation, which is equivalent to the coupled Langevin equations. Chesca finds analytical solutions for the dc SQUID in the limit $\beta_L < 1/\pi$. The noise energy ε scales as $\varepsilon \propto \Gamma^4$, for fixed L, and the optimum SQUID inductance is found to be $L = L_{\rm th}/\pi$ (≈ 10 pH at T=77 K) for $\Gamma > 1$.

In a systematic study of the transfer function and thermal noise of YBCO dc SQUIDs, Barthel *et al.* (1999) compare both numerical simulations and Chesca's analytical approach with experimental results obtained for a wide range of noise parameters up to $\Gamma = 5$. Several predictions of the analytical theory could be verified experimentally, and a good qualitative agreement with both theories is observed. Furthermore, the numerical simulations performed in the limit of large thermal fluctuations show excellent agreement with the analytic theory.

Zhang *et al.* (1999) demonstrated a design of a planar multiturn flux transformer integrated with a superconducting labyrinth resonator serving as the planar tank circuit for a YBCO thin film rf SQUID magnetometer. When coupled to a 210 pH double-hole washer SQUID in flip-chip configuration the magnetometer showed a white magnetic field noise as low as 11.5 fT $Hz^{-1/2}$ (above $f \approx 3$ kHz). However, the noise at 10 Hz was more than one order of magnitude above the whate noise level, presumably due to $1/f$ noise from poor film quality.

Kittel *et al.* (1998) have fabricated and tested a planar, thin-film, second-derivative gradiometer. The flux transformer consisted of two identical pickup loops placed one on each side of a smaller loop that was inductively coupled to a directly coupled magnetometer; this configuration can be envisioned as a second pickup loop coupled to the left-hand side of the smaller loop in Fig. 33(b). The overall length of the flux transformer was 80 mm, and the baselines for the first- and second-derivatives were 62 mm and 31 mm, respectively. By mechanically adjusting the separation between the magnetometer and the flux transformer, the authors achieved a typical rejection of uniform magnetic fields of 50 ppm. The residual first-order gradient response was at most 1.4% relative to the second-order gradient response.

Fleet *et al.* (1999) have described a high T_c scanning SQUID microscope for detecting flaws in computer chips. The room-temperature sample could be brought to within 30 μm of the SQUID, which was cooled by a cryocooler. A 3 kHz current was passed through the circuit, which was on the far side of the chip from the SQUID, and the magnetic field images obtained by the SQUID were inverted to generate two-dimensional current density distributions. This technique enabled the authors to achieve a spatail resolution of 75 μm, substantially less than the SQUID-circuit separation of 340 μm. A short-circuit on the chip was located.

ACKNOWLEDGMENTS

In preparing this review we have benefitted from help from many people. We gratefully acknowledge discussions with L. Alff, K. Barthel, R. Cantor, B. Chesca, R. Dittmann, O. Dössel, D. Drung, R. Gross, R. H. Koch, H.-J. Krause, A. Marx, M. Mück, and M. Siegel. We are indebted to A. I. Braginski, B. Chesca, and R. Gross, each of whom read one section and made constructive comments. The following authors supplied us with figures: R. Cantor, B. Chesca, G. M. Daalmans, D. Drung, M. I. Faley, R. Gross, R. Hohmann, H.-J. Krause, R. H. Koch, A. Marx, M. Mück, T. Nagaishi, J. Z. Sun, Y. Tavrin, F. C. Wellstood, and Y. Zhang. B. Salisbury prepared the entire manuscript. This work was partly supported by the Director, Office of Energy Research, Office of Basic Energy Sciences, Materials Sciences Division of the U.S. Department of Energy under Contract No. DE-AC03-76SF00098.

REFERENCES

Aarnink, W. A. M., P. J. van den Bosch, T.-M. Roelofs, M. Verbiesen, H. J. Holland, H. J. M. ter Brake, and H. Rogalla, 1995, IEEE Trans. Appl. Supercond. **5**, 2470.

Alff, L., G. M. Fischer, R. Gross, F. Kober, A. Beck, K. D. Husemann, T. Nissel, F. Schmidl, and C. Burckhardt, 1992, Physica C **200**, 277.

Alff, L. S., S. Kleefisch, U. Schoop, M. Zittartz, T. Kemen, T. Bauch, A. Marx, and R. Gross, 1998, Eur. Phys. J. B **5**, 423.

Ambegaokar, V., and B. I. Halperin, 1969, Phys. Rev. Lett. **22**, 1364.

Aminov, B. A., A. A. Golubov, and M. Y. Kupriyanov, 1996, Phys. Rev. B **53**, 365.

Banchet, J., J. Jouglar, P.-L. Vuillermoz, P. Waltz, and H. Weinstock, 1995, IEEE Trans. Appl. Supercond. **5**, 2486.
Barbour, J. C., E. L. Venturini, D. S. Ginley, and J. F. Kwak, 1992, Nucl. Instrum. Methods Phys. Res. B **65**, 531.
Barone, A., and G. Paterno, 1982, *Physics and Applications of the Josephson Effect* (Wiley, New York).
Barth, R., B. Spangenberg, C. Jäckel, H. G. Roskos, H. Kurz, and B. Holzapfel, 1993, Appl. Phys. Lett. **63**, 1149.
Barthel, K., D. Koelle, B. Chesca, A. I. Braginski, A. Marx, R. Gross, and R. Kleiner, 1999, Appl. Phys. Lett. (in press).
Beck, A., O. M. Froehlich, D. Koelle, R. Gross, H. Sato, and M. Naito, 1996, Appl. Phys. Lett. **68**, 3341.
Beck, A., A. Stenzel, O. M. Froehlich, R. Gerber, R. Gerdemann, L. Alff, B. Mayer, R. Gross, A. Marx, J. C. Villegier, and H. Moriceau, 1995, IEEE Trans. Appl. Supercond. **5**, 2192.
Bednorz, J. G., and K. A. Müller, 1986, Z. Phys. B **64**, 189.
Berberich, P., B. Utz, W. Prusseit, and H. Kinder, 1994, Physica C **219**, 497.
Beyer, J., D. Drung, F. Ludwig, T. Minotani, and K. Enpuku, 1998, Appl. Phys. Lett. **72**, 203.
Black, R. C., 1995, Ph.D. thesis, University of Maryland.
Black, R. C., A. Mathai, F. C. Wellstood, E. Dantsker, A. H. Miklich, D. T. Nemeth, J. J. Kingston, and J. Clarke, 1993, Appl. Phys. Lett. **62**, 2128.
Black, R. C., F. C. Wellstood, E. Dantsker, A. H. Miklich, J. J. Kingston, D. T. Nemeth, and J. Clarke, 1994, Appl. Phys. Lett. **64**, 1.
Black, R. C., F. C. Wellstood, E. Dantsker, A. H. Miklich, D. Koelle, F. Ludwig, and J. Clarke, 1995, IEEE Trans. Appl. Supercond. **5**, 2137.
Black, R. C., F. C. Wellstood, E. Dantsker, A. H. Miklich, D. T. Nemeth, D. Koelle, F. Ludwig, and J. Clarke, 1995a, Appl. Phys. Lett. **66**, 99.
Black, R. C., F. C. Wellstood, E. Dantsker, A. H. Miklich, D. T. Nemeth, D. Koelle, F. Ludwig, and J. Clarke, 1995b, Appl. Phys. Lett. **66**, 1267.
Bode, M., M. Grove, M. Siegel, and A. I. Braginski, 1996, J. Appl. Phys. **80**, 6378.
Borgmann, J., P. David, G. Ockenfuß, R. Otto, J. Schubert, W. Zander, and A. I. Braginski, 1997, Rev. Sci. Instrum. **68**, 2730.
Braginski, A. I., 1993, in *The New Superconducting Electronics*, NATO ASI series, edited by H. Weinstock and R. W. Ralston (Kluwer Academic, Dordrecht), p. 89.
Braginski, A. I., 1996, in *SQUID Sensors: Fundamentals, Fabrication and Applications*, NATO ASI Series, edited by H. Weinstock (Kluwer Academic, Dordrecht), p. 235.
Bruines, J. J. P., V. J. de Waal, and J. E. Mooji, 1982, J. Low Temp. Phys. **46**, 383.
Burghoff, M., L. Trahms, Y. Zhang, H. Bousack, and J. Borgmann, 1996, J. Clin. Eng. **21**, 62.
Cantor, R., 1996, in *SQUID Sensors: Fundamentals, Fabrication and Applications*, NATO ASI Series, edited by H. Weinstock (Kluwer Academic, Dordrecht), p. 179.
Cantor, R., L. P. Lee, M. Teepe, V. Vinetskiy, and J. Longo, 1995, IEEE Trans. Appl. Supercond. **5**, 2927.
Carr, C., D. McA. McKirdy, E. J. Romans, and G. B. Donaldson, 1997, IEEE Trans. Appl. Supercond. **7**, 3275.
Chang, W. H., 1981, IEEE Trans. Magn. **MAG-17**, 764.
Char, K., M. S. Colclough, L. P. Lee, and G. Zaharchuk, 1991, Appl. Phys. Lett. **59**, 2177.
Chaudhari, P., J. Mannhart, D. Dimos, C. C. Tsuei, C. C. Chi, M. M. Oprysko, and M. Scheuermann, 1988, Phys. Rev. Lett. **60**, 1653.
Chemla, Y. R., T. S. Lee, J. Clarke, M. Adamkiewicz, and B. Buchanan, 1997, in *Extended Abstracts of the 6th International Superconductive Electronics Conference (ISEC'97)*, Berlin, edited by H. Koch and S. Knappe (Physikalisch-Technische Bundesanstalt, Braunschweig), Vol. 1, p. 140.
Chen, J., T. Yamashita, H. Suzuki, K. Nakajima, H. Kurosawa, Y. Mutoh, Y. Hirotsu, H. Myoren, and Y. Osaka, 1991, Jpn. J. Appl. Phys., Part 1 **30**, 1964.
Chen, Y. F., Z. G. Ivanov, E. A. Stepantsov, A. Ya. Tzalenchuk, S. Zarembinski, T. Claeson, and L.-G. Johansson, 1996, J. Appl. Phys. **79**, 9221.
Chesca, B., 1998a, J. Low Temp. Phys. **110**, 963.
Chesca, B., 1998b, J. Low Temp. Phys. **112**, 165.
Chesca, B., 1999, IEEE Trans. Appl. Supercond. (in press).
Clarke, J., 1983, IEEE Trans. Magn. **MAG-19**, 288.
Clarke, J., 1996, in *SQUID Sensors: Fundamentals, Fabrication and Applications*, NATO ASI Series, edited by H. Weinstock (Kluwer Academic, Dordrecht), p. 1.
Clarke, J., T. D. Gamble, W. M. Goubau, R. H. Koch, and R. F. Miracky, 1983, Geophys. Pros. **31**, 149.
Clarke, J., W. M. Goubau, and M. B. Ketchen, 1976, J. Low Temp. Phys. **25**, 99.
Clem, J., 1996, unpublished.
Clem, T. R., J. W. Purpura, R. F. Wiegert, and W. L. Goodman, 1993, IEEE Trans. Appl. Supercond. **3**, 1848.
Colclough, M. S., C. E. Gough, M. Keene, C. M. Muirhead, N. Thomas, J. S. Abell, and S. Sutton, 1987, Nature (London) **328**, 47.
Curio, G., D. Drung, H. Koch, W. Müller, U. Steinhoff, L. Trahms, Y. Q. Shen, P. Vase, and T. Freltoft, 1996, Neurosci. Lett. **206**, 204.
Daalmans, G. M., 1995, Appl. Supercond. **3**, 399.
Daalmans, G. M., L. Bär, M. Kühnl, D. Uhl, M. Selent, and J. Ramos, 1995, IEEE Trans. Appl. Supercond. **5**, 3109.
Daly, K. P., J. Burch, S. Coons, and R. Hu, 1991, IEEE Trans. Magn. **MAG-27**, 3066.
Danilov, V. V., K. K. Likharev, and O. V. Snigirev, 1980, in *SQUID'80, Superconducting Quantum Interference Devices and their Applications*, edited by H. D. Hahlbohm and H. Lübbig (Walter de Gruyter, Berlin), p. 473.
Dantsker, E., O. Froehlich, S. Tanaka, K. Kouznetsov, J. Clarke, Z. Lu, V. Matijasevic, and K. Char, 1997, Appl. Phys. Lett. **71**, 1712.
Dantsker, E., D. Koelle, A. H. Miklich, D. T. Nemeth, F. Ludwig, J. Clarke, J. T. Longo, and V. Vinetskiy, 1994, Rev. Sci. Instrum. **65**, 3809.
Dantsker, E., F. Ludwig, R. Kleiner, J. Clarke, M. Teepe, L. P. Lee, N. McN. Alford, and T. Button, 1995, Appl. Phys. Lett. **67**, 725.
Dantsker, E., S. Tanaka, and J. Clarke, 1997, Appl. Phys. Lett. **70**, 2037.
Dantsker, E., S. Tanaka, P.-Å. Nilsson, R. Kleiner, and J. Clarke, 1996, Appl. Phys. Lett. **69**, 4099.
David, B., O. Dössel, V. Doormann, R. Eckart, W. Hoppe, J. Krüger, H. Laudan, and G. Rabe, 1997, IEEE Trans. Appl. Supercond. **7**, 3267.
David, B., D. Grundler, R. Eckart, K. Fanghänel, J. P. Krumme, V. Doormann, and O. Dössel, 1994, Supercond. Sci. Technol. **7**, 287.

David, B., D. Grundler, S. Krey, V. Doormann, R. Eckart, J. P. Krumme, G. Rabe, and O. Dössel, 1996, Supercond. Sci. Technol. **9**, A96.
David, B., D. Grundler, J.-P. Krumme, and O. Dössel, 1995, IEEE Trans. Appl. Supercond. **5**, 2935.
Delin, K. A., and A. W. Kleinsasser, 1996, Supercond. Sci. Technol. **9**, 227.
Deutscher, G., and K. A. Müller, 1987, Phys. Rev. Lett. **59**, 1745.
de Waal, V. J., P. Schrijner, and R. Llurba, 1984, J. Low Temp. Phys. **54**, 215.
Dieckmann, N., A. Bock, and U. Merkt, 1996, Appl. Phys. Lett. **68**, 3626.
DiIorio, M. S., K.-Y. Yang, and S. Yoshizumi, 1995, Appl. Phys. Lett. **67**, 1926.
DiIorio, M. S., S. Yoshizumi, K.-Y. Yang, M. Maung, and B. Power, 1993, in *Advances in Superconductivity V*, edited by Y. Bando and H. Yamauchi (Springer, Tokyo), p. 1161.
DiIorio, M. S., S. Yoshizumi, K.-Y. Yang, M. Maung, J. Zhang, and B. Power, 1993, IEEE Trans. Appl. Supercond. **3**, 2011.
DiIorio, M. S., S. Yoshizumi, K.-Y. Yang, J. Zhang, and M. Maung, 1991, Appl. Phys. Lett. **58**, 2552.
Dillmann, F., V. N. Glyantsev, and M. Siegel, 1996, Appl. Phys. Lett. **69**, 1948.
Dimos, D., P. Chaudhari, and J. Mannhart, 1990, Phys. Rev. B **41**, 4038.
Dimos, D., P. Chaudhari, J. Mannhart, and F. K. LeGoues, 1988, Phys. Rev. Lett. **61**, 219.
Dömel, R., C. Horstmann, M. Siegel, A. I. Braginski, and M. Y. Kupriyanov, 1995, Appl. Phys. Lett. **67**, 1775.
Donaldson, G., S. Evanson, M. Otaka, K. Hasegawa, T. Shimizu, and K. Takaku, 1990, Br. J. Non-Destr. Test. **32**, 238.
Dörrer, L., S. Wunderlich, F. Schmidl, H. Schneidewind, U. Hübner, and P. Seidel, 1997, Appl. Supercond. (in press).
Dössel, O., B. David, M. Fuchs, W. H. Kullmann, and K.-M. Lüdeke, 1991, IEEE Trans. Magn. **MAG-27**, 2797.
Drung, D., 1994, IEEE Trans. Appl. Supercond. **4**, 121.
Drung, D., 1995, Appl. Phys. Lett. **67**, 1474.
Drung, D., 1996, in *SQUID Sensors: Fundamentals, Fabrication and Applications*, NATO ASI Series, edited by H. Weinstock (Kluwer Academic, Dordrecht), p. 63.
Drung, D., R. Cantor, M. Peters, T. Ryhänen, and H. Koch, 1991, IEEE Trans. Magn. **MAG-27**, 3001.
Drung, D., R. Cantor, M. Peters, H.-J. Scheer, and H. Koch, 1990, Appl. Phys. Lett. **57**, 406.
Drung, D., E. Dantsker, F. Ludwig, H. Koch, R. Kleiner, J. Clarke, S. Krey, D. Reimer, B. David, and O. Doessel, 1996, Appl. Phys. Lett. **68**, 1856.
Drung, D., S. Knappe, and H. Koch, 1995, J. Appl. Phys. **77**, 4088.
Drung, D. and H. Koch, 1993, IEEE Trans. Appl. Supercond. **3**, 2594.
Drung, D., F. Ludwig, W. Müller, U. Steinhoff, L. Trahms, Y. Q. Shen, M. B. Jensen, P. Vase, T. Holst, T. Freltoft, and G. Curio, 1996, Appl. Phys. Lett. **68**, 1421.
Drung, D., T. Radic, H. Matz, H. Koch, S. Knappe, S. Menkel, and H. Burkhardt, 1997, IEEE Trans. Appl. Supercond. **7**, 3283.
Ehnholm, G. J., 1977, J. Low Temp. Phys. **29**, 1.
Eidelloth, W., B. Oh, R. P. Robertazzi, W. J. Gallagher, and R. H. Koch, 1991, Appl. Phys. Lett. **59**, 3473.
Enpuku, K., 1993, Jpn. J. Appl. Phys., Part 2 **32**, L1407.
Enpuku, K., H. Doi, G. Tokita, and T. Maruo, 1995, IEEE Trans. Appl. Supercond. **5**, 2762.
Enpuku, K., T. Maruo, and T. Minotani, 1996, J. Appl. Phys. **80**, 1207.
Enpuku, K., T. Maruo, and T. Minotani, 1997, IEEE Trans. Appl. Supercond. **7**, 3355.
Enpuku, K., T. Muta, K. Yoshida, and F. Irie, 1985, J. Appl. Phys. **58**, 1916.
Enpuku, K., Y. Shimomura, and T. Kisu, 1993, J. Appl. Phys. **73**, 7929.
Enpuku, K., K. Sueoka, K. Yoshida, and F. Irie, 1985, J. Appl. Phys. **57**, 1691.
Enpuku, K., G. Tokita, and T. Maruo, 1994, J. Appl. Phys. **76**, 8180.
Enpuku, K., G. Tokita, T. Maruo, and T. Minotani, 1995, J. Appl. Phys. **78**, 3498.
Erné, S. N., H.-D. Hahlbohm, and H. Lübbig, 1976, J. Appl. Phys. **47**, 5440.
Falco, C. M. and W. H. Parker, 1975, J. Appl. Phys. **46**, 3238.
Faley, M. I., U. Poppe, C. L. Jia, U. Dähne, Yu. Goncharov, N. Klein, K. Urban, V. N. Glyantsev, G. Kunkel, and M. Siegel, 1995, IEEE Trans. Appl. Supercond. **5**, 2091.
Faley, M. I., U. Poppe, K. Urban, H. Hilgenkamp, H. Hennes, W. Aarnink, J. Flokstra, and H. Rogalla, 1995, Appl. Phys. Lett. **67**, 2087.
Faley, M. I., U. Poppe, K. Urban, H.-J. Krause, H. Soltner, R. Hohmann, D. Lomparski, R. Kutzner, R. Wördenweber, H. Bousack, A. I. Braginski, V. Y. Slobodchikov, A. V. Gapelyuk, V. V. Khanin, and Y. V. Maslennikov, 1997, IEEE Trans. Appl. Supercond. **7**, 3702.
Ferrari, M. J., M. Johnson, F. C. Wellstood, J. Clarke, A. Inam, X. D. Wu, L. Nazar, and T. Venkatesan, 1989, Nature (London) **341**, 723.
Ferrari, M. J., M. Johnson, F. C. Wellstood, J. Clarke, P. A. Rosenthal, R. H. Hammond, and M. R. Beasley, 1988, Appl. Phys. Lett. **53**, 695.
Ferrari, M. J., M. Johnson, F. C. Wellstood, J. J. Kingston, T. J. Shaw, and J. Clarke, 1994, J. Low Temp. Phys. **94**, 15.
Ferrari, M. J., J. J. Kingston, F. C. Wellstood, and J. Clarke, 1991, Appl. Phys. Lett. **58**, 1106.
Fife, A. A., G. Anderson, V. Angus, C. Backhouse, K. Betts, M. B. Burbank, R. A. Cragg, K. Ferguson, F. Habib, P. R. Kubik, J. Nomura, M. Smith, P. Spear, W. Westera, Hu Zhou, S. Govorkov, B. Heinrich, J. C. Irwin, and W. B. Xing, 1995, IEEE Trans. Appl. Supercond. **5**, 3113.
Fleet, E. H., S. Chatraphorn, F. C. Wellstood, S. M. Green, and L. A. Knauss, 1999, IEEE Trans. Appl. Supercond. (in press).
Foglietti, V., W. J. Gallagher, M. B. Ketchen, A. W. Kleinsasser, R. H. Koch, S. I. Raider, and R. L. Sandstrom, 1986, Appl. Phys. Lett. **49**, 1393.
Foglietti, V., R. H. Koch, W. J. Gallagher, B. Oh, B. Bumble, and W. Y. Lee, 1989, Appl. Phys. Lett. **54**, 2259.
Foglietti, V., R. H. Koch, J. Z. Sun, R. B. Laibowitz, and W. J. Gallagher, 1995, J. Appl. Phys. **77**, 378.
Forgacs, R. L., and A. F. Warnick, 1967, Rev. Sci. Instrum. **38**, 214.
Freltoft, T., Y. Q. Shen, and P. Vase, 1993, IEEE Trans. Appl. Supercond. **3**, 2937.
Friedl, G., M. Vildić, B. Roas, D. Uhl, F. Bömmel, M. Römheld, B. Hillenbrand, B. Stritzker, and G. M. Daalmans, 1992, Appl. Phys. Lett. **60**, 3048.

Gao, J., W. A. M. Aarnink, G. J. Gerritsma, and H. Rogalla, 1990, Physica C **171**, 126.
Gao, J., Y. Boguslavskij, B. B. G. Klopman, D. Terpstra, D. Wijbrans, G. J. Gerritsma, and H. Rogalla, 1992, J. Appl. Phys. **72**, 525.
Gerber, R., D. Koelle, R. Gross, R. P. Huebener, F. Ludwig, E. Dantsker, R. Kleiner, and J. Clarke, 1996, Appl. Phys. Lett. **68**, 1555.
Giffard, R. P., 1980, in *Superconducting Quantum Interference Devices and Their Applications*, edited by H. D. Hahlbohm and H. Lübbig (de Gruyter, Berlin), p. 445.
Giffard, R. P., J. C. Gallop, and B. N. Petley, 1976, Prog. Quantum Electron. **4**, 301.
Glyantsev, V. N., Y. Tavrin, W. Zander, J. Schubert, and M. Siegel, 1996, Supercond. Sci. Technol. **9**, A105.
Golubov, A. A., and M. Y. Kupriyanov, 1996, Physica C **259**, 27.
Govorkov, S., A. A. Fife, G. Anderson, V. Haid, Hu Zhou, B. Heinrich, and J. Chrzanowski, 1997, IEEE Trans. Appl. Supercond. **7**, 3235.
Gross, R., in *Interfaces in High-T_c Superconducting Systems*, edited by S. L. Shinde and D. A. Rudman (Springer, New York), p. 176.
Gross, R., L. Alff, A. Beck, O. M. Froehlich, R. Gerber, R. Gerdemann, A. Marx, B. Mayer, and D. Koelle, 1995, in *Proceedings of the 2nd Workshop on HTS Applications and New Materials*, edited by D. H. Blank (University of Twente, The Netherlands), p. 8.
Gross, R., L. Alff, A. Beck, O. M. Froehlich, D. Koelle, and A. Marx, 1997, IEEE Trans. Appl. Supercond. **7**, 2929.
Gross, R., and P. Chaudhari, 1992, in *Principles and Applications of Superconducting Quantum Interference Devices*, edited by A. Barone (World Scientific, Singapore), p. 419.
Gross, R., P. Chaudhari, D. Dimos, A. Gupta, and G. Koren, 1990, Phys. Rev. Lett. **64**, 228.
Gross, R., P. Chaudhari, M. Kawasaki, and A. Gupta, 1990, Phys. Rev. B **42**, 10735.
Gross, R., P. Chaudhari, M. Kawasaki, and A. Gupta, 1991, IEEE Trans. Magn. **MAG-27**, 3227.
Gross, R., P. Chaudhari, M. Kawasaki, M. B. Ketchen, and A. Gupta, 1990a, Appl. Phys. Lett. **57**, 727.
Gross, R., P. Chaudhari, M. Kawasaki, M. B. Ketchen, and A. Gupta, 1990b, Physica C **170**, 315.
Gross, R., and B. Mayer, 1991, Physica C **180**, 235.
Grove, M., R. Dittmann, M. Bode, M. Siegel, and A. I. Braginski, 1996, Appl. Phys. Lett. **69**, 696.
Grundler, D., B. David, R. Eckart, and O. Dössel, 1993, Appl. Phys. Lett. **63**, 2700.
Grundler, D., B. David, and O. Dössel, 1995, in *Proceedings of the Second European Conference on Applied Superconductivity (EUCAS'95)*, Institute of Physics Conference Series No. **148**, Edinburgh, edited by D. Dew-Hughes (Institute of Physics, Bristol/Philadelphia), p. 1625.
Grundler, D., R. Eckart, B. David, and O. Dössel, 1993, Appl. Phys. Lett. **62**, 2134.
Gupta, A., J. Z. Sun, and C. C. Tsuei, 1994, Science **265**, 1075.
Gurvitch, M., M. A. Washington, and H. A. Huggins, 1983, Appl. Phys. Lett. **42**, 472.
Hagerhorst, J. M., J. D. Mannhart, M. M. Oprysko, M. R. Scheuermann, and C. C. Tsuei, 1989, *Laser and Particle-Beam Modification of Chemical Processes on Surfaces*, edited by A. W. Johnson, G. L. Loper and T. W. Sigmon, Mat. Res. Soc. Symp. Proc. Vol. 129, 347.
Hämäläinen, M., R. Hari, R. J. Ilmoniemi, J. Knuutila, and O. V. Lounasmaa, 1993, Rev. Mod. Phys. **65**, 413.
Hansma, P. K., 1973, J. Appl. Phys. **44**, 4191.
He, D. F., X. H. Zeng, H.-J. Krause, H. Soltner, F. Rüders, and Y. Zhang, 1998, Appl. Phys. Lett. **72**, 696.
Hein, M. A., S. Schmöe, M. Strupp, H. Piel, Y. Zhang, and A. I. Braginski, 1995, IEEE Trans. Appl. Supercond. **5**, 2501.
Herrmann, K., Y. Zhang, M. Mück, J. Schubert, and A. I. Braginski, 1991, Supercond. Sci. Technol. **4**, 583.
Herrmann, K., G. Kunkel, M. Siegel, J. Schubert, W. Zander, A. I. Braginski, C. L. Jia, B. Kabius, and K. Urban, 1995, J. Appl. Phys. **78**, 1131.
Hildebrandt, G., and F. H. Uhlmann, 1995, IEEE Trans. Appl. Supercond. **5**, 2766.
Hilgenkamp, J. W. M., G. C. S. Brons, J. G. Soldevilla, R. P. J. Ijsselsteijn, J. Flokstra, and H. Rogalla, 1994, Appl. Phys. Lett. **64**, 3497.
Hilgenkamp, J. W. M., R. P. J. Ijsselsteijn, A. J. H. M. Rijnders, P. A. C. Tavares, J. Flokstra, and H. Rogalla, 1993, J. Alloys Compd. **195**, 707.
Hilgenkamp, H., J. Mannhart, and B. Mayer, 1996, Phys. Rev. B **53**, 14586.
Hilgenkamp, J. W. M., F. J. G. Roesthuis, S. Hoogeveen, L. D. Vargas Llona, J. Flokstra, and H. Rogalla, 1995, in *Proceedings of the 2nd Workshop on HTS Applications and New Materials*, edited by D. H. A. Blank (Enschede, The Netherlands), p. 117.
Hoenig, H. E., G. M. Daalmans, L. Bär, F. Bömmel, A. Paulus, D. Uhl, H. J. Weisse, S. Schneider, H. Seifert, H. Reichenberger, and K. Abram-Fuchs, 1991, IEEE Trans. Magn. **MAG-27**, 2777.
Hohmann, R., H.-J. Krause, H. Soltner, Y. Zhang, C. A. Copetti, H. Bousack, and A. I. Braginski, 1997, IEEE Trans. Appl. Supercond. **7**, 2860.
Hollenhorst, H. N., and R. P. Giffard, 1980, J. Appl. Phys. **51**, 1719.
Hollin, C. A., J. S. Abell, S. W. Goodyear, N. G. Chew, and R. G. Humphreys, 1994, Appl. Phys. Lett. **64**, 918.
Hosoya, M., E. Goto, N. Shimizu, and Y. Harada, 1989, IEEE Trans. Magn. **MAG-25**, 1111.
Humphreys, R. G., J. S. Satchell, N. G. Chew, J. A. Edwards, S. W. Goodyear, and M. N. Keene, 1991, Mater. Sci. Eng., B **10**, 293.
Husemann, K.-D., R. Gross, R. P. Huebener, and B. Roas, 1993, Appl. Phys. Lett. **62**, 2871.
Il'ichev, E., V. Zakosarenko, V. Schultze, H.-G. Meyer, H. E. Hoenig, V. N. Glyantsev, and A. Golubov, 1998, Appl. Phys. Lett. **72**, 731.
Itozaki, H., S. Tanaka, T. Nagaishi, and H. Kado, 1994, IEICE Trans. Electron. **E77-C**, 1185.
Itozaki, H., S. Tanaka, H. Toyoda, T. Hirano, Y. Haruta, M. Nomura, T. Saijou, and H. Kado, 1996, Supercond. Sci. Technol. **9**, A38.
Ivanov, Z. G., P. Å. Nilsson, D. Winkler, J. A. Alarco, T. Claeson, E. A. Stepantsov, and A. Ya. Tzalenchuk, 1991, Appl. Phys. Lett. **59**, 3030.
Jackel, L. D., and R. A. Buhrman, 1975, J. Low Temp. Phys. **19**, 201.
Jaklevic, R. C., J. Lambe, A. H. Silver, and J. E. Mercereau, 1964, Phys. Rev. Lett. **12**, 159.
Jaycox, J. M., and M. B. Ketchen, 1981, IEEE Trans. Magn. **17**, 400.

Jia, C. L., B. Kabius, K. Urban, K. Herrmann, G. J. Cui, J. Schubert, W. Zander, A. I. Braginski, and C. Heiden, 1991, Physica C **175**, 545.
Jia, C. L., B. Kabius, K. Urban, K. Herrmann, J. Schubert, W. Zander, and A. I. Braginski, 1992, Physica C **196**, 211.
Josephson, B. D., 1962, Phys. Lett. **1**, 251.
Josephson, B. D., 1965, Adv. Phys. **14**, 419.
Kang, D.-J., W. E. Booij, M. G. Blamire, and E. J. Tarte, 1997, in *Extended Abstracts of the 6th International Superconductive Electronics Conference (ISEC'97)*, Berlin, edited by H. Koch and S. Knappe (Physikalisch-Technische Bundesanstalt, Braunschweig), Vol. 3, p. 40.
Kasai, N., N. Ishikawa, H. Yamakawa, K. Chinone, S. Nakayama, and A. Odawara, 1997, IEEE Trans. Appl. Supercond. **7**, 2315.
Kawasaki, M., P. Chaudhari, and A. Gupta, 1992, Phys. Rev. Lett. **68**, 1065.
Kawasaki, M., P. Chaudhari, T. H. Newman, and A. Gupta, 1991, Appl. Phys. Lett. **58**, 2555.
Kawasaki, M., E. Sarnelli, P. Chaudhari, A. Gupta, A. Kussmaul, J. Lacey, and W. Lee, 1993, Appl. Phys. Lett. **62**, 417.
Keene, M. N., N. G. Chew, S. W. Goodyear, J. A. Edwards, R. G. Humphreys, K. Lander, and J. S. Satchell, 1994, Physica C **230**, 110.
Keene, M. N., N. J. Exon, R. G. Humphreys, and N. G. Chew, 1996, J. Appl. Phys. **79**, 8783.
Keene, M. N., S. W. Goodyear, N. G. Chew, R. G. Humphreys, J. S. Satchell, J. A. Edwards, and K. Lander, 1994, Appl. Phys. Lett. **64**, 366.
Keene, M. N., S. W. Goodyear, J. S. Satchell, J. A. Edwards, N. G. Chew, and R. G. Humphreys, 1993, IEEE Trans. Appl. Supercond. **3**, 2430.
Keene, N. M., J. S. Satchell, S. W. Goodyear, R. G. Humphreys, J. A. Edwards, N. G. Chew, and K. Lander, 1995, IEEE Trans. Appl. Supercond. **5**, 2923.
Ketchen, M. B., 1981, IEEE Trans. Magn. **17**, 387.
Ketchen, M. B., W. J. Gallagher, A. W. Kleinsasser, S. Murphy, and J. R. Clem, 1985, in *SQUID'85, Superconducting Quantum Interference Devices and their Applications*, edited by H. D. Hahlbohm and H. Lübbig (Walter de Gruyter, Berlin), p. 865.
Ketchen, M. B., W. M. Goubau, J. Clarke, and G. B. Donaldson, 1978, Appl. Phys. **49**, 4111.
Kittel A., K. A. Kouznetsov, R. McDermott, B. Oh, and John Clarke, 1998, Appl. Phys. Lett. **73**, 2197.
Kleiner, R., 1996, unpublished.
Kleiner, R., and P. Müller, 1994, Phys. Rev. B **49**, 1327.
Kleiner, R., F. Steinmeyer, G. Kunkel, and P. Müller, 1992, Phys. Rev. Lett. **68**, 2394.
Kleinsasser, A. W., and K. A. Delin, 1995, Appl. Phys. Lett. **66**, 102.
Knappe, S., D. Drung, T. Schurig, H. Koch, M. Klinger, and J. Hinken, 1992, Cryogenics **32**, 881.
Koch, H., R. Cantor, D. Drung, S. N. Erne, K. P. Matthies, M. Peters, T. Ryhänen, H. J. Scheer, and H. D. Hahlbohm, 1991, IEEE Trans. Magn. **MAG-27**, 2793.
Koch, R. H. 1994, unpublished.
Koch, R. H. 1997, private communication.
Koch, R. H., J. Clarke, W. M. Goubau, J. M. Martinis, C. M. Pegrum, and D. J. Van Harlingen, 1983, J. Low Temp. Phys. **51**, 207.
Koch, R. H., W. Eidelloth, B. Oh, R. P. Robertazzi, S. A. Andrek, and W. J. Gallagher, 1992, Appl. Phys. Lett. **60**, 507.
Koch, R. H., V. Foglietti, J. R. Rozen, K. G. Stawiasz, M. B. Ketchen, D. K. Lathrop, J. Z. Sun, and W. J. Gallagher, 1994, Appl. Phys. Lett. **65**, 100.
Koch, R. H., W. J. Gallagher, B. Bumble, and W. Y. Lee, 1989, Appl. Phys. Lett. **54**, 951.
Koch, R. H., M. B. Ketchen, W. J. Gallagher, R. L. Sandstrom, A. W. Kleinsasser, D. R. Gambrel, T. H. Field, and H. Matz, 1991, Appl. Phys. Lett. **58**, 1786.
Koch, R. H., J. R. Rozen, J. Z. Sun, and W. J. Gallagher, 1993, Appl. Phys. Lett. **63**, 403.
Koch, R. H., J. R. Rozen, P. Wöltgens, T. Picunko, W. J. Goss, D. Gambrel, D. Lathrop, R. Wiegert, and D. Overway, 1996, Rev. Sci. Instrum. **67**, 2968.
Koch, R. H., J. Z. Sun, V. Foglietti, and W. J. Gallagher, 1995, Appl. Phys. Lett. **67**, 709.
Koch, R. H., C. P. Umbach, G. J. Clark, P. Chaudhari, and R. B. Laibowitz, 1987, Appl. Phys. Lett. **51**, 200.
Koelle, D., E. Dantsker, D. T. Nemeth, F. Ludwig, and J. Clarke, 1993, unpublished.
Koelle, D., A. H. Miklich, E. Dantsker, F. Ludwig, D. T. Nemeth, J. Clarke, W. Ruby, and K. Char, 1993, Appl. Phys. Lett. **63**, 3630.
Koelle, D., A. H. Miklich, F. Ludwig, E. Dantsker, D. T. Nemeth, and J. Clarke, 1993, Appl. Phys. Lett. **63**, 2271.
Kötitz, R., H. Matz, L. Trahms, H. Koch, W. Weitschies, T. Rheinländer, W. Semmler, and T. Bunte, 1997, IEEE Trans. Appl. Supercond. **7**, 3678.
Krause, H.-J. Y. Zhang, R. Hohmann, M. Grüneklee, M. I. Faley, D. Lomparski, M. Maus, H. Bousack, and A. I. Braginski, 1997, in *Proceedings of the Third European Conference on Applied Superconductivity (EUCAS'97)*, Ueldhoven Institute of Physics Conference Series No. 158, edited by H. Rogalla and D. H. A. Blank (Institute of Physics, Philadelphia), p. 775.
Kreutzbruck, M. v., M. Mück, U. Baby, and C. Heiden, 1998, in *Studies in Applied Electromagnetics and Mechanics* (IOS Press Amsterdam, The Netherlands), Vol. 13, p. 345.
Kreutzbruck, M. v., J. Tröll, M. Mück, C. Heiden, and Y. Zhang, 1997, IEEE Trans. Appl. Supercond. **7**, 3279.
Kromann, R., J. J. Kingston, A. H. Miklich, L. T. Sagdahl, and J. Clarke, 1993, Appl. Phys. Lett. **63**, 559.
Kugai, H., T. Nagaishi, and H. Itozaki, 1996, in *Advances in Superconductivity VIII*, edited by H. Hayakawa and Y. Enomoto (Springer, Tokyo), p. 1145.
Kupriyanov, M. Y., and K. K. Likharev, 1990, Sov. Phys. Usp. **160**, 49.
Kurkijärvi, J., 1972, Phys. Rev. B **6**, 832.
Kurkijärvi, J., 1973, J. Appl. Phys. **44**, 3729.
Kuzmin, L. S., K. K. Likharev, V. V. Migulin, E. A. Polunin, and N. A. Simonov, 1985, in *SQUID'85, Superconducting Quantum Interference Devices and their Applications*, edited by H.-D. Hahlbohm and H. Lübbig (Walter de Gruyter, Berlin), p. 1029.
Lee, L. P., K. Char, M. S. Colclough, and G. Zaharchuk, 1991, Appl. Phys. Lett. **59**, 3051.
Lee, L. P., J. Longo, V. Vinetskiy, and R. Cantor, 1995, Appl. Phys. Lett. **66**, 1539.
Lee, T. S., Y. R. Chemla, E. Dantsker, and J. Clarke, 1997, IEEE Trans. Appl. Supercond. **7**, 3147.
Lee, T. S., E. Dantsker, and J. Clarke, 1996, Rev. Sci. Instrum. **67**, 4208.
Likhachev, A. G., V. N. Polushkin, S. V. Uchaikin, and B. V. Vasiliev, 1990, Supercond. Sci. Technol. **3**, 148.

Likharev, K. K., 1986, *Dynamics of Josephson Junctions and Circuits* (Gordon and Breach, New York).
Likharev, K. K. and B. T. Ulrich, 1978, *Dynamics of Josephson Junction Circuits: Basic Theory* (Moscow University, Moscow; in Russian).
Ludwig, F., J. Beyer, D. Drung, S. Bechstein, and Th. Schurig, 1997, Appl. Supercond. **5**, 345.
Ludwig, F., E. Dantsker, R. Kleiner, D. Koelle, J. Clarke, S. Knappe, D. Drung, H. Koch, N. McN. Alford, and T. W. Button, 1995, Appl. Phys. Lett. **66**, 1418.
Ludwig, F., E. Dantsker, D. Koelle, R. Kleiner, A. H. Miklich, and J. Clarke, 1995, Appl. Supercond. **3**, 383.
Ludwig, F., E. Dantsker, D. Koelle, R. Kleiner, A. H. Miklich, D. T. Nemeth, J. Clarke, D. Drung, J. Knappe, and H. Koch, 1995, IEEE Trans. Appl. Supercond. **5**, 2919.
Ludwig, F., E. Dantsker, D. T. Nemeth, D. Koelle, A. H. Miklich, J. Clarke, S. Knappe, H. Koch, and R. E. Thomson, 1994, Supercond. Sci. Technol. **7**, 273.
Ludwig, F., D. Koelle, E. Dantsker, D. T. Nemeth, A. H. Miklich, J. Clarke, and R. E. Thomson, 1995, Appl. Phys. Lett. **66**, 373.
Mannhart, J., P. Chaudhari, D. Dimos, C. C. Tsuei, and T. R. McGuire, 1988, Phys. Rev. Lett. **61**, 2476.
Martinis, J. M., and J. Clarke, 1985, J. Low Temp. Phys. **61**, 227.
Marx, A., L. Alff, and R. Gross, 1995, Appl. Phys. Lett. **67**, 1929.
Marx, A., U. Fath, W. Ludwig, R. Gross, and T. Amrein, 1995, Phys. Rev. B **51**, 6735.
Marx, A., and R. Gross, 1997, Appl. Phys. Lett. **70**, 120.
Mathai, A., D. Song, Y. Gim, and F. C. Wellstood, 1993, IEEE Trans. Appl. Supercond. **3**, 2609.
Matijasevic, V., Z. Lu, T. Kaplan, and C. Huang, 1997, in *Proceedings of the Third European Conference on Applied Superconductivity (EUCAS'97)*, Veldhoven Institute of Physics Conference Series No. 158, p. 189.
Matsuda, M., Y. Murayama, S. Kiryu, N. Kasai, S. Kashiwaya, M. Koyanagi, and T. Endo, 1991, IEEE Trans. Magn. **MAG-27**, 3043.
Matzander, U., U. Kalberkamp, V. Rath, K.-D. Husemann, G. Panaitow, E. Zimmermann, and Y. Zhang, 1997, in *Extended Abstracts of the 6th International Superconductive Electronics Conference (ISEC'97)*, Berlin, edited by H. Koch and S. Knappe (Physikalisch-Technische Bundesanstalt, Braunschweig), Vol. 3, p. 355.
Mayer, B., L. Alff, T. Träuble, R. Gross, P. Wagner, and H. Adrian, 1993, Appl. Phys. Lett. **63**, 996.
McCumber, D. E., 1968, J. Appl. Phys. **39**, 3113.
McDaniel, E. B., S. C. Gausephohl, C.-T. Li, M. Lee, J. W. P. Hsu, R. A. Rao, and C. B. Eom, 1997, Appl. Phys. Lett. **70**, 1882.
Mercereau, J. E., 1970, Rev. Phys. Appl. **5**, 13.
Meservey, R., and P. M. Tedrow, 1969, J. Appl. Phys. **40**, 2028.
Miklich, A. H., J. Clarke, M. S. Colclough, and K. Char, 1992, Appl. Phys. Lett. **60**, 1899.
Miklich, A. H., J. J. Kingston, F. C. Wellstood, J. Clarke, M. S. Colclough, K. Char, and G. Zaharchuk, 1991, Appl. Phys. Lett. **59**, 988.
Miklich, A. H., D. Koelle, E. Dantsker, D. T. Nemeth, J. J. Kingston, R. F. Kroman, and J. Clarke, 1993, IEEE Trans. Appl. Supercond. **3**, 2434.
Miklich, A. H., D. Koelle, F. Ludwig, D. T. Nemeth, E. Dantsker, and J. Clarke, 1995, Appl. Phys. Lett. **66**, 230.
Miklich, A. H., D. Koelle, T. J. Shaw, F. Ludwig, D. T. Nemeth, E. Dantsker, and J. Clarke, 1994, Appl. Phys. Lett. **64**, 3494.
Milliken, F. P., S. L. Brown, and R. H. Koch, 1997, Appl. Phys. Lett. **71**, 1857.
Milliken, F. P., R. H. Koch, S. L. Brown, R. A. Altman, W. J. Gallagher, S. G. Haupt, and D. K. Lathrop, 1997, J. Appl. Phys. **82**, 6301.
Minotani, T., K. Enpuku, and Y. Kuroki, 1997, J. Appl. Phys. **82**, 457.
Minotani, T., S. Kawakami, T. Kiss, Y. Kuroki, and K. Enpuku, 1997, Jpn. J. Appl. Phys., Part 2 **36**, L1092.
Missert, N., T. E. Harvey, and R. H. Ono, 1993, Appl. Phys. Lett. **63**, 1690.
Moeckley, B. H., D. K. Lathrop, and R. A. Buhrman, 1993, Phys. Rev. B **47**, 400.
Mück, M., 1993, IEEE Trans. Appl. Supercond. **3**, 2003.
Mück, M., J. Clarke, and C. Heiden, 1994, Proc. SPIE **2160**, p. 180.
Mück, M., C. Heiden, and J. Clarke, 1994, J. Appl. Phys. **75**, 4588.
Mück, M., M. v. Kreutzbruck, U. Baby, J. Tröll, and C. Heiden, 1997, Physica C **282-287**, 407.
Nagaishi, T., H. Kugai, H. Toyoda, and H. Itozaki, 1997, IEEE Trans. Appl. Supercond. **7**, 2886.
Nakane, H., Y. Tarutani, T. Nishino, H. Yamada, and U. Kawabe, 1987, Jpn. J. Appl. Phys., Part 2 **26**, L1925.
Nichols, D. G., E. Dantsker, R. Kleiner, M. Mück, and J. Clarke, 1996, J. Appl. Phys. **80**, 6032.
Nisenoff, M., 1970, Rev. Phys. Appl. **5**, 21.
Ockenfuß, G. J., J. Borgmann, M. Reese, and R. Wördenweber, 1997, IEEE Trans. Appl. Supercond. **7**, 3698.
Ockenfuß, G. J., R. Wördenweber, T. A. Scherer, R. Unger, and W. Jutzi, 1995, Physica C **243**, 24.
Oh, B. D., R. H. Koch, W. J. Gallagher, R. P. Robertazzi, and W. Eidelloth, 1991, Appl. Phys. Lett. **59**, 123.
Ono, R. H., J. A. Beall, M. W. Cromar, T. E. Harvey, M. E. Johansson, C. D. Reintsema, and D. A. Rudman, 1991, Appl. Phys. Lett. **59**, 1126.
Ono, R. H., L. R. Vale, K. R. Kimminau, J. A. Beall, M. W. Cromar, C. D. Reintsema, T. E. Harvey, P. A. Rosenthal, and D. A. Rudman, 1993, IEEE Trans. Appl. Supercond. **3**, 2389.
Ott, H. W., 1988, *Noise Reduction Techniques in Electronic Systems*, Second Edition (Wiley, New York), p. 233.
Penny, R. D., D. K. Lathrop, E. E. Magnuson, B. D. Thorson, B. R. Whitecotton, R. H. Koch, and J. R. Rosen, 1997, IEEE Trans. Appl. Supercond. **7**, 2323.
Pettiette-Hall, C. L., J. A. Luine, J. Murduck, J. F. Burch, R. Hu, M. Sergant, and D. St. John, 1995, IEEE Trans. Appl. Supercond. **5**, 2087.
Phillips, J., 1993, in *The New Superconducting Electronics*, NATO ASI series, edited by H. Weinstock and R. W. Ralston (Kluwer Academic, Dordrecht), p. 59.
Phillips, J., 1996, J. Appl. Phys. **79**, 1829.
Pitzius, P., V. Dworak, and U. Hartmann, 1997, in *Extended Abstracts of the 6th International Superconductive Electronics Conference (ISEC'97)*, Berlin, edited by H. Koch and S. Knappe (Physikalisch-Technische Bundesanstalt, Braunschweig), Vol. 3, p. 395.
Purpura, J. W., T. R. Clem, and R. F. Wiegert, 1993, IEEE Trans. Appl. Supercond. **3**, 2445.
Quincey, P. G., 1994, Appl. Phys. Lett. **64**, 517.

Radic, T. D. Drung, S. Knappe, and S. Menkel, 1997, in *Extended Abstracts of the 6th International Superconductive Electronics Conference (ISEC'97)*, Berlin, edited by H. Koch and S. Knappe (Physikalisch-Technische Bundesanstalt, Braunschweig), Vol. 3, p. 352.

Reimer, D., F. Ludwig, M. Schilling, S. Knappe, and D. Drung, 1995, in *Proceedings of the Second European Conference on Applied Superconductivity (EUCAS'95)*, Edinburgh, edited by D. Dew-Hughes (Institute of Physics, Bristol, Philadelphia) Institute of Physics Conference Series No. 148, p. 1605.

Reimer, D., M. Schilling, S. Knappe, and D. Drung, 1995, IEEE Trans. Appl. Supercond. **5**, 2342.

Reintsema, C. D., R. H. Ono, G. Barnes, L. Borcherdt, T. E. Harvey, G. Kunkel, D. A. Rudman, L. R. Vale, N. Missert, and P. A. Rosenthal, 1995, IEEE Trans. Appl. Supercond. **5**, 3405.

Roas, B., L. Bär, M. Kühnl, G. Daalmans, and F. Bömmel, 1993, in *Proceedings of European Conference on Applied Superconductivity (EUCAS'93)*, edited by H. C. Freyhardt (DGM Informationsgesellschaft, Oberursel), p. 1335.

Rosenthal, P. A., E. N. Grossman, R. H. Ono, and L. R. Vale, 1993, Appl. Phys. Lett. **63**, 1984.

Russek, S. E., D. K. Lathrop, B. H. Moeckly, R. A. Buhrman, D. H. Shin, and J. Silcox, 1990, Appl. Phys. Lett. **57**, 1155.

Russek, S. E., S. C. Sanders, A. Roshko, and J. W. Ekin, 1994, Appl. Phys. Lett. **64**, 3649.

Russek, S. E., S. C. Sanders, C. C. Clickner, and J. W. Ekin, 1996, Applied Superconductivity Conference (ASC'96), Pittsburgh, PA (unpublished).

Ryhänen, T., H. Seppä, R. Ilmoniemi, and J. Knuutila, 1989, J. Low Temp. Phys. **76**, 287.

Satoh, T., M. Y. Kupriyanov, J. Tsai, M. Hidaka, and H. Tsuge, 1995, IEEE Trans. Appl. Supercond. **5**, 2612.

Savo, B., F. C. Wellstood, and J. Clarke, 1987, Appl. Phys. Lett. **50**, 1757.

Scharnweber, R., and M. Schilling, 1996, Appl. Phys. Lett. **69**, 1303.

Scharnweber, R., and M. Schilling, 1997, IEEE Trans. Appl. Supercond. **7**, 3485.

Scharnweber, R., K.-O. Subke, and M. Schilling, 1995, in *Proceedings of the Second European Conference on Applied Superconductivity (EUCAS'95)*, Edinburgh, edited by D. Dew-Hughes (Institute of Physics, Bristol/Philadelphia) Institute of Physics Conference Series No. 148, p. 1609.

Scheel, H. J., M. Berkowski, and B. Chabotes, 1991, J. Cryst. Growth **115**, 19.

Schilling, M., 1997, IEEE Trans. Appl. Supercond. **7**, 2960.

Schilling, M., S. Krey, and R. Scharnweber, 1996, Appl. Phys. Lett. **69**, 2751.

Schilling, M., R. Scharnweber, and S. Völkl, 1995, IEEE Trans. Appl. Supercond. **5**, 2346.

Schmidl, R., S. Wunderlich, L. Dörrer, H. Specht, J. Heinrich, K.-U. Barholz, H. Schneidewind, U. Hübner, and P. Seidel, 1997, in *Proceedings of the Third European Conference on Applied Superconductivity (EUCAS'97)*, Veldhoven, edited by H. Rogalla and D. H. A. Blank (Institute of Physics, Philadelphia), Vol. 158, p. 651.

Schmidl, R., S. Wunderlich, L. Dörrer, H. Specht, S. Linzen, H. Schneidewind, and P. Seidel, 1997, IEEE Trans. Appl. Supercond. **7**, 2756.

Schmidt, J. M., L. P. Lee, A. Matlashov, M. Teepe, V. Vinetskiy, and R. Cantor, 1996, Biomag'96, Santa Fe, New Mexico, Abstracts p. 340.

Schneider, J., H. Kohlstedt, and R. Wördenweber, 1993, Appl. Phys. Lett. **63**, 2426.

Schneidewind, H., F. Schmidl, S. Linzen, and P. Seidel, 1995, Physica C **250**, 191.

Schultze, V., R. Ijsselsteijn, V. Zakosarenko, F. Thrum, E. Il'ichev, and H. G. Meyer, 1997, in *Extended Abstracts of the 6th International Superconductive Electronics Conference (ISEC'97)*, Berlin, edited by H. Koch and S. Knappe (Physikalisch-Technische Bundesanstalt, Braunschweig), Vol. 3, p. 71.

Schultze, V., R. Stolz, R. Ijsselsteijn, V. Zakosarenko, L. Fritzsch, F. Thrum, E. Il'ichev, and H.-G. Meyer, 1997, IEEE Trans. Appl. Supercond. **7**, 3473.

Seidel, P., R. Weidl, S. Brabetz, F. Schmidl, H. Nowak, and U. Leder, 1997, in *Extended Abstracts of the 6th International Superconductive Electronics Conference (ISEC'97)*, Berlin, edited by H. Koch and S. Knappe (Physikalisch-Technische Bundesanstalt, Braunschweig), Vol. 3, p. 321.

Shaw, T. J., J. Clarke, R. B. van Dover, L. F. Schneemeyer, and A. E. White, 1996, Phys. Rev. B **54**, 15411.

Sheen, D. M., S. M. Ali, D. E. Oates, R. S. Withers, and J. A. Kong, 1991, IEEE Trans. Appl. Supercond. **1**, 108.

Shen, Y. Q., Z. J. Sun, R. Kromann, T. Holst, P. Vase, and T. Freltoft, 1995, Appl. Phys. Lett. **67**, 2081.

Simon, R., J. B. Bulman, J. F. Burch, S. B. Coons, K. P. Daly, W. D. Dozier, R. Hu, A. E. Lee, J. A. Luine, C. E. Platt, and M. J. Zani, 1991, IEEE Trans. Magn. **MAG-27**, 3209.

Sivakov, A. G., A. P. Zhuravel, O. G. Turutanov, I. M. Dmitrenko, J. W. M. Hilgenkamp, G. C. S. Brons, J. Flokstra, and H. Rogalla, 1994, Physica C **232**, 93.

Somekh, R. E. and Z. H. Barber, 1992, in *Physics and Materials Science of High Temperature Superconductors, II*, edited by R. Kossowsky, B. Raveau, D. Wohlleben, and S. K. Patapis (Kluwer Academic, Dordrecht), p. 443.

Stewart, W. C., 1968, Appl. Phys. Lett. **12**, 277.

Strikovskiy, M. D., and A. Engelhardt, 1996, Appl. Phys. Lett. **69**, 2918.

Sun, J. Z., W. J. Gallagher, A. C. Callegari, V. Foglietti, and R. H. Koch, 1993, Appl. Phys. Lett. **63**, 1561.

Sun, J. Z., W. J. Gallagher, and R. H. Koch, 1992, Appl. Phys. Lett. **61**, 3190.

Sun, J. Z., W. J. Gallagher, and R. H. Koch, 1993, IEEE Trans. Appl. Supercond. **3**, 2022.

Sun, J. Z., W. J. Gallagher, and R. H. Koch, 1994, Phys. Rev. B **50**, 13664.

Tanaka S., H. Itozaki, and H. Kado, 1995, in *Proceedings of the 7th International Symposium on Superconductivity (ISS '94)*, Advances in Superconductivity VII, edited by K. Yamafuji and T. Morishita (Springer, Tokyo), p. 1117.

Tanaka, S., H. Itozaki, H. Toyoda, N. Harada, A. Adachi, K. Okajima, and H. Kado, 1994, Appl. Phys. Lett. **64**, 514.

Tavrin, Y., H.-J. Krause, W. Wolf, V. Glyantsev, J. Schubert, W. Zander, and H. Bousack, 1995, Cryogenics **36**, 83.

Tavrin Y., and M. Siegel, 1997, in *Proceedings of the Third European Conference on Applied Superconductivity (EUCAS'97)*, Veldhoven, edited by H. Rogalla and D. H. A. Blank (Institute of Physics, Philadelphia), No. 158, p. 719.

Tavrin, Y., M. Siegel, and J. Hinken, 1999, IEEE Trans. Appl. Supercond. (in press).

Tavrin, Y., Y. Zhang, M. Mück, A. I. Braginski, and C. Heiden, 1993a, IEEE Trans. Appl. Supercond. **3**, 2477.

Tavrin, Y., Y. Zhang, M. Mück, A. I. Braginski, and C. Heiden, 1993b, Appl. Phys. Lett. **62**, 1824.

Tavrin, Y., Y. Zhang, W. Wolf, and A. I. Braginski, 1994, Supercond. Sci. Technol. **7**, 265.
ter Brake, H. J. M., W. A. M. Aarnink, P. J. van den Bosch, J. W. M. Hilgenkamp, J. Flokstra, and H. Rogalla, 1997, Supercond. Sci. Technol. **10**, 512.
ter Brake, H. J. M., N. Janssen, J. Flokstra, D. Veldhuis, and H. Rogalla, 1997, IEEE Trans. Appl. Supercond. **7**, 2545.
ter Brake, H. J. M., R. Karunanithi, H. J. Holland, J. Flokstra, D. Veldhuis, L. Vargas, J. W. M. Hilgenkamp, W. Jaszczuk, N. Janssen, F. J. G. Roesthuis, and H. Rogalla, 1997, Meas. Sci. Technol. **8**, 927.
Tesche, C. D., and J. Clarke, 1977, J. Low Temp. Phys. **29**, 301.
Tesche, C. D., and J. Clarke, 1979, J. Low Temp. Phys. **37**, 397.
Tinchev, S. S., 1997, in *Microwave Physics and Technique* (Kluwer Academic, Dordrecht), p. 173.
Tinchev, S. S., and J. H. Hinken, 1992, in *Superconducting Devices and their Applications*, edited by H. Koch and H. Lübbig, Springer Proceedings in Physics, (Springer, Berlin/Heidelberg), Vol. 64, p. 102.
TonThat, Dinh M., M. Ziegeweid, Y.-Q. Song, E. J. Munson, S. Appelt, A. Pines, and J. Clarke, 1997, Chem. Phys. Lett. **272**, 245.
Töpfer, H., 1991, in *Superconductivity and Cryoelectronics*, edited by W. Krech, P. Seidel, and H. G. Meyer (World Scientific, Singapore), p. 170.
Töpfer, H., and F. H. Uhlmann, 1994, in *Proceedings of the Seventh International Symposium on Weak Superconductivity*, Smolenice, p. 336.
Tsuei, C. C., J. R. Kirtley, C. C. Chi, L. S. Yu-Jahnes, A. Gupta, T. Shaw, J. Z. Sun, and M. B. Ketchen, 1994, Phys. Rev. Lett. **73**, 593.
Tsuei, C. C., J. Mannhart, and D. Dimos, 1989, in *Proceedings of the Topical Conference on High T_c Superconducting Thin Films, Devices and Applications*, Atlanta, GA, 1988, edited by G. Mararitondo, R. Joint, and M. Onellion (AIP, New York), p. 194.
Uhlmann, H., H. Töpfer, F. Verwiebe, and J. Uhlig, 1992, in *Superconducting Devices and their Applications*, edited by H. Koch and H. Lübbig, Springer Proceedings in Physics (Springer, Berlin/Heidelberg), Vol. 64, p. 292.
Vale, L. R., R. H. Ono, and D. A. Rudman, 1997, IEEE Trans. Appl. Supercond. **7**, 3193.
van der Harg, A. J. M., E. van der Drift, and P. Hadley, 1995, IEEE Trans. Appl. Supercond. **5**, 1448.
Voss, R. F., 1981, J. Low Temp. Phys. **42**, 151.
Vrba, J., 1996, in *SQUID Sensors: Fundamentals, Fabrication and Applications*, NATO ASI Series, edited by H. Weinstock (Kluwer Academic, Dordrecht), p. 117.
Vu, L. N., and D. J. Van Harlingen, 1993, IEEE Trans. Appl. Supercond. **3**, 1918.
Wang, S. G., L. H. Zhang, C. J. Wang, and Y. D. Dai, 1997, M2S-HTSC-V, *Fifth International Conference, Materials and Mechanisms of Superconductivity, High-Temperature Superconductors*, Beijing, China, p. 31.
Weidl, R., S. Brabetz, F. Schmidl, F. Klemm, S. Wunderlich, and P. Seidel, 1997, Supercond. Sci. Technol. **10**, 95.
Weinstock H., 1996, Ed., *SQUID Sensors: Fundamentals, Fabrication and Applications* (Kluwer Academic, Dordrecht).
Wellstood, F., C. Heiden, and J. Clarke, 1984, Rev. Sci. Instrum. **55**, 952.
Wellstood, F. C., J. J. Kingston, and J. Clarke, 1994, J. Appl. Phys. **75**, 683.
Wellstood, F. C., J. J. Kingston, M. J. Ferrari, and J. Clarke, 1990, Appl. Phys. Lett. **57**, 1930.
Wellstood, F. C., J. J. Kingston, M. J. Ferrari, and J. Clarke, 1991, IEEE Trans. Magn. **27**, 2569.
Wellstood, F. C., A. H. Miklich, J. J. Kingston, M. J. Ferrari, J. Clarke, M. S. Colclough, K. Char, and G. Zaharchuk, 1992, in *Superconducting Devices and their Applications*, edited by H. Koch and H. Lübbig, Springer Proceedings in Physics (Springer, Berlin/Heidelberg), Vol. 64, p. 162.
Wen, C. P., 1969, IEEE Trans. Microwave Theory Tech. **MTT-17**, 1087.
Wikswo, Jr., J. P., 1995, IEEE Trans. Appl. Supercond. **5**, 74.
Woeltgens, P. J. M., R. H. Koch, R. Matthews, S. L. Brown, R. A. Altman, W. J. Gallagher, S. G. Haupt, and D. K. Lathrop, 1996, Applied Superconductivity Conference (ASC'96), Pittsburgh (unpublished).
Wu, M. K., J. R. Ashburn, C. J. Torng, P. H. Hor, R. L. Meng, L. Gao, N. Z. Huang, Y. Q. Wang, and C. W. Chu, 1987, Phys. Rev. Lett. **58**, 908.
Yanamoto, K., B. M. Lairson, J. C. Bravman, and T. H. Geballe, 1991, J. Appl. Phys. **69**, 7189.
Yi, H. R., M. Gustafsson, D. Winkler, E. Olsson, and T. Claeson, 1996, J. Appl. Phys. **79**, 9213.
Zakosarenko, V., F. Schmidl, H. Schneidewind, L. Dörrer, and P. Seidel, 1994, Appl. Phys. Lett. **65**, 779.
Zani, M. J., J. A. Luine, G. S. Lee, J. M. Murduck, R. Ha, M. J. Levis, R. A. Davidheiser, and L. R. Eaton, 1991, IEEE Trans. Magn. **MAG-27**, 2557.
Zhang, Y., M. Gottschlich, H. Soltner, E. Sodtke, J. Schubert, W. Zander, and A. I. Braginski, 1995, Appl. Phys. Lett. **67**, 3183.
Zhang, Y., U. Krüger, R. Kutzner, R. Wördenweber, J. Schubert, W. Zander, E. Sodtke, and A. I. Braginski, 1994, Appl. Phys. Lett. **65**, 3380.
Zhang, Y., M. Mück, M. Bode, K. Herrmann, J. Schubert, W. Lander, A. I. Braginski, and C. Heiden, 1992, Appl. Phys. Lett. **60**, 2303.
Zhang, Y., M. Mück, K. Herrmann, J. Schubert, W. Zander, A. I. Braginski, and C. Heiden, 1993, IEEE Trans. Appl. Supercond. **3**, 2465.
Zhang, Y., M. Mück, K. Herrmann, W. Zander, J. Schubert, A. I. Braginski, and Ch. Heiden, 1992, Appl. Phys. Lett. **60**, 645.
Zhang, Y., H. Soltner, H.-J. Krause, E. Sodtke, W. Zander, J. Schubert, M. Grüneklee, D. Lomparski, M. Banzer, H. Bousack, and A. I. Braginski, 1997, IEEE Trans. Appl. Supercond. **7**, 2866.
Zhang, Y., H. Soltner, N. Wolters, W. Zander, J. Schubert, M. Banzet, and A. I. Braginski, 1997, IEEE Trans. Appl. Supercond. **7**, 2870.
Zhang, Y., Y. Tavrin, M. Mück, A. I. Braginski, C. Heiden, S. Hampson, C. Pantev, and T. Elbert, 1993, Brain Topography **5**, 379.
Zhang, Y., N. Wolters, X. H. Zeng, J. Schubert, W. Zander, H. Soltner, M. Banzet, F. Rüders, and A. I. Braginski, 1997, Appl. Supercond. (in press).
Zhang, Y., W. Zander, J. Schubert, F. Rüders, H. Soltner, M. Banzet, N. Wolters, X. H. Zeng, and A. I. Braginski, 1997, Appl. Phys. Lett. **71**, 704.
Zhang, Y., H. R. Yi, J. Schubert, W. Zander, M. Banzet, and A. I. Braginski, 1998, Appl. Phys. Lett. **72**, 2029.

Zhang, Y., H. R. Yi, J. Schubert, W. Zander, H.-J. Krause, H. Bousack, and A. I. Braginski, 1999, IEEE Trans. Appl. Supercond. (in press).
Zimmerman, J. E., 1971, J. Appl. Phys. **42**, 4483.
Zimmerman, J. E., J. A. Beall, M. W. Cromar, and R. H. Ono, 1987, Appl. Phys. Lett. **51**, 617.
Zimmerman, J. E., and N. V. Frederick, 1971, Appl. Phys. Lett. **19**, 16.
Zimmerman, J. E., P. Thiene, and J. T. Harding, 1970, J. Appl. Phys. **41**, 1572.